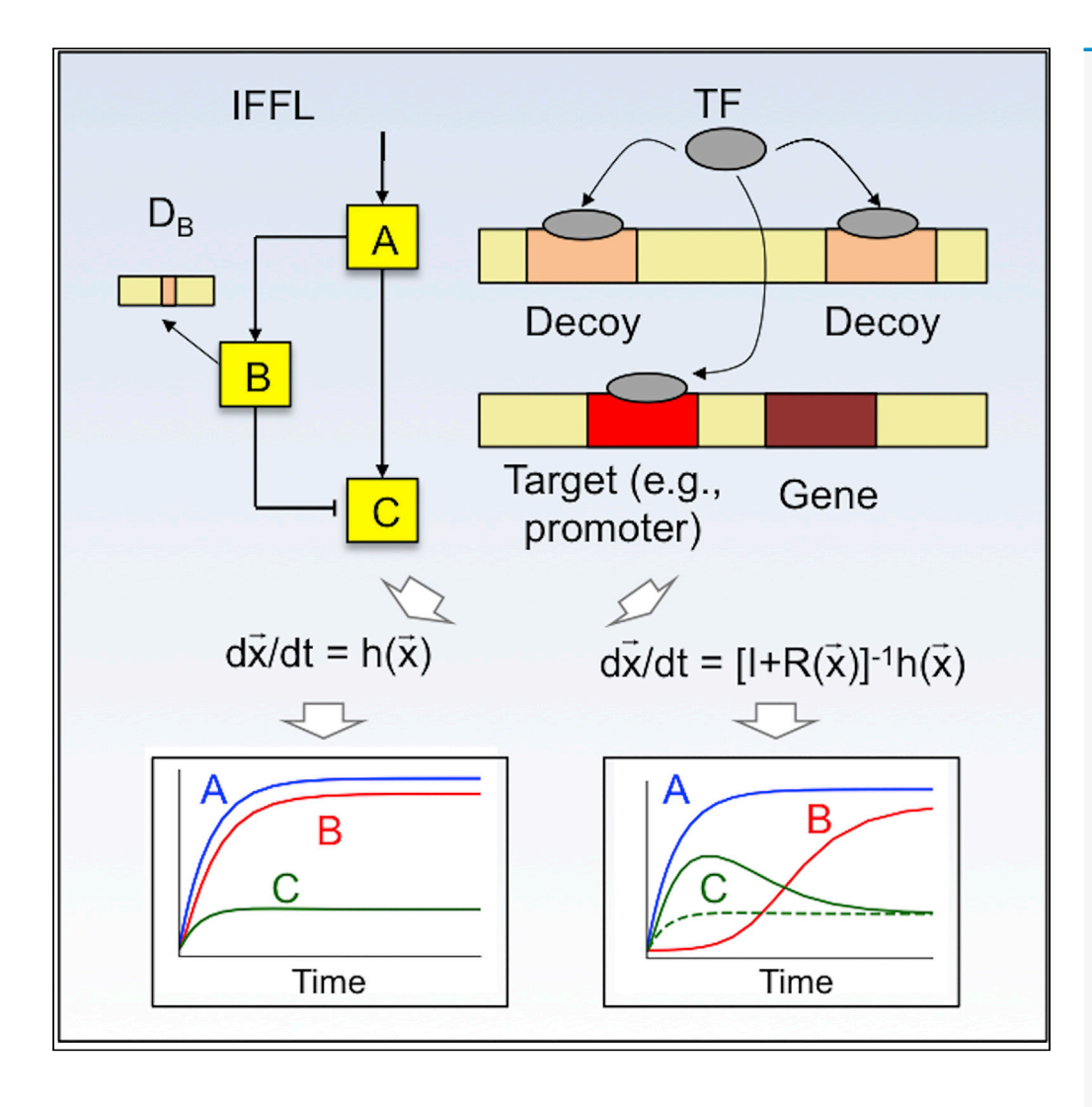
iScience



Article

How Retroactivity Affects the Behavior of Incoherent Feedforward Loops



Junmin Wang, Calin Belta, Samuel A. Isaacson

dawang@bu.edu

HIGHLIGHTS

Study of how retroactivity affects behaviors of incoherent feedforward loops (IFFLs)

Increasing retroactivity in IFFLs can speed up or slow down the response

Increasing retroactivity in negative autoregulatory loops only slows the response

Tuning retroactivity could be used to improve the performance of synthetic IEEI s

Wang et al., iScience 23, 101779 December 18, 2020 © 2020 The Authors. https://doi.org/10.1016/ j.isci.2020.101779



iScience



Article

How Retroactivity Affects the Behavior of Incoherent Feedforward Loops

Junmin Wang, 1,3,* Calin Belta, 1 and Samuel A. Isaacson²

SUMMARY

An incoherent feedforward loop (IFFL) is a network motif known for its ability to accelerate responses and generate pulses. It remains an open question to understand the behavior of IFFLs in contexts with high levels of retroactivity, where an upstream transcription factor binds to numerous downstream binding sites. Here we study the behavior of IFFLs by simulating and comparing ODE models with different levels of retroactivity. We find that increasing retroactivity in an IFFL can increase, decrease, or keep the network's response time and pulse amplitude constant. This suggests that increasing retroactivity, traditionally considered an impediment to designing robust synthetic systems, could be exploited to improve the performance of IFFLs. In contrast, we find that increasing retroactivity in a negative autoregulated circuit can only slow the response. The ability of an IFFL to flexibly handle retroactivity may have contributed to its significant abundance in both bacterial and eukaryotic regulatory networks.

INTRODUCTION

Living cells sense and respond to the environment via a large variety of mechanisms. How do diverse biochemical networks, which are at the core of the process by which cells sense and respond to signals, yield and maintain specific functional behaviors? A widely held hypothesis in systems biology is that recurring network sub-structures, also known as network motifs, play important roles therein. Network motifs capable of performing biological functions are preserved over the course of evolution, resulting in a rate of occurrence higher than if nodes and edges were connected at random (Alon, 2007).

One of the most common three-gene network motifs in transcriptional regulatory networks (TRN) is the incoherent feedforward loop (IFFL), where a transcription factor (TF) activates and inhibits a downstream gene directly and indirectly (Figure 1A). In a pioneering study guided by ordinary differential equation (ODE) models, IFFLs were established as a sign-sensitive response accelerator and pulse generator (Mangan and Alon, 2003) (Figure 1B). These findings were supported by subsequent efforts in synthetic biology with compelling experimental evidence (Mangan and Alon, 2003). Using the gal system in *Escherichia coli* (*E. coli*), it was shown that compared with simple regulation, IFFLs can accelerate the response times of a target gene (Alon, 2007). The feasibility of creating synthetic pulse-generating IFFL circuits under the guidance of ODE models was demonstrated in another study (Basu et al., 2004). In addition, IFFLs can provide fold-change detection and buffer noise (Goentoro et al., 2009). It was shown that miRNA-mediated IFFLs confer precision and stability to the target protein level despite fluctuations in upstream regulators (Osella et al., 2011; Siciliano et al., 2013; Grigolon et al., 2016).

Although a wealth of literature has shed light on this topic, it remains an open area of research to understand the full functional capabilities of IFFLs. In ODE-model-based studies, it was generally assumed that changes in protein concentrations arise from first-order decay and protein production rates regulated by upstream TFs (Mangan and Alon, 2003; Basu et al., 2004). This assumption aligns with the traditional view of TRNs as modular systems, where the temporal dynamics of a protein depend solely upon the TFs that regulate its expression. In other words, under this assumption, the dynamics of the protein are not affected by the components it regulates even if the protein is also a TF. However, growing theoretical and experimental evidence suggests that TRNs are not modular but quasi-modular. A fraction of the TF molecules are employed to form complexes with downstream binding sites, hence becoming unavailable for additional



¹The Bioinformatics Graduate Program, Boston University, Boston, MA 02215,

²Department of Mathematics and Statistics, Boston University, Boston, MA 02215, USA

³¹ ead Contact

^{*}Correspondence: dawang@bu.edu

https://doi.org/10.1016/j.isci. 2020.101779





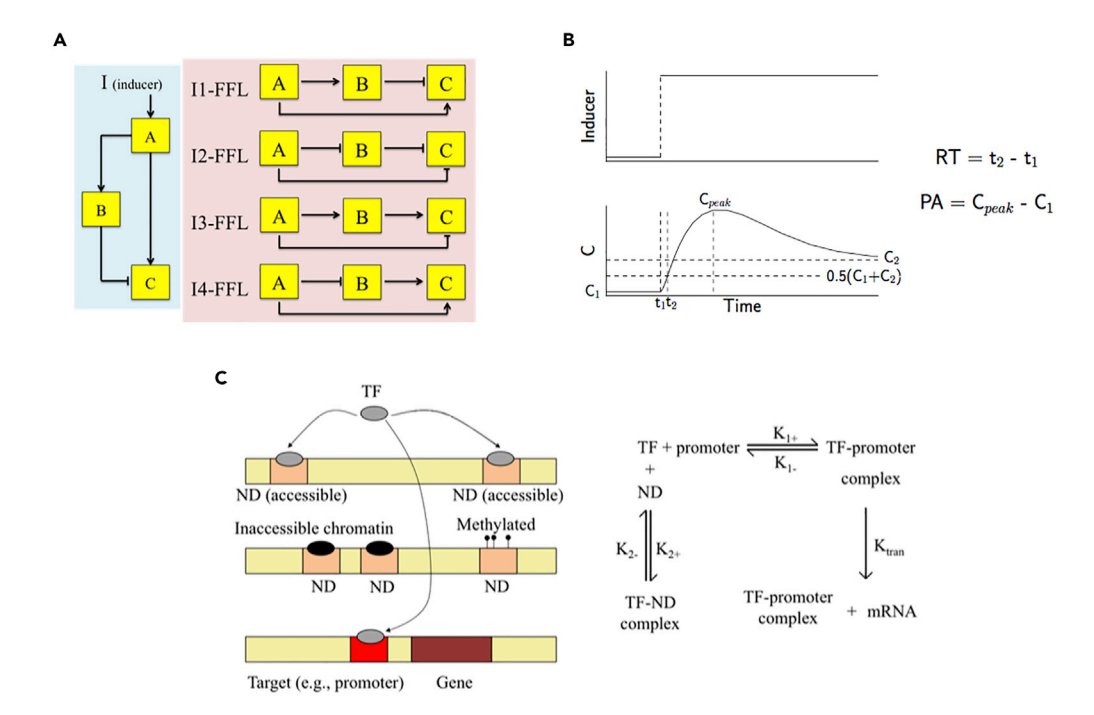


Figure 1. IFFLs, Response Time, Pulse Amplitude, and Accessible ND-Binding Sites

(A) Graphical representations of four types of IFFL: I1-FFL, I2-FLL, I3-FFL, and I4-FFL. An IFFL is a three-node network motif, where the input A, stimulated by an external inducer I, regulates the output C in two opposing directions. Arrows indicate activation, and edges with bars at the ends, inhibition.

(B) Definitions of response time and pulse amplitude. Response time, abbreviated as RT, is defined as the time needed to reach the midpoint between the pre-induction and the post-induction steady states (t_2-t_1) , whereas pulse amplitude, abbreviated as PA, is defined as the difference between the pre-induction steady state and the peak concentration $(C_{\text{peak}}-C_1)$.

(C) The effect of accessible ND-binding sites on the dynamics of the TF. Non-functional NDs sequester some of the upstream TF, so only a fraction of the upstream TF molecules are available to bind to functional target sites (e.g., promoters and enhancers).

molecular activities, such as degradation, protein-protein interaction, or regulation of other genes. Examples of such TFs include p53 (Pariat et al., 1997) and MyoD (Abu Hatoum et al., 1998), both of which become resistant to degradation when bound to DNA. This phenomenon, where downstream binding sites can alter the dynamics of the upstream system, is known as retroactivity (Del Vecchio et al., 2008).

In TRNs, retroactivity is large when the amount of TF is comparable to, or smaller than, the copy number of the downstream bindings sites, or when the affinity of such binding is high (Del Vecchio et al., 2008). In synthetic biology, retroactivity is widely recognized as an essential parameter to consider in model-based circuit design (Brophy and Voigt, 2014). In the context of endogenous regulatory networks, retroactivity is seldom discussed, as the level of retroactivity that arises from TF binding in the genome is typically assumed to be negligible (Jayanthi et al., 2013). However, results from chromatin immunoprecipitation (ChIP)-on-chip and ChIP sequencing (ChIP-seq) methods suggest that the validity of this assumption is dependent on the biological context of the network (Kemme et al., 2016). In particular, genome-wide studies driven by the Encyclopedia of DNA Elements (ENCODE) project have shown that in eukaryotic cells, TFs bind to not only functional sites in the cis-regulatory elements (e.g., promoters and enhancers) but also numerous high-affinity sequence-specific binding sites that are seemingly non-functional (Consortium, 2012; Fisher et al., 2012; Li et al., 2008) (Figure 1C). It has been suggested that these high-affinity sequence-specific binding sites can serve as natural decoys (NDs), which compete with functional target sites for TF binding (Burger et al., 2010, 2012; Lee and Maheshri, 2012; Liu et al., 2007; Wang et al., 2016). While the majority of ND sites are inaccessible due to chromatin structure, CpG methylation, or competing proteins, an average TF in the human genome still has approximately 10^4-10^5 accessible ND sites, which typically have greater or at least comparable binding affinity compared with sequence-specific



TF-binding sites (Kemme et al., 2015, 2016; Esadze et al., 2014) (Figure 1C). As such, in studying many eukaryotic TRNs retroactivity must be taken into account (Kemme et al., 2016).

The goal of our study is to understand how retroactivity affects response acceleration and pulsing of IFFLs. In the simplest case where an input is coupled to a downstream promoter-binding region, it was demonstrated that retroactivity increases response times and dampens pulse amplitude (Del Vecchio et al., 2008). In the context of more complicated topologies, changing retroactivity can lead to more sophisticated, often undesired effects on circuit behaviors (Sepulchre and Ventura, 2013; Gyorgy and Del Vecchio, 2014; Wang and Belta, 2019). This raises the question whether retroactivity is simply an impediment to overcome in designing synthetic IFFL circuits. Another natural question is the potential role of retroactivity in motif evolution. As the levels of retroactivity differ sharply in prokaryotes and higher eukaryotes due to the number of accessible ND sites, could the behaviors of a network motif under different levels of retroactivity have affected its abundance, as one progresses from bacterial TRNs to eukaryotic ones? Note, we focus on IFFLs in particular because synthesizing functional IFFLs has proved to be experimentally feasible (Basu et al., 2004; Bleris et al., 2011), making our predictions experimentally testable in controlled synthetic systems.

A systematic modeling framework was developed to account for retroactivity in TRNs (Gyorgy and Del Vecchio, 2014). Using this framework, we study IFFL networks by simulating, comparing, and mathematically analyzing ODE models with varying levels of retroactivity. Similar to previous computational studies (Shi et al., 2017; Ma et al., 2009; Castillo-Hair et al., 2015), we performed time course simulations of IFFLs repeatedly with kinetic parameters representing different regions of parameter space. We quantified the response time, as well as the pulse amplitude, for each parameter set (see Figure 1B for the definitions of response time and pulse amplitude). Building from these simulations, we compared the dynamics of the corresponding ODE systems to understand how retroactivity affects the behavior of IFFLs. To demonstrate that our findings are parameter-independent, we carried out mathematical proofs where model parameters can take arbitrary positive values.

We find that increasing retroactivity can increase, decrease, or keep the response time and the pulse amplitude constant in an IFFL. This suggests that in contrast to the traditional perception of retroactivity as an impediment to circuit design (Del Vecchio et al., 2008), increasing retroactivity could actually be harnessed to improve the performance of IFFLs. Our results predict that the introduction of synthetic decoy binding sites into a synthetic IFFL system would affect its response time and pulse amplitude, and the magnitude of this effect would depend on kinetic parameters (e.g., Hill coefficients) and circuit topologies (e.g. I1-FFLs). Hence, retroactivity should be considered in connection with circuit parts to optimize the behavior of IFFL circuits. Our observations of IFFLs led us to examine a few other motifs capable of sign-sensitive response acceleration. Comparing the behavior of IFFLs to that of negative autoregulation, we found that increasing retroactivity in a negative autoregulated circuit can only decelerate the response. Interestingly, we observed that IFFLs are conserved in bacteria, mouse, and human networks, whereas negative autoregulatory loops are only present in significant numbers in bacteria. The functional versatility of IFFLs at increasing levels of retroactivity, thus, may have provided IFFLs a selective advantage over negative autoregulation in cases where decreasing or keeping the response time constant was beneficial.

RESULTS

Modeling Transcriptional Regulatory Networks

In this section, we describe our approach to modeling the effect of retroactivity on TRNs. A TRN can be mapped to a graph, where each node represents a gene/protein, each edge transcriptional regulation, and the direction of an edge the direction of the regulation, activation or inhibition. The time evolution of each node can be described by an ODE, where the time derivative represents the rate of change of the protein concentration contributed by protein production and first-order decay. Mathematically, the rates of changes of proteins in the network can be expressed as:

$$\frac{d\overrightarrow{x}}{dt} = h(\overrightarrow{x}), mtext{(Equation 1)}$$

where





$$h(\overrightarrow{x}) = \begin{pmatrix} \beta_{1} \cdot \left[(1 - \gamma_{1}) H_{1}(\overrightarrow{p_{1}}) + \gamma_{1} \right] - \delta_{1} x_{1} \\ \beta_{2} \cdot \left[(1 - \gamma_{2}) H_{2}(\overrightarrow{p_{2}}) + \gamma_{2} \right] - \delta_{2} x_{2} \\ \dots \\ \beta_{n} \cdot \left[(1 - \gamma_{n}) H_{n}(\overrightarrow{p_{n}}) + \gamma_{n} \right] - \delta_{n} x_{n} \end{pmatrix},$$
 (Equation 2)

where x_i denotes the concentration of the i-th protein, and δ_i , the decay rate. $\overrightarrow{p_i}$, the concentration of the parent(s) of the i-th protein, is a subset of \overrightarrow{x} . β_i represents the maximal production rate of the i-th protein, and γ_i , the basal fraction of the promoter that is active. H_i is the Hill function describing the transcriptional regulation of x_i by its parent(s). If the i-th protein species x_i has only one parent species p_i , then Hill function $H_i(p_i)$ can be expressed as:

$$H_{i}(p_{i}) = \begin{cases} \frac{1}{1 + \left(\frac{p_{i}}{K_{i}}\right)^{h_{i}}}, & \text{if species p}_{i} \text{ is an inhibitor} \\ \frac{\left(\frac{p_{i}}{K_{i}}\right)^{h_{i}}}{1 + \left(\frac{p_{i}}{K_{i}}\right)^{h_{i}}}, & \text{if species p}_{i} \text{ is an activator,} \end{cases}$$
 (Equation 3)

where $H_i(p_i)$ accounts for the fraction of the promoter that is active, K_i is the dissociation constant, and h_i is the Hill coefficient. Co-regulation by multiple TFs can be modeled by simple logic models. Unless otherwise specified, throughout this work we consider an AND logic, where the regulated gene is turned on only when all activators are abundant and all inhibitors are scarce (see Transparent Methods Section 1 for Hill functions describing co-regulation).

To account for retroactivity, we adopt a previously developed framework (Gyorgy and Del Vecchio, 2014). The major assumptions needed to apply this framework are that (1) there is a separation of time scales between protein production/degradation and reversible binding reactions between TFs and DNA and (2) the corresponding quasi-steady state is locally exponentially stable (Gyorgy and Del Vecchio, 2014). The first assumption is valid as protein turnover and binding reactions typically occur on different time scales (Milo et al., 2002). The second assumption is implicit in our use of the Hill-function-based models, and its validity is explained in a previous study (Gyorgy and Del Vecchio, 2014). Under these assumptions, the rates of changes of protein concentrations with retroactivity considered can be described as:

$$\frac{d\overrightarrow{x}}{dt} = [I + R(\overrightarrow{x})]^{-1}h(\overrightarrow{x}),$$
 (Equation 4)

where $R(\vec{x})$, known as the retroactivity matrix (Gyorgy and Del Vecchio, 2014), can be calculated as:

$$R(\overrightarrow{x}) = \begin{cases} \Sigma_{i|x_i \in \Phi} V_i^T R_i(\overrightarrow{p_i}) V_i & \text{if } \Phi \neq \varphi, \\ 0_{N \times N} & \text{if } \Phi = \varphi. \end{cases}$$
 (Equation 5)

Here V_i is a binary matrix, containing as many rows as the length of $\overrightarrow{p_i}$ and as many columns as the number of nodes in the network. The element in the j-th row and k-th column of V_i is 1 if the j-th parent of node i is node k and 0 otherwise. AND logic is a special case of independent binding, in which case $R_i(\overrightarrow{p_i})$ is a diagonal matrix (see Transparent Methods Section 2 for calculation of $R_i(\overrightarrow{p_i})$). This in turn implies that $V_i^T R_i(\overrightarrow{p_i}) V_i$ is also a diagonal matrix (Transparent Methods Section 3). Hence, $R(\overrightarrow{x})$ is also diagonal. More details about retroactivity, including its derivation, can be found in a previous study (Gyorgy and Del Vecchio, 2014). Models of IFFL networks with and without retroactivity are given in Transparent Methods Section 4.

Simulation of IFFLs

In this section, we describe the specific IFFL models in which we study the effect of retroactivity and outline our simulation protocol. IFFLs are known to be sign-sensitive response accelerators and pulse generators: they accelerate or delay responses to stimulus steps only in one direction (Alon, 2007; Mangan and Alon, 2003). Considering sign-sensitivity of IFFLs, we separated the four IFFL motifs into two groups: one group (i.e., I1-FFL and I4-FFL) capable of response acceleration and pulse generation in response to an ON step (i.e., inducer level x_i changes from 0 to ∞) and the other (i.e., I2-FFL and I3-FFL) capable of response acceleration and pulse generation in response to an OFF step (i.e.,



inducer level x_l changes from ∞ to 0). Here we focused on I1-FFLs and I4-FFLs, as similar analysis could be performed for I2-FFLs and I3-FFLs. We constructed non-dimensionalized ODE models for I1-FFLs and I4-FFLs (details of non-dimensionalization and non-dimensionalized models can be found in Transparent Methods Sections 5 and 6) and simulated each model using the DifferentialEquations.jl package version 5.3.1 in Julia version 1.1.0 (Rackauckas and Nie, 2017; Bezanson et al., 2017). We connected genes A, B, and/or C of the IFFL to additional downstream binding sites denoted by D_X (X = A, B, or C). The degree of retroactivity arising from additional downstream binding sites was allowed to vary, with the retroactivity coefficient $\tilde{\eta}_{AD_A}$ ($\tilde{\eta}_{BD_B}$, $\tilde{\eta}_{CD_C}$) set to 0, 1.0, 10.0, and 100.0 (see Transparent Methods Section 5 for definition of $\tilde{\eta}_{XD_X}$ (X = A, B, or C)). By contrast, we assumed that genes A, B, and C themselves are single-copy genes, and hence, retroactivity that arises from binding of A, B, or C to the functional target site(s) (e.g., promoter that controls the expression of B and C) is negligible. Note, a model without retroactivity is equivalent to a model where $\tilde{\eta}_{XD_X}$ equals zero.

As an example, the non-dimensionalized model of an I1-FFL (Figure 1A) without retroactivity is given here:

$$\frac{d\tilde{x}_{A}}{d\tau} = f_{\tilde{A}} = (1 - \gamma_{A}) \frac{\left(\frac{x_{I}}{K_{IA}}\right)^{h_{IA}}}{1 + \left(\frac{x_{I}}{K_{IA}}\right)^{h_{IA}}} + \gamma_{A} - \tilde{x}_{A}$$

$$\frac{d\tilde{x}_{B}}{d\tau} = f_{\tilde{B}} = (1 - \gamma_{B}) \frac{\left(\frac{\tilde{x}_{A}}{\tilde{K}_{AB}}\right)^{h_{AB}}}{1 + \left(\frac{\tilde{x}_{A}}{\tilde{K}_{AB}}\right)^{h_{AB}}} + \gamma_{B} - \tilde{x}_{B}$$
(Equation 6)
$$\frac{d\tilde{x}_{C}}{d\tau} = f_{\tilde{C}} = (1 - \gamma_{C}) \frac{\left(\frac{\tilde{x}_{A}}{\tilde{K}_{AC}}\right)^{h_{AC}}}{\left(1 + \left(\frac{\tilde{x}_{A}}{\tilde{K}_{AC}}\right)^{h_{AC}}\right)\left(1 + \left(\frac{\tilde{x}_{B}}{\tilde{K}_{BC}}\right)^{h_{BC}}\right)} + \gamma_{C} - \tilde{x}_{C}.$$

With retroactivity applied on all three nodes, the non-dimensionalized model of an I1-FFL becomes:

$$\begin{bmatrix} \frac{d\tilde{x}_{A}}{d\tau} \\ \frac{d\tilde{x}_{B}}{d\tau} \\ \frac{d\tilde{x}_{C}}{d\tau} \end{bmatrix} = \begin{bmatrix} \frac{1}{a} & 0 & 0 \\ 0 & \frac{1}{b} & 0 \\ 0 & 0 & \frac{1}{c} \end{bmatrix} \begin{bmatrix} f_{\tilde{A}} \\ f_{\tilde{B}} \\ f_{\tilde{C}} \end{bmatrix} = \begin{bmatrix} \frac{1}{r_{AD_{A}} + 1} & 0 & 0 \\ 0 & \frac{1}{r_{BD_{B}} + 1} & 0 \\ 0 & 0 & \frac{1}{r_{CD_{C}} + 1} \end{bmatrix} \begin{bmatrix} f_{\tilde{A}} \\ f_{\tilde{B}} \\ f_{\tilde{C}} \end{bmatrix},$$
 (Equation 7)

where

$$r_{AD_{A}} = \tilde{\eta}_{AD_{A}} h_{AD_{A}}^{2} \left(\frac{\tilde{X}_{A}}{\tilde{K}_{AD_{A}}}\right)^{h_{AD_{A}}-1} \left(1 + \left(\frac{\tilde{X}_{A}}{\tilde{K}_{AD_{A}}}\right)^{h_{AD_{A}}}\right)^{-2}$$

$$r_{BD_{B}} = \tilde{\eta}_{BD_{B}} h_{BD_{B}}^{2} \left(\frac{\tilde{X}_{B}}{\tilde{K}_{BD_{B}}}\right)^{h_{BD_{B}}-1} \left(1 + \left(\frac{\tilde{X}_{B}}{\tilde{K}_{BD_{B}}}\right)^{h_{BD_{B}}}\right)^{-2}$$

$$r_{CD_{C}} = \tilde{\eta}_{CD_{C}} h_{CD_{C}}^{2} \left(\frac{\tilde{X}_{C}}{\tilde{K}_{CD_{C}}}\right)^{h_{CD_{C}}-1} \left(1 + \left(\frac{\tilde{X}_{C}}{\tilde{K}_{CD_{C}}}\right)^{h_{CD_{C}}}\right)^{-2}.$$
(Equation 8)

In Equations (6) and (7), \tilde{x}_A , \tilde{x}_B , and \tilde{x}_C are the nondimensionalized concentrations of proteins A, B, and C, whereas τ is the nondimensionalized time. $f_{\tilde{A}}$, $f_{\tilde{B}}$, and $f_{\tilde{C}}$ are the sums of regulated protein production and protein decay (Transparent Methods Section 6). a, b, and c, defined as the reduction factors of $\frac{d\tilde{x}_A}{d\tau}$, $\frac{d\tilde{x}_B}{d\tau}$ and $\frac{d\tilde{x}_C}{d\tau}$ due to retroactivity, are equal to 1 if retroactivity is not considered. Note that for I4-FFLs, the only changes in Equations (6) and (7) are in the definitions of $f_{\tilde{A}}$, $f_{\tilde{B}}$, and $f_{\tilde{C}}$ due to the different regulatory interactions, i.e., r_{AD_A} , r_{BD_B} , and r_{CD_C} are still given by the same Equation (8). Note also that retroactivity does not affect steady-state values of \tilde{x}_A , \tilde{x}_B , and \tilde{x}_C .





In terms of model simulation, we selected parameters based on values chosen in an earlier study (Mangan and Alon, 2003), exploring several orders of magnitude of parameter space. Specifically we considered Hill coefficients h_i less than, equal to, and larger than 1 (Equation 3). If h_i is non-integer, then the underlying reaction between the promoter and the TF is likely the resultant of several mechanisms, such as chain reactions (Boekel, 2009). In this scenario, h_i , which is also the reaction order, can be considered an approximation of the detailed mechanisms (Boekel, 2009). An h_i larger than, equal to, and less than 1 stands for positive, zero, and negative cooperativity, respectively. Details of the parameters can be found in Transparent Methods Section 5.

In the absence of regulatory interactions, we assumed that only the expression of gene A is modulated by an external inducer, whereas genes B and C are constitutively expressed. We initialize our models at a steady state corresponding to a fixed inducer concentration, and subsequently induce changes in concentrations of proteins A, B, and C via a sudden increase in the inducer's concentration. In the case of an ON (OFF) step, the inducer level x_1 changes from 0 (∞) to ∞ (0). By integrating the ODEs until solutions reached a new steady state, we obtained one trajectory of proteins A, B, and C for each set of kinetic parameters we sampled.

Retroactivity Changes Behaviors of IFFLs

We begin by studying how varying levels of retroactivity on just one gene of an IFFL can alter its behaviors. That is, we allowed retroactivity on one and only one gene of the IFFL to vary, keeping retroactivity on the rest of the genes equal to zero. The response time of gene C was then calculated for each parameter set at each different level of retroactivity. Our results show that changing retroactivity on each node has different effects on response times, as each node of the IFFL serves a different function (Tables S1-S8). Increasing $ilde{\eta}_{CDc}$ expectedly slows the response time of gene C (Table S1), whereas we observed that the response time of gene C decreases as $\tilde{\eta}_{BD_n}$ increases, most notably for $h_{BD_n} \le 1$ (Figure 2A; see Table S2 for data). To generalize our observation, we proved that increasing $\tilde{\eta}_{BD_B}$ shortens the response time of gene C regardless of the values of any other parameters for I1-FFLs (see Transparent Methods Section 7 for the mathematical proof). Serving as the regulatory node in the network, gene B controls the time gap between the opposing forces of regulation exerted on gene C. In response to an ON step, the expression level of protein B monotonically increases. Increasing the level of retroactivity $\tilde{\eta}_{BD_B}$ in turn slows the approach of B to steady state. Consequently, it takes protein B a longer time to effectively repress gene C, allowing protein C to reach the half point over a shorter period of time (Figure 2A). Thus, we find that increasing $\tilde{\eta}_{BD_0}$ shortens the response time of gene C. As Table S2 indicates, the magnitude by which the response time shortens depends on h_{BD_n} as well as the IFFL topology. A detailed discussion of the underlying association will be provided later.

When the repressor (activator) B has a strong inhibitory (activating) effect on the production of the target protein, the dynamics of C exhibit a pulse-like shape (Alon, 2007). In addition to response times, we examined how retroactivity affects pulse amplitude, when for a given set of parameters the IFFL generates a pulse. Increasing $\tilde{\eta}_{CD_C}$ expectedly slows down the response of gene C, resulting in a lower pulse amplitude for all parameters (Table S3). In contrast, we observed and subsequently proved that increasing $\tilde{\eta}_{BD_B}$ always increases the pulse amplitude (Figure S1; see Table S4 for data and Transparent Methods Section 7 for the proof). The underlying mechanism can again be traced back to the delayed response of $\tilde{\chi}_B$ due to increased $\tilde{\eta}_{BD_B}$. While a decreased initial rate of growth of B shortens the response time of gene C, it also causes protein B to take a longer time to effectively repress gene C, allowing protein C to develop a larger response over time (Figure S1). In Transparent Methods Section 8, we extend our analysis by exploring the behavior of an IFFL when it is embedded in a larger network and node B serves as an input to other circuits (Figure S2), investigating the effect of intermodular retroactivity on IFFL behaviors. Similar to before, we find that increasing intermodular retroactivity on node B decreases the response time and increases the pulse amplitude of node C.

As the input node of the IFFL, gene A regulates gene C in opposing directions. Our simulations show that changing $\tilde{\eta}_{AD_A}$ affects the response time and pulse amplitude of gene C in a more complicated manner than changing $\tilde{\eta}_{BD_B}$ and $\tilde{\eta}_{CD_C}$. While increasing $\tilde{\eta}_{AD_A}$ slows down the direct activation of gene C, it counteracts this delay by decelerating the activation of gene B, thus attenuating the inhibition of C by B and allowing C a longer time to develop a response. To demonstrate the counteracting effects, we compared the response time of an IFFL with that of a two-input circuit under different levels of $\tilde{\eta}_{AD_A}$. In a two-input circuit,



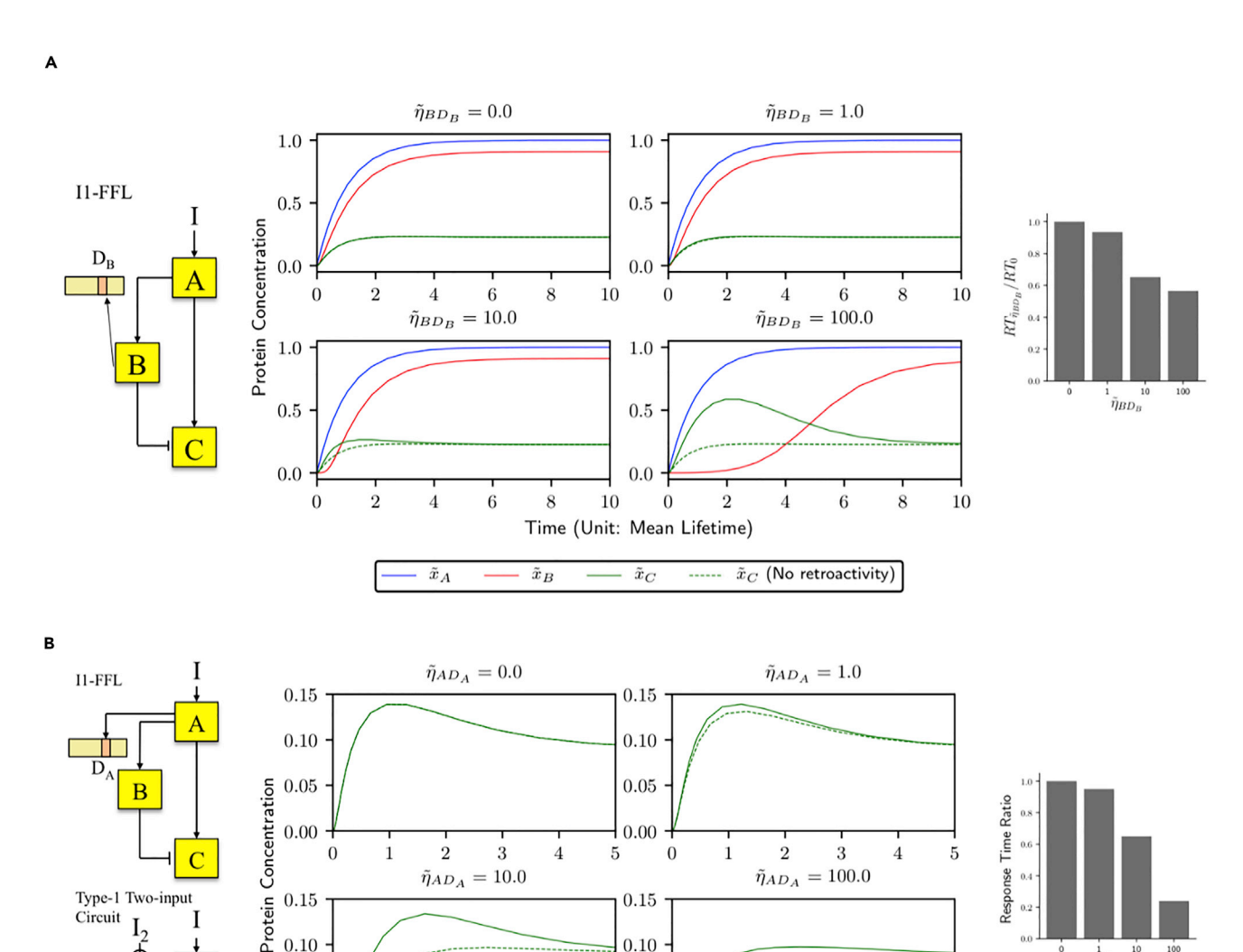


Figure 2. $\tilde{\eta}_{BD_8}$ and $\tilde{\eta}_{AD_A}$ Affect the Response Time of I1-FFLs (A) Shortened response time due to increasing $\tilde{\eta}_{BD_8}$ in an I1-FFL. $\tilde{\eta}_{BD_8}$ increases in the order of top left, top right, bottom left, and bottom right. Values of the other parameters are: $\tilde{K}_{AB} = \tilde{K}_{AC} = \tilde{K}_{BC} = \tilde{K}_{BC} = 0.1$, $h_{AB} = h_{AC} = 1.0$, $h_{BC} = h_{BD_R} = 0.5$. For comparison, the green dashed curve represents the trajectory of \tilde{x}_C when $\tilde{\eta}_{BD_R}$ equals 0. The bar plot shows the response time for different $\tilde{\eta}_{BD_R}$ compared with the response time without retroactivity. (B) Shorter response time in an I1-FFL than in a type-1 two-input circuit at different levels of $\tilde{\eta}_{AD_A}$. Values of the parameters are: $\tilde{K}_{AB} = \tilde{K}_{AC} = \tilde{K}_{AD_A} = \tilde{K}$ $\tilde{K}_{BC} = 0.1$, $h_{AB} = h_{A_2B} = h_{AC} = h_{AD_A} = h_{BC} = 1.0$. The bar plot shows the ratio of the response time in an I1-FFL to the response time in a type-1 two-input circuit.

0.10

0.05

0.00 5

Time (Unit: Mean Lifetime)

 $ilde{x}_C$ (Type-1 Two-input Circuit)

gene C is simultaneously activated by gene A, which is induced by inducer I, and inhibited by gene A2, which is induced by a separate inducer I₂ (Figure 2B). To facilitate a meaningful comparison between an IFFL and a two-input circuit, we assumed that genes A and A_2 have the same production rates upon induction, but only allowed retroactivity of gene A (not A2) to vary (see Transparent Methods Section 9 for the model). We find that because of the counteracting effects, increasing $\tilde{\eta}_{AD_A}$ leads to a smaller increase in response time and a smaller decrease in pulse amplitude in an IFFL than in a two-input circuit where gene A regulates C with no feedforward mechanism (see Tables S5-S8 for data).

 $ilde{x}_C$ (I1-FFL)

0.10

0.05

0.00

В

12

15

 $\tilde{\eta}_{AD_A}$ 10



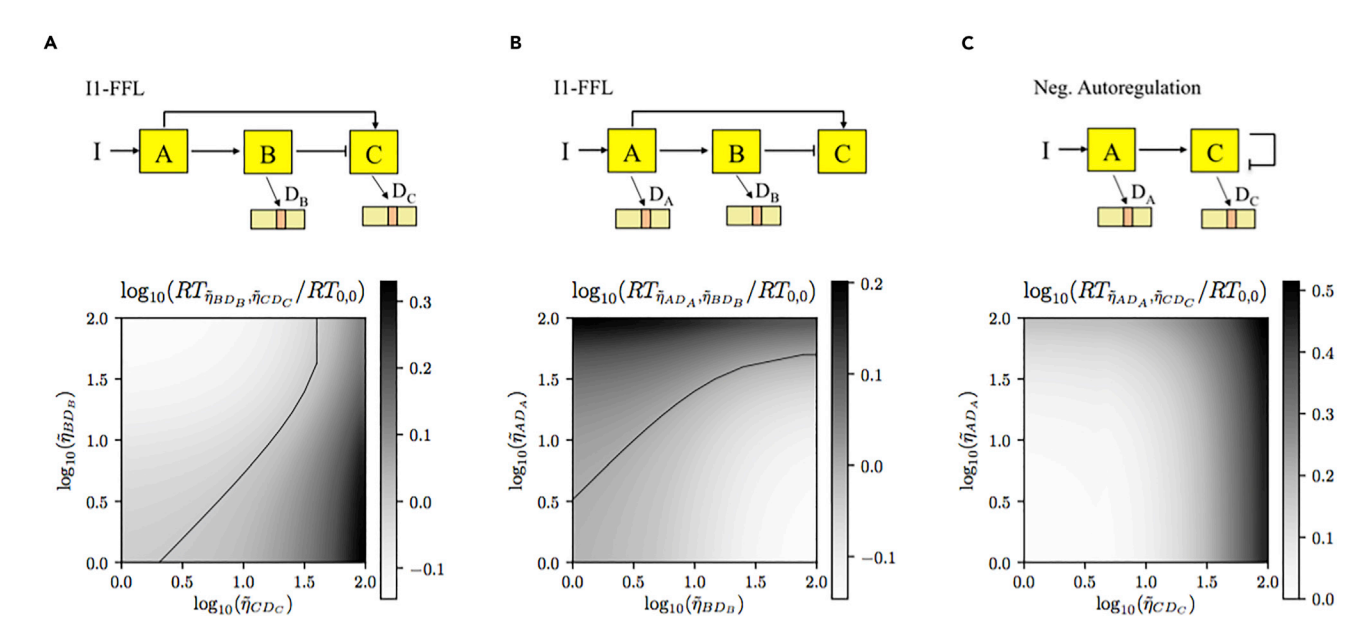


Figure 3. Joint Changes of $\tilde{\eta}_{AD_A}$, $\tilde{\eta}_{BD_B}$, and/or $\tilde{\eta}_{CD_C}$ in I1-FFLs and Negative Autoregulated Circuits

(A) Response times of the I1-FFL model at different levels of $\tilde{\eta}_{BD_B}$ and $\tilde{\eta}_{CD_C}$ compared with that of the model with no retroactivity.

(B) Response times of the I1-FFL model at different levels of $\tilde{\eta}_{AD_A}$ and $\tilde{\eta}_{BD_B}$ compared with that of the model with no retroactivity.

(C) Response times of the negative autoregulated circuit model at different levels of $\tilde{\eta}_{AD_A}$ and $\tilde{\eta}_{CD_C}$ compared with that of the model with no retroactivity. Values of parameters used for making the plots are: in (A), $\tilde{K}_{AB} = \tilde{K}_{AC} = \tilde{K}_{CD_C} = 0.01$, $\tilde{K}_{BC} = \tilde{K}_{BD_B} = 0.1$, $h_{AB} = h_{AC} = h_{BC} = h_{BD_B} = h_{CD_C} = 0.5$; in (B), $\tilde{K}_{AB} = \tilde{K}_{AC} = \tilde{K}_{AD_A} = 0.01$, $\tilde{K}_{BC} = \tilde{K}_{BD_B} = 0.1$, $h_{AB} = h_{AC} = h_{AD_A} = h_{BC} = h_{BD_B} = 0.5$; in (C), $\tilde{K}_{AD_A} = \tilde{K}_{AC} = \tilde{K}_{CD_C} = 0.01$, $h_{AD_A} = h_{AC} = h_{CC} = h_{CD_C} = 0.5$. We chose $\tilde{\eta}_{XD_X}(X = A,B,C)$ to be the midpoints of the 50 subintervals that we split the interval [log₁₀(1.0),log₁₀(100.0)] evenly into. The magnitude of the ratio is shown by the color. For values of $\tilde{\eta}_{XD_X}(X = A,B,C)$ that were not chosen for simulation, the ratio was interpolated. The black curve, which we refer to as the "iso-response-time" curve, represents values of $\tilde{\eta}_{XD_X}(X = A,B,C)$ at which the response time is the same as the response time of the model with no retroactivity. Note that in (C) there is no "iso-response-time" curve because $\log_{10}(RT\tilde{\eta}_{AD_A},\tilde{\eta}_{CD_C}/RT\tilde{\eta}_{0,0})$ is always larger than 1.

Joint Increases of Retroactivity Can Keep Response Time Constant

Next, we investigated how joint increases of retroactivity on multiple nodes affect response times by letting $\tilde{\eta}_{BD_B}$ and $\tilde{\eta}_{CD_C}$ ($\tilde{\eta}_{AD_A}$) vary simultaneously. The I1-FFL model was simulated for different values of $\tilde{\eta}_{BD_B}$ and $\tilde{\eta}_{CD_C}$ ($\tilde{\eta}_{AD_A}$) within the interval of 1.0 and 100.0. The ratio of the response time under each combination of $\tilde{\eta}_{BD_B}$ and $\tilde{\eta}_{CD_C}$ ($\tilde{\eta}_{AD_A}$) to the response time without retroactivity was then calculated (Figures 3A and 3B). We find that in an I1-FFL, if $\tilde{\eta}_{BD_B}$ and $\tilde{\eta}_{CD_C}$ ($\tilde{\eta}_{AD_A}$) increase simultaneously, response time can be increased, decreased, or kept constant depending on the values of $\tilde{\eta}_{BD_B}$ and $\tilde{\eta}_{CD_C}$ ($\tilde{\eta}_{AD_A}$). This is because increasing $\tilde{\eta}_{BD_B}$ and $\tilde{\eta}_{CD_C}$ ($\tilde{\eta}_{AD_A}$) affects response time in opposing directions, and the resulting counteracting effects can be canceled when the values of $\tilde{\eta}_{BD_B}$ and $\tilde{\eta}_{CD_C}$ ($\tilde{\eta}_{AD_A}$) satisfy a certain relationship (the solid black curves in Figures 3A and 3B, which we call the "isoresponse-time" curves).

Moreover, we compared the behavior of an IFFL under increasing levels of retroactivity to that of negative autoregulation (Figure 3C), another motif known for sign-sensitive response acceleration (Rosenfeld et al., 2002). We found that in contrast to IFFLs, increasing $\tilde{\eta}_{AD_A}$ and/or $\tilde{\eta}_{CD_C}$ in a negative autoregulatory circuit can only slow down the response regardless of the values of any other parameters, as the response time of the model with retroactivity is always larger than that of the model without retroactivity (Figure 3C; see Transparent Methods Section 10 for the proof).

Besides IFFLs and negative autoregulation, our simulations suggest that two-node negative feedback loops (NFBLs) can also act as sign-sensitive response accelerators (Figure S3; see Transparent Methods Section 11 for the model). Moreover, we find that if $\tilde{\eta}_{BD_B}$ and $\tilde{\eta}_{AD_A}$ increase simultaneously, then response times of gene A can be increased, decreased, or kept constant depending on the values of $\tilde{\eta}_{BD_B}$ and $\tilde{\eta}_{AD_A}$ (Figure S3).



Effects of Retroactivity Depend on the Motif

We now examine how varying regulatory logic, e.g., I1- versus I4-FFLs and "OR" logic, can lead to different responses in the presence of retroactivity. As is demonstrated earlier, increasing retroactivity $\tilde{\eta}_{BD_B}$ accelerates the response and increases the pulse amplitude of gene C. Our simulations also suggest that how much retroactivity affects response time and pulse amplitude depends on the actual type of the IFFL. In response to an ON step, increasing $\tilde{\eta}_{BD_B}$ accelerates the response times in an I1-FFL but not in an I4-FFL for $h_{BD_B} \leq 1$, and increases the pulse amplitude more strongly in an I1-FFL than in an I4-FFL (Figures 4A and 4B; see Tables S2 and S4).

The different effects of retroactivity on response time and pulse amplitude in different IFFLs is likely an outcome of how much $d\tilde{x}_B/d\tau$ decreases in different phases of the response. To explain this argument, we take the derivative of the reduction factor b (Equation 7) with respect to \tilde{x}_B :

$$\frac{db(\tilde{x}_B)}{d\tilde{x}_B} = \frac{\tilde{\eta}_{BD_B}h_{BD_B}^2 - 1}{\tilde{K}_{BD_B}^{h_{BD_B} - 1}} \cdot \tilde{x}_B^{h_{BD_B} - 2} \left(1 + \left(\frac{\tilde{x}_B}{\tilde{K}_{BD_B}}\right)^{h_{BD_B}}\right)^{-2} \cdot \left[\left(h_{BD_B} - 1\right) - 2h_{BD_B} \cdot \frac{\tilde{x}_B^{h_{BD_B}}}{\tilde{K}_{BD_B}^{h_{BD_B}} + \tilde{x}_B^{h_{BD_B}}}\right]. \quad \text{(Equation 9)}$$

If h_{BD_B} is a value between 0 and 1, then $db(\tilde{x}_B)/d\tilde{x}_B$ is always negative, indicating that $b(\tilde{x}_B)$ is monotonically decreasing in the interval of (0,1]. In an I1-FFL, \tilde{x}_B transitions from a low pre-stimulus steady state to a high post-stimulus steady state in response to an ON step. Based on monotonicity of $b(\tilde{x}_B)$, we know that the reduction factor is the largest when \tilde{x}_B is close to 0, which significantly lowers the initial value of $|d\tilde{x}_B/d\tau|$ relative to the no retroactivity case (Figure 4C). Consequently, \tilde{x}_B increases more slowly, and hence $d\tilde{x}_C/d\tau$ is significantly increased during the initial response phase. This results in a shortened response time and increased pulse amplitude. On the other hand, in an I4-FFL, \tilde{x}_B transitions from a high pre-stimulus steady state to a low post-stimulus steady state in response to an ON step (Figure 4C). Due to monotonicity of $b(\tilde{x}_B)$, the reduction factor is smallest when \tilde{x}_B is close to 1. This means that initially $d\tilde{x}_C/d\tau$ is minimally affected in an I4-FFL, so the effects of $\tilde{\eta}_{BD_B}$ on response time and pulse amplitude are not as strong in an I4-FFL as in an I1-FFL.

If h_{BD_B} is larger than 1, then $b(\tilde{x}_B)$ reaches its maximum for some value of \tilde{x}_B between 0 and 1. Moreover, $b(\tilde{x}_B)$ monotonically increases (decreases) to the left (right) of arg $\max_{\tilde{x}_b} b(\tilde{x}_B)$. Setting $db(\tilde{x}_B)/d\tilde{x}_B$ equal to zero, we can obtain the following expression for arg $\max_{\tilde{x}_b} b(\tilde{x}_B)$:

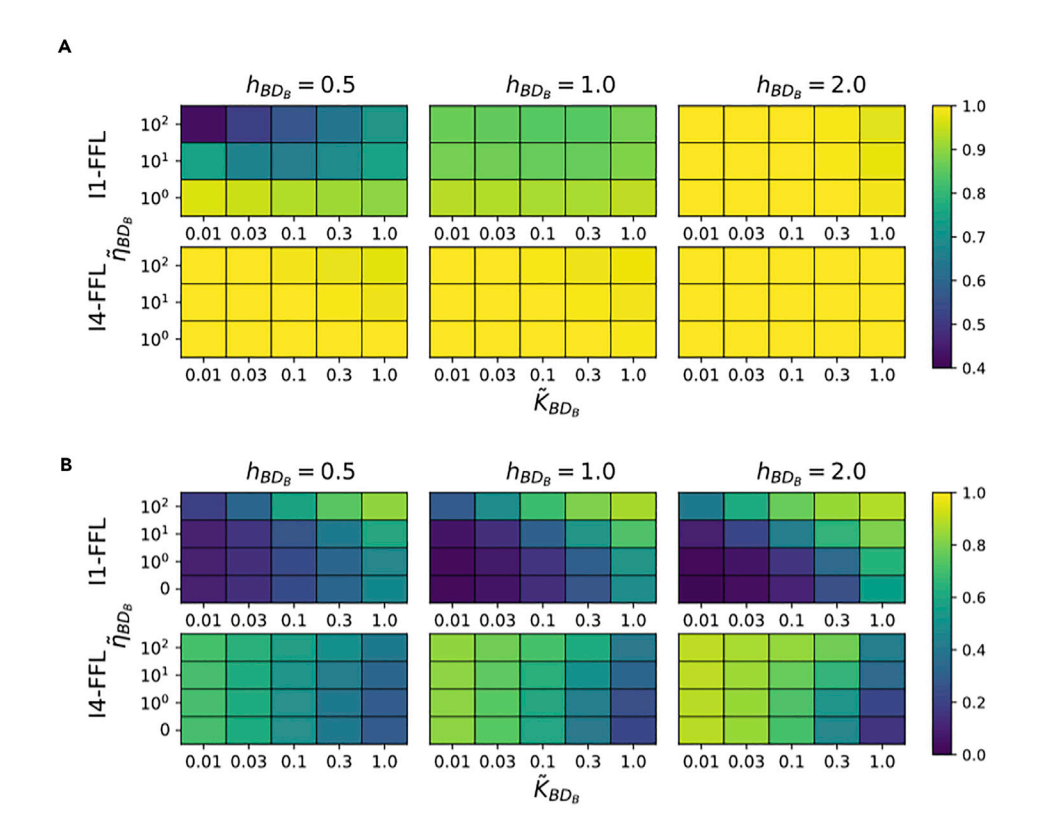
$$\arg\max_{\tilde{X}_B} b(\tilde{x}_B) = \left(\frac{h_{BD_B} - 1}{h_{BD_B} + 1}\right)^{\frac{1}{h_{BD_B}}} \cdot \tilde{K}_{BD_B}.$$
 (Equation 10)

The qualitative behavior of the IFFL for $h_{BD_B} > 1$ is similar to the $h_{BD_B} = 2$ case. When h_{BD_B} equals 2, $\tilde{\eta}_{BD_B}$ minimally affects response times in either I1-FFLs or I4-FFLs (Figure 4A). This is likely because for h_{BD_B} equal to 2, $b(\tilde{x}_B)$ reaches its maximum when \tilde{x}_B reaches approximately 50% of \tilde{K}_{BD_B} , which happens much later than when \tilde{x}_C reaches its half response point even in I1-FFLs (Table S9). As a result, retroactivity $\tilde{\eta}_{BD_B}$ barely affects the response time when h_{BD_B} equals 2.

On the other hand, an I1-FFL generally experiences a more significant change in pulse amplitude than an I4-FFL as $\tilde{\eta}_{BD_B}$ increases (Figure 4B). To generate a pulse, $\tilde{\chi}_B$ often needs to get larger (smaller) than \tilde{K}_{BC} so that it can effectively inhibit C in an I1-FFL (I4-FFL) (Table S10), which happens after $b(\tilde{\chi}_B)$ reaches its maximum. In response to an ON step, $\tilde{\chi}_B$ transitions from a low state to a high state in an I1-FFL, so according to Equation (9), the reduction factor is the largest in the initial response phase before $\tilde{\chi}_B$ becomes large relative to \tilde{K}_{BC} , greatly lowering the initial value of $|d\tilde{\chi}_B/d\tau|$ (Figure S4). In contrast, in an I4-FFL, because $\tilde{\chi}_B$ transitions from a high state to a low state, the reduction factor is the largest when $\tilde{\chi}_B$ becomes small relative to \tilde{K}_{BC} somewhere in the return phase (Equation 9) (Figure S4). As a result, $\tilde{\eta}_{BD_B}$ affects pulse amplitude more strongly in an I1-FFL than in an I4-FFL for h_{BD_B} larger than 1, similar to the $h_{BD_B} \leq 1$ case.

Under the assumption of OR logic, 11-FFLs and I4-FFLs become sign-sensitive response accelerators in response to an OFF step (inducer level x_l changes from ∞ to 0). OR logic is another special case of independent binding, where either the presence of an activator or the absence of an inhibitor is sufficient to turn on the expression of the regulated gene (see Transparent Methods Section 12 for model details). Although response time is more sensitive to changes in $\tilde{\eta}_{BD_B}$ in an I1-FFL than in an I4-FFL under the assumption of AND logic, the reverse becomes true under the assumption of OR logic: in response to an OFF step,





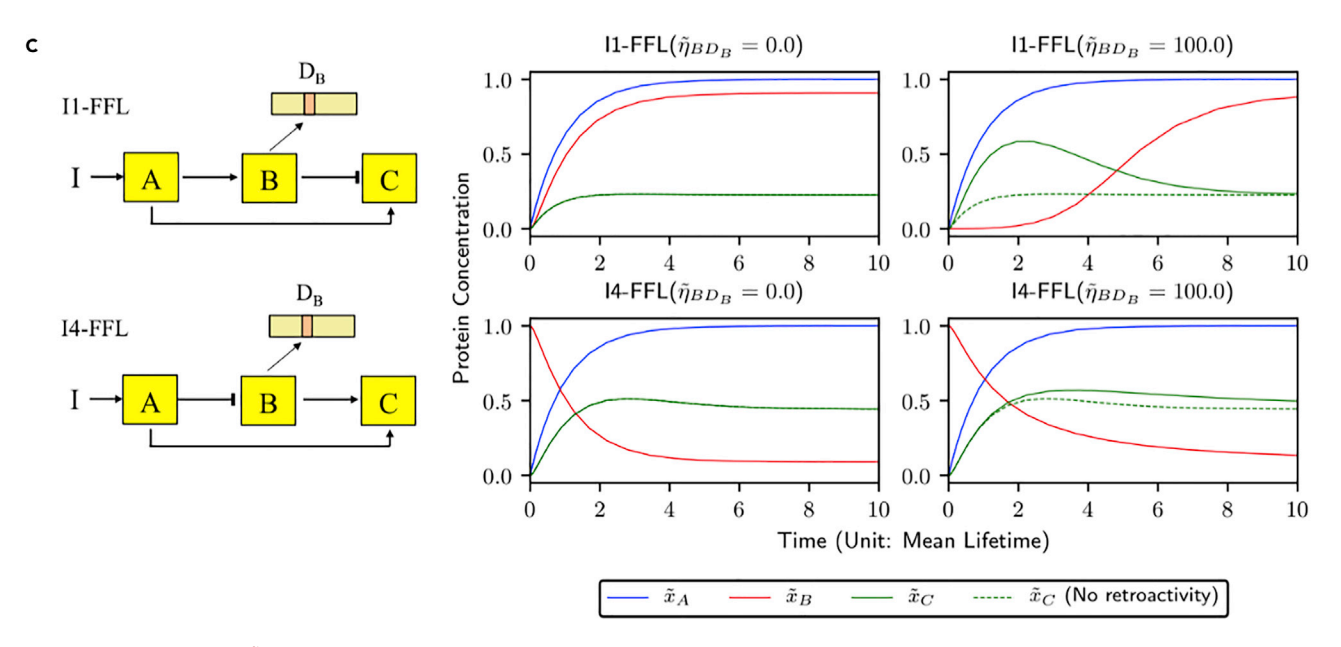


Figure 4. Effects of $\tilde{\eta}_{BD_8}$, \tilde{K}_{BD_8} , and h_{BD_8} on the Response Times of I1-FFLs and I4-FFLs

(A) Relative response time of I1-FFL and I4-FFL models with different values of \tilde{K}_{BD_B} . Here, relative response time is defined as the ratio of the response time of the model to the response time of the model without retroactivity. Values of the parameters are: $\tilde{K}_{AB} = \tilde{K}_{AC} = 0.1$, $h_{AB} = h_{AC} = 1.0$.

(B) Pulse amplitude of I1-FFL and I4-FFL models with different values of \tilde{K}_{BD_B} . Values of the parameters are the same as in (A). Note that pulse amplitudes of I1-FFLs and I4-FFLs should not be compared column-wise, as I1-FFLs generate larger pulses with larger \tilde{K}_{BD_B} , whereas I4-FFLs generate larger pulses with smaller \tilde{K}_{BD_B} .

(C) The effect of retroactivity $\tilde{\eta}_{BD_8}$ on response times is more pronounced in an I1-FFL (top row) than in an I4-FFL (bottom row) for $h_{BD_8} \leq 1$. For comparison, the green dashed curves represent the trajectories of $\tilde{\chi}_C$ when $\tilde{\eta}_{BD_8}$ equals 0. Values of the parameters are: $\tilde{K}_{AB} = \tilde{K}_{AC} = \tilde{K}_{BC} = \tilde{K}_{BD_8} = 0.1$, $h_{AB} = h_{AC} = 1.0$, $h_{BC} = h_{BD_8} = 0.5$.



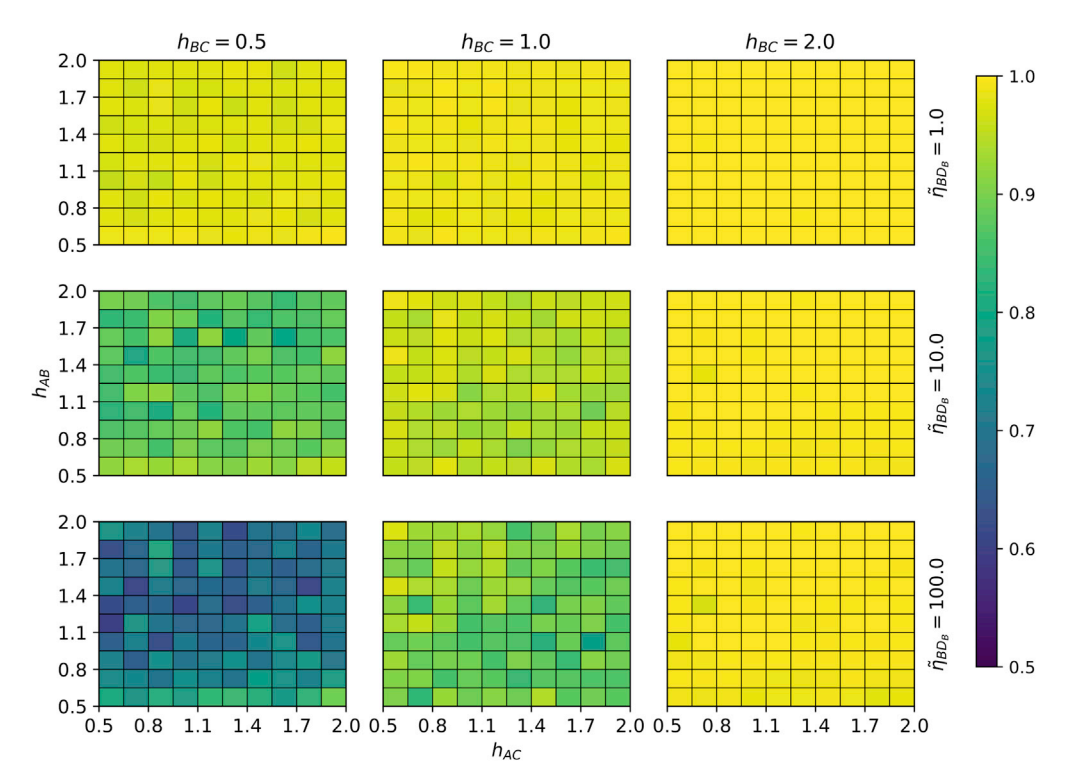


Figure 5. Response Acceleration Can Occur Over a Wide Set of Parameters When Node B Regulates Node C through Negative or Neutral Cooperativity

Median relative response time of I1-FFLs as model parameters are systematically varied, with random sampling of h_{BD_B} and \tilde{K}_{BD_B} within the intervals $0.8h_{BC} \le h_{BD_B} \le 1.2h_{BC}$ and $0.8\tilde{K}_{BC} \le \tilde{K}_{BD_B} \le 1.2\tilde{K}_{BC}$. The trajectories are separated evenly by h_{AB} and h_{AC} into 100 voxels, the color of which represents the median relative response time of the 100 simulated trajectories within that bin, where for each trajectory the remaining parameters were chosen via random Latin Hypercube Sampling. Here, relative response time is defined as the ratio of the response time of the model to the response time of the model without retroactivity.

See Transparent Methods Section 13 for details of parameter sampling.

increasing $\tilde{\eta}_{BD_B}$ decreases the response time more strongly in an I4-FFL than in an I1-FFL (Figure S5). This is because in response to an OFF step, $\tilde{\chi}_B$ transitions from a high pre-stimulus steady state to a low post-stimulus steady state in an I1-FFL whereas $\tilde{\chi}_B$ transitions from a low pre-stimulus steady state to a high post-stimulus steady state in an I4-FFL (Figure S5; see Transparent Methods Section 12 for the model and Table S11 for the data).

Effects of Retroactivity Are Independent of Parameter Isometry

To demonstrate the robustness of our findings, we performed extensive simulations on an I1-FFL model, where Hill coefficients, binding affinity, and decay rates were all allowed to vary. Similar to our earlier simulations, we set $\tilde{\eta}_{BD_B}$ equal to 0, 1.0, 10.0, and 100.0, and h_{BC} equal to 0.5, 1.0, and 2.0, to represent different levels of retroactivity and cooperativity. The rest of the parameters were sampled from their corresponding ranges via Latin Hypercube Sampling (details of parameter sampling can be found in Transparent Methods Section 13). The assumption of isometry, where TFs bind to the functional target site and non-functional decoy sites with equal affinity and cooperativity (i.e., $h_{BC} = h_{BD_B}$ and $\tilde{K}_{BC} = \tilde{K}_{BD_B}$) was also relaxed. Instead, we assume that h_{BC} (h_{BD_B}) and \tilde{K}_{BC} (\tilde{K}_{BD_B}) may be unequal but correlated, as the target sites and decoy sites we considered here have the same binding motifs. To preserve correlation, we sampled h_{BD_B} and \tilde{K}_{BD_B} from the intervals $(1-c)h_{BC} \leq h_{BD_B} \leq (1+c)h_{BC}$ and $(1-c)\tilde{K}_{BC} \leq \tilde{K}_{BD_B} \leq (1+c)h_{BC}$ and $(1-c)\tilde{K}_{BC} \leq \tilde{K}_{BD_B} \leq (1+c)h_{BC}$ where flexibility coefficient c equals 0, 0.2, or 0.5. The process of ODE simulation was repeated for 10,000 sets of parameters.

After the simulation was completed, we separated the trajectories by h_{AB} and h_{AC} evenly into 10 \times 10 voxels. Within each voxel, we calculated the median relative response time (Figure 5) as well as the percent of





trajectories achieving relative response time less than 90% of the model in the absence of retroactivity (i.e., 10% response acceleration) (Figure S6). The results suggest that parameter isometry, which we had assumed earlier (e.g., $h_{AB} = h_{AC}$, $\tilde{K}_{AB} = \tilde{K}_{AC}$, $h_{BC} = h_{BD_B}$, $\tilde{K}_{BC} = \tilde{K}_{BD_B}$, $\delta_A = \delta_B = \delta_C$), is not essential to our conclusions. Moreover, the model exhibits significant response acceleration in a large region of parameter space (Figure 5 and Figure S6), including regions where $h_{AB} > 1$ and/or $h_{AC} > 1$. Simulation results assuming flexibility coefficient c equal to 0 and 0.5 exhibit similar patterns (Figures S7–S10) and further corroborate the mathematical proof in Transparent Methods Section 7.

DISCUSSION

In this work, we studied how retroactivity affects the behavior of IFFLs via simulation and mathematical analysis. Our findings can be summarized as follows. First, in IFFLs, increasing retroactivity of the input node A, $\tilde{\eta}_{AD_A}$, induces counteracting effects on response time and pulse amplitude, slowing both the direct activation and the indirect inhibition of node C. Second, increasing retroactivity of the regulatory node B, $\tilde{\eta}_{BD_B}$, can shorten response times and increase pulse amplitudes, particularly in an I1-FFL with AND logic and an I4-FFL with OR logic. As a result, compared with negative autoregulation, IFFLs exhibit a larger variety of functional capabilities at high levels of retroactivity. While mathematical proofs in Transparent Methods Sections 7 and 8 demonstrate that our second finding is parameter-independent, the simulations systematically exploring parameter space in the Results section show that the magnitude by which retroactivity affects response times in IFFLs is significant in large regions of parameter space.

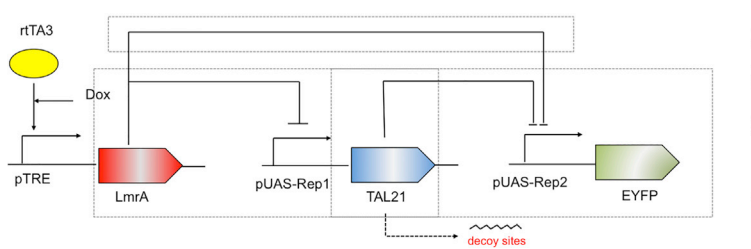
Tuning Retroactivity in Synthetic IFFLs

In synthetic biology, our work lends insights into designing gene circuits. Most prior studies have focused on the disruptive effects of retroactivity on the intended behavior of circuits, e.g., shrinking the bistable region of a toggle switch (Gyorgy and Del Vecchio, 2014; Gardner et al., 2000). In contrast, here we showed that increasing retroactivity may be used as a strategy to improve the behavior of IFFLs, i.e., creating synthetic IFFLs with shorter response times and larger pulse amplitudes while maintaining the same steady-state behaviors. One approach to changing retroactivity in synthetic systems is to mimic NDs by adding synthetic decoy sites, i.e., recombined bacterial plasmids that contain high-affinity sequence-specific binding sites. Biologically, the number of synthetic decoys can be adjusted by changing the transformation/transfection protocol, including the plasmid dose, the transformation/transfection reagent, and/or the method of transformation/transfection. By a mechanism similar to NDs, synthetic decoys can affect the behavior of synthetic circuits by sequestering TFs.

Our work also suggests that topology alone does not constitute the entire solution to circuit design. As shown by Figures 4 and 5, retroactivity affects the behaviors of I1-FFLs much more strongly for $h_{BD_B} \le 1$ (negative cooperativity) than for $h_{BD_B} \ge 1$ (positive cooperativity). Importantly, negative cooperativity and non-cooperativity are typical of the synthetic transcriptional repressors/activators used in constructing mammalian gene circuits. A synthetic biology group constructed four ABA/GA-inducible VPR-Sp/Sa dCas9 gene activators (Gao et al., 2016), with Hill coefficients ranging from 0.70 to 0.97 (coefficients fit from source data to Figure 2, Gao et al., 2016). Another group constructed and characterized a library of 26 transcription activator-like effector repressors (TALERs) that bind designed hybrid promoters (Li et al., 2015). The Hill coefficients of the characterized TALER-binding promoters range from 0.67 to 1.15, whereas the Hill coefficients of TALERs range from 0.51 to 1.56 (Li et al., 2015).

As a practical example, we consider a mammalian-cell-based IFFL circuit composed of biological parts built and tested in a previous study (Davidsohn et al., 2015) (Figure 6). Induced by Dox, the pTRE promoter turns on the expression of LmrA, which inhibits EYFP directly and activates EYFP indirectly through TAL21. As an I2-FFL, this construct mediates response acceleration in response to an OFF step. Using parameter estimates from the literature (Wang et al., 2018, 2019), we simulate its behaviors in the absence and presence of retroactivity (see Transparent Methods Section 14 for details). As Figure 6 suggests, the response time of EYFP decreases by more than 18% from 2.2 to 1.8 h when the concentration of the decoy sites increases from 0 to 8.7 \times 106 MEFL (30 times the binding affinity of TAL21 to pUAS-Rep2). Compared with manipulation of kinetic parameters, the strategy we propose may allow more precise control of the circuit as introduction of plasmids containing TAL21-binding sites does not interfere with the circuit's steady state.





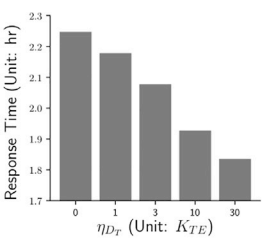


Figure 6. Tuning Retroactivity in a Synthetic IFFL

Tuning retroactivity is predicted by models to increase the response time of a synthetic IFFL construct (Davidsohn et al., 2015; Wang et al., 2018, 2019). The level of retroactivity may be adjusted via the delivery of plasmids containing synthetic decoy binding sites.

See Transparent Methods Section 14 for details.

A Potential Role of Retroactivity in Motif Evolution

From an evolutionary perspective, we hypothesize that the behaviors of IFFLs and negative autoregulated circuits under increasing levels of retroactivity may have shaped the relative abundance of sign-sensitive response-accelerating motifs in different organisms. Using published databases of *E. coli*, mouse, and human TRNs (*E. coli*: RegulonDB v10, Santos-Zavaleta et al., 2018; mouse and human: TTRUST v2, Han et al., 2018), we compared the number of times an IFFL is observed in the TRN of each organism to the number of times an IFFL is expected in the corresponding randomized Erdos-Renyi (ER) networks. We observed a total of 1,258, 470, and 1,171 IFFLs in *E. coli*, mouse, and human TRNs, whereas only 11, 5, and 7 would be expected, respectively, if TF-gene interactions were completely randomized (Table S12; see Transparent Methods Section 15 for details). The number of times an IFFL is observed versus expected suggests that IFFLs are conserved in both prokaryotic and eukaryotic organisms. In contrast, the occurrence of negative autoregulation differs drastically between prokaryotes and higher eukaryotes. In agreement with a previous study (Stewart et al., 2013), we found that whereas almost half of all repressors in *E. coli* are negatively self-regulated, approximately only 1% of repressors in the mouse and the human genomes are negatively autoregulated (Table S13; see Transparent Methods Section 15 for details).

From a general standpoint, higher eukaryotes have much larger genomes and non-coding genomes than prokaryotes. A direct consequence is that whereas an average $E.\ coli$ TF has 3–25 binding sites in the genome (Gao et al., 2018), an average human TF, as is mentioned in the Introduction section, has approximately 10^4-10^5 accessible ND sites. The degree of retroactivity that arises from accessible ND sites is, thus, expected to be substantially higher in higher eukaryotes such as mouse and human TRNs than in bacterial TRNs.

Due to technical challenges, studies quantifying the cooperativity of TF-DNA binding are much less common in natural systems than in synthetic systems. Nevertheless, a previous ChIP-seq-based study (Ghosh et al., 2019) examining the DNA binding of eight common TFs (i.e., OCT4, NANOG, CTCF, IRF2, FOXA1, NFAT, IRF1, and RELA) suggested that negative cooperativity and non-cooperativity may be a prevalent phenomenon of TF-DNA binding in mammalian cells (Figure S5B, Ghosh et al., 2019). It was observed that the ChIP-seq signal strength of most of these TFs stays relatively constant or decreases as the number of binding sites increases (Ghosh et al., 2019), which indicates non- and negative cooperativity. Querying these TFs against the TTRUST v2 database (Han et al., 2018), we found that three TFs, namely, RELA, IRF1, and CTCF, act as intermediate regulators (node B) in 101 IFFLs in human TRNs. RELA and IRF1, of which the latter exhibits clear negative cooperativity (Figure S5B, Ghosh et al., 2019), serve as the input node (node A) and regulatory node (node B) of IFFLs regulating BCL2, CCNB1, CDK4, CDKN1A, and FOXP3, as a part of the interferon pathway (Han et al., 2018; Kochupurakkal et al., 2015). As such, they are physical examples of IFFLs where protein B binds to DNA with negative cooperativity.

As is shown in the Results section and Transparent Methods Section 10, higher retroactivity in a negative autoregulatory loop results in a longer response time. This indicates that a negative autoregulatory loop achieves its minimum response time under the condition of zero retroactivity. In contrast, as is shown in the Results section and Transparent Methods Section 7, an IFFL with retroactivity on the regulatory node B can achieve response times shorter than that of an IFFL with zero retroactivity, especially if protein





B binds to DNA with negative cooperativity or non-cooperativity. One can speculate that network motifs that exhibit a larger diversity of functional capabilities under a high level of retroactivity are more likely to be conserved in higher eukaryotes. This is because the desired outcome of increasing retroactivity, i.e., whether the response time should increase, decrease, or stay constant, depends on the actual biological context, and a network motif that exhibits a larger diversity of functions is more likely to meet the expectation of the context. This suggests that IFFLs could enable organisms to better adapt to a large number of accessible ND sites during evolution than negative autoregulation in cases where a response time shorter than that of the circuit under zero retroactivity is desired. Therefore, IFFLs might confer upon the organism a selective advantage compared with negative autoregulation at high levels of retroactivity.

It is interesting to note that, in contrast to the decreased abundance of autoregulatory loops, we have observed an increased abundance of two-node NFBLs in higher eukaryotic TRNs compared with bacterial TRNs (Table S14; see Transparent Methods Section 15 for details). This may be because, similar to IFFLs, two-node NFBLs also exhibit a larger diversity of functional capabilities than negative autoregulatory loops under high levels of retroactivity.

Future Directions

Our work can be generalized and extended in several directions. First, it would be interesting to explore how the connection of IFFLs to additional network motifs, such as NFBLs, affects the ability of IFFLs to accelerate responses. In a modeling study (Joanito et al., 2018), it was proposed that in *Arabidopsis thaliana*, the CCA1/LHY-PRR9/7(PRR5/TOC1)-CCA1/LHY IFFL circuit serves to break the bistability generated by the double NBFLs between CCA1/LHY and PRR5/TOC1. Compared with a plain NFBL, the IFFL-NFBL combination allows cells to switch between the two states more rapidly (Joanito et al., 2018). In addition, it was demonstrated that conjoining an NFBL to an IFFL can also increase the robustness of IFFL-mediated adaptation (Reeves, 2019; Ma et al., 2009). That is, perfect or near-perfect adaptation can be achieved over a wider region of parameter space in an IFFL-NFBL combination than in either motif alone. Studying the effect of retroactivity that arises from the interconnection of an IFFL to an NFBL will serve to inform the design of a robust IFFL-NFBL synthetic system.

More generally, the modeling framework we apply here is based on ODEs. Other approaches to studying retroactivity include stochastic gene expression models, which take transcriptional bursting into consideration. Via stochastic simulation, it was found that retroactivity can dampen fluctuations and lengthen correlations in the output signal noise when the output of a network is connected to a downstream module (Kim and Sauro, 2011). It will be interesting to study whether retroactivity can further enhance the ability of IFFLs to attenuate the stochastic variation in gene expression.

Limitations of the Study

This study presents a minimal model of IFFL circuits with and without retroactivity. In cases where two transcription factors bind to the same promoter, the model excludes binding types other than AND and OR logics, such as the competitive logic.

METHODS

All methods can be found in the accompanying Transparent Methods supplemental file.

Resource Availability

Lead Contact

Further information and requests for resources should be directed to and will be fulfilled by the Lead Contact, Junmin Wang (dawang@bu.edu).

Materials Availability

This study did not generate any new unique reagent.

Data and Code Availability

A Julia script for implementing and solving the ODEs that model IFFLs, type-1 two-input circuits, and negative autoregulated circuits can be found online at https://github.com/wang-junmin/IFFL.



SUPPLEMENTAL INFORMATION

Supplemental Information can be found online at https://doi.org/10.1016/j.isci.2020.101779.

ACKNOWLEDGMENTS

The authors thank Prof. Domitilla Del Vecchio, Prof. Daniel Segrè, and Brian Teague for helpful discussions and constructive feedbacks. C.B. was supported by NSF CBET-0939511. S.A.I. was supported by National Science Foundation award DMS-1902854.

AUTHOR CONTRIBUTIONS

J.W. conceptualized the ideas, took the lead in writing the manuscript, and supervised this work. J.W., C.B., and S.A.I. developed the computational models. J.W. performed the simulations, interpreted the results, and wrote the mathematical proofs with input from S.A.I, who provided critical feedback and co-interpreted the results. All authors contributed to the writing of the manuscript.

DECLARATION OF INTERESTS

The authors declare no competing interests.

Received: July 15, 2020 Revised: September 24, 2020 Accepted: November 2, 2020 Published: December 18, 2020

REFERENCES

Abu Hatoum, O., Gross-Mesilaty, S., Breitschopf, K., Hoffman, A., Gonen, H., Ciechanover, A., and Bengal, E. (1998). Degradation of myogenic transcription factor myod by the ubiquitin pathway in vivo and in vitro: regulation by specific dna binding. Mol. Cell. Biol. 18, 5670–5677.

Alon, U. (2007). An Introduction to Systems Biology - Design Principles of Biological Circuits (Chapman and Hall).

Basu, S., Mehreja, R., Thiberge, S., Chen, M.-T., and Weiss, R. (2004). Spatiotemporal control of gene expression with pulse-generating networks. Proc. Natl. Acad. Sci. U S A 101, 6355–6360.

Bezanson, J., Edelman, A., Karpinski, S., and Shah, V. (2017). Julia: a fresh approach to numerical computing. SIAM Rev. *59*, 65–98.

Bleris, L., Xie, Z., Glass, D., Adadey, A., Sontag, E., and Benenson, Y. (2011). Synthetic incoherent feedforward circuits show adaptation to the amount of their genetic template. Mol. Syst. Biol. 7. 519.

Boekel, M.A.J.S. (2009). Kinetic Modeling of Reactions in Foods (Boca Raton, FL: CRC Press).

Brophy, J.A.N., and Voigt, C.A. (2014). Principles of genetic circuit design. Nat. Methods 11, 508–520.

Burger, A., Walczak, A.M., and Wolynes, P.G. (2010). Abduction and asylum in the lives of transcription factors. Proc. Natl. Acad. Sci. U S A 107, 4016–4021.

Burger, A., Walczak, A.M., and Wolynes, P.G. (2012). Influence of decoys on the noise and dynamics of gene expression. Phys. Rev. E Stat. Nonlin. Soft Matter Phys. 86, 041920.

Castillo-Hair, S.M., Villota, E.R., and Coronado, A.M. (2015). Design principles for robust oscillatory behavior. Syst. Synth. Biol. *9*, 125–133.

Consortium, E.P. (2012). An integrated encyclopedia of dna elements in the human genome. Nature 489, 57–74.

Davidsohn, N., Beal, J., Kiani, S., Adler, A., Yaman, F., Li, Y., Xie, Z., and Weiss, R. (2015). Accurate predictions of genetic circuit behavior from part characterization and modular composition. ACS Synth. Biol. 4, 673–681.

Del Vecchio, D., Ninfa, A.J., and Sontag, E.D. (2008). Modular cell biology: retroactivity and insulation. Mol. Syst. Biol. *4*, 161.

Esadze, A., Kemme, C.A., Kolomeisky, A.B., and Iwahara, J. (2014). Positive and negative impacts of nonspecific sites during target location by a sequence-specific dna-binding protein: origin of the optimal search at physiological ionic strength. Nucleic Acids Res. 42, 7039–7046.

Fisher, W.W., Li, J.J., Hammonds, A.S., Brown, J.B., Pfeiffer, B.D., Weiszmann, R., MacArthur, S., Thomas, S., Stamatoyannopoulos, J.A., Eisen, M.B., et al. (2012). Dna regions bound at low occupancy by transcription factors do not drive patterned reporter gene expression in drosophila. Proc. Natl. Acad. Sci. U S A 109, 21330–21335.

Gao, Y., Xiong, X., Wong, S., Charles, E.J., Lim, W.A., and Qi, L.S. (2016). Complex transcriptional modulation with orthogonal and inducible dcas9 regulators. Nat. Methods 13, 1043–1049.

Gao, Y., Yurkovich, J.T., Seo, S.W., Kabimoldayev, I., Dräger, A., Chen, K., Sastry, A.V., Fang, X., Mih, N., Yang, L., et al. (2018). Systematic discovery of uncharacterized transcription factors in

escherichia coli k-12 mg1655. Nucleic Acids Res. 46, 10682–10696.

Gardner, T., Cantor, C., and Collins, J.; 1 (2000). Construction of a genetic toggle switch in escherichia coli. Nature 403, 339–342.

Ghosh, R.P., Shi, Q., Yang, L., Reddick, M.P., Nikitina, T., Zhurkin, V.B., Fordyce, P., Stasevich, T.J., Chang, H.Y., Greenleaf, W.J., and Liphardt, J.T. (2019). Satb1 integrates dna binding site geometry and torsional stress to differentially target nucleosome-dense regions. Nat. Commun. 10, 3221.

Goentoro, L., Shoval, O., Kirschner, M.W., and Alon, U. (2009). The incoherent feedforward loop can provide fold-change detection in gene regulation. Mol. Cell 36, 894–899.

Grigolon, S., Di Patti, F., De Martino, A., and Marinari, E. (2016). Noise processing by micrornamediated circuits: the incoherent feed-forward loop, revisited. Heliyon 2, e00095.

Gyorgy, A., and Del Vecchio, D. (2014). Modular composition of gene transcription networks. PLoS Comput. Biol.

Han, H., Cho, J.-W., Lee, S., Yun, A., Kim, H., Bae, D., Yang, S., Kim, C.Y., Lee, M., Kim, E., et al. (2018). Trrust v2: an expanded reference database of human and mouse transcriptional regulatory interactions. Nucleic Acids Res. 46, D380–D386.

Jayanthi, S., Nilgiriwala, K.S., and Del Vecchio, D. (2013). Retroactivity controls the temporal dynamics of gene transcription. ACS Synth. Biol. *2*, 431–441.

Joanito, I., Chu, J.-W., Wu, S.-H., and Hsu, C.-P. (2018). An incoherent feed-forward loop switches





the arabidopsis clock rapidly between two hysteretic states. Sci. Rep. 8, 13944.

Kemme, C.A., Esadze, A., and Iwahara, J. (2015). Influence of quasi-specific sites on kinetics of target dna search by a sequence-specific dnabinding protein. Biochemistry 54, 6684–6691.

Kemme, C.A., Nguyen, D., Chattopadhyay, A., and Iwahara, J. (2016). Regulation of transcription factors via natural decoys in genomic dna. Transcription 7, 115–120.

Kim, K.H., and Sauro, H.M. (2011). Measuring retroactivity from noise in gene regulatory networks. Biophys. J. 100, 1167–1177.

Kochupurakkal, B.S., Wang, Z.C., Hua, T., Culhane, A.C., Rodig, S.J., Rajkovic-Molek, K., Lazaro, J.-B., Richardson, A.L., Biswas, D.K., and Iglehart, J.D. (2015). Rela-induced interferon response negatively regulates proliferation. PLoS One 10, 1–33.

Lee, T.-H., and Maheshri, N. (2012). A regulatory role for repeated decoy transcription factor binding sites in target gene expression. Mol. Syst. Biol. 8, 576.

Li, X.-y., MacArthur, S., Bourgon, R., Nix, D., Pollard, D.A., Iyer, V.N., Hechmer, A., Simirenko, L., Stapleton, M., Luengo Hendriks, C.L., et al. (2008). Transcription factors bind thousands of active and inactive regions in the drosophila blastoderm. PLoS Biol. 6, e27.

Li, Y., Jiang, Y., Chen, H., Liao, W., Li, Z., Weiss, R., and Xie, Z. (2015). Modular construction of mammalian gene circuits using tale transcriptional repressors. Nat. Chem. Biol. *11*, 207–213

Liu, X., Wu, B., Szary, J., Kofoed, E.M., and Schaufele, F. (2007). Functional sequestration of transcription factor activity by repetitive dna. J. Biol. Chem. *282*, 20868–20876. Ma, W., Trusina, A., El-Samad, H., Lim, W.A., and Tang, C. (2009). Defining network topologies that can achieve biochemical adaptation. Cell *138*, 760–773.

Mangan, S., and Alon, U. (2003). Structure and function of the feed-forward loop network motif. Proc. Natl. Acad. Sci. U S A 100, 11980–11985.

Milo, R., Shen-Orr, S., Itzkovitz, S., Kashtan, N., Chklovskii, D., and Alon, U. (2002). Network motifs: simple building blocks of complex networks. Science *298*, 824–827.

Osella, M., Bosia, C., Corá, D., and Caselle, M. (2011). The role of incoherent microma-mediated feedforward loops in noise buffering. PLoS Comput. Biol. 7, 1–16.

Pariat, M., Carillo, S., Molinari, M., Salvat, C., Debüssche, L., Bracco, L., Milner, J., and Piechaczyk, M. (1997). Proteolysis by calpains: a possible contribution to degradation of p53. Mol. Cell. Biol. 17, 2806–2815.

Rackauckas, C., and Nie, Q. (2017). DifferentialEquations.jl – a performant and feature-rich ecosystem for solving differential equations in Julia. J. Open Source Softw. 5, 15.

Reeves, G.T. (2019). The engineering principles of combining a transcriptional incoherent feedforward loop with negative feedback. J. Biol. Eng. 13, 62.

Rosenfeld, N., Elowitz, M.B., and Alon, U. (2002). Negative autoregulation speeds the response times of transcription networks. J. Mol. Biol. 323, 785–793.

Santos-Zavaleta, A., Sánchez-Pérez, M., Salgado, H., Velázquez-Ramírez, D.A., Gama-Castro, S., Tierrafría, V.H., Busby, S.J.W., Aquino, P., Fang, X., Palsson, B.O., et al. (2018). A unified resource for transcriptional regulation in escherichia coli k-12 incorporating high-throughput-generated binding data into regulondb version 10.0. BMC Biol. 16, 91.

Sepulchre, J.-A., and Ventura, A.C. (2013). Intrinsic feedbacks in MAPK signaling cascades lead to bistability and oscillations. Acta Biotheor. *61*, 59–78.

Shi, W., Ma, W., Xiong, L., Zhang, M., and Tang, C. (2017). Adaptation with transcriptional regulation. Sci. Rep. 7, 42648.

Siciliano, V., Garzilli, I., Fracassi, C., Criscuolo, S., Ventre, S., and di Bernardo, D. (2013). Mirnas confer phenotypic robustness to gene networks by suppressing biological noise. Nat. Commun. 4, 2364.

Stewart, A.J., Seymour, R.M., Pomiankowski, A., and Reuter, M. (2013). Under-dominance constrains the evolution of negative autoregulation in diploids. PLoS Comput. Biol. 9, e1002992.

Wang, J., and Belta, C. (2019). Retroactivity affects the adaptive robustness of transcriptional regulatory networks. In 2019 American Control Conference (ACC)), pp. 5396–5401.

Wang, J., Isaacson, S.A., Belta, C., 2018. Predictions of genetic circuit behaviors based on modular composition in transiently transfected mammalian cells. 2018 IEEE Life Sciences Conference (LSC), 85–88.

Wang, J., Isaacson, S.A., and Belta, C. (2019). Modeling genetic circuit behavior in transiently transfected mammalian cells. ACS Synth. Biol. 8, 407, 707

Wang, Z., Potoyan, D.A., and Wolynes, P.G. (2016). Molecular stripping, targets and decoys as modulators of oscillations in the nf-lob/ilob1±/dna genetic network. J. R. Soc. Interface 13, 20160606.

iScience, Volume 23

Supplemental Information

How Retroactivity Affects
the Behavior of Incoherent
Feedforward Loops

Junmin Wang, Calin Belta, and Samuel A. Isaacson

Supplemental Figures

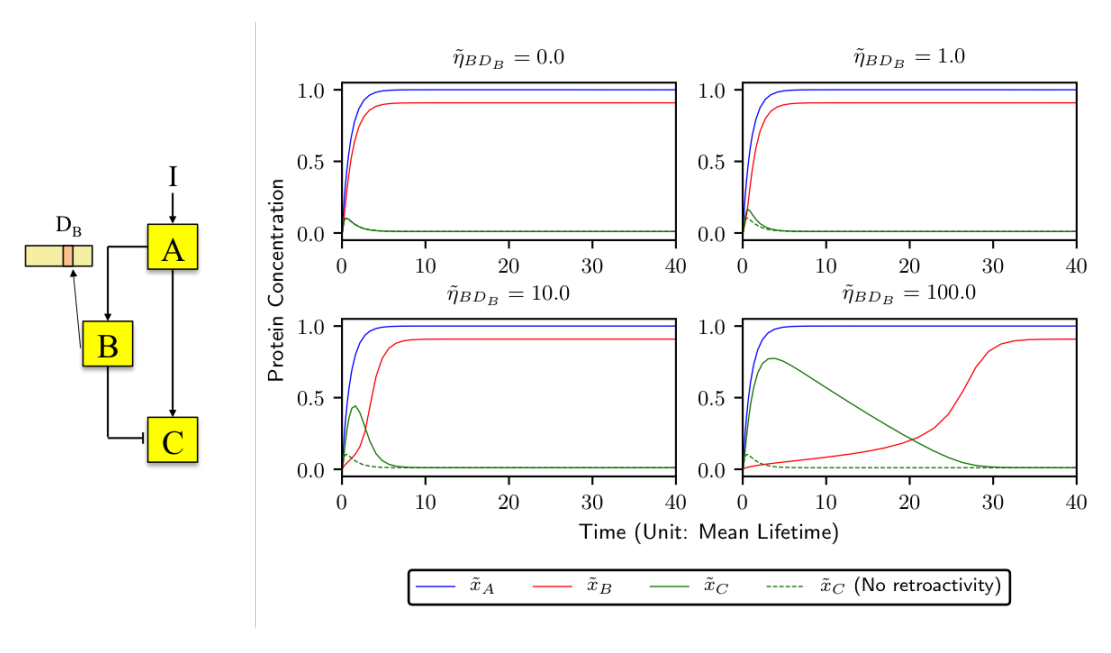


Figure S1: Increasing pulse amplitude due to increasing $\tilde{\eta}_{BD_B}$ in an I1-FFL. Related to Figure 2A. $\tilde{\eta}_{BD_B}$ increases in the order of top left, top right, bottom left, and bottom right. Values of the other parameters are: $\tilde{K}_{AB} = \tilde{K}_{AC} = \tilde{K}_{BC} = \tilde{K}_{BD_B} = 0.1$, $h_{AB} = h_{AC} = 1.0$, $h_{BC} = h_{BD_B} = 2.0$. For comparison, the green dashed curve represents the trajectory of \tilde{x}_C when $\tilde{\eta}_{BD_B}$ equals 0.

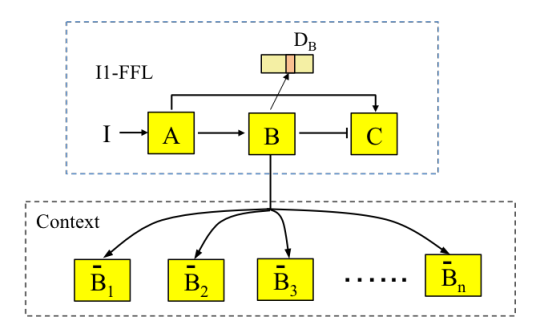


Figure S2: An I1-FFL connected to $\it n$ additional circuits, i.e., its context. Related to Figure 2A and Transparent Methods Section 8.

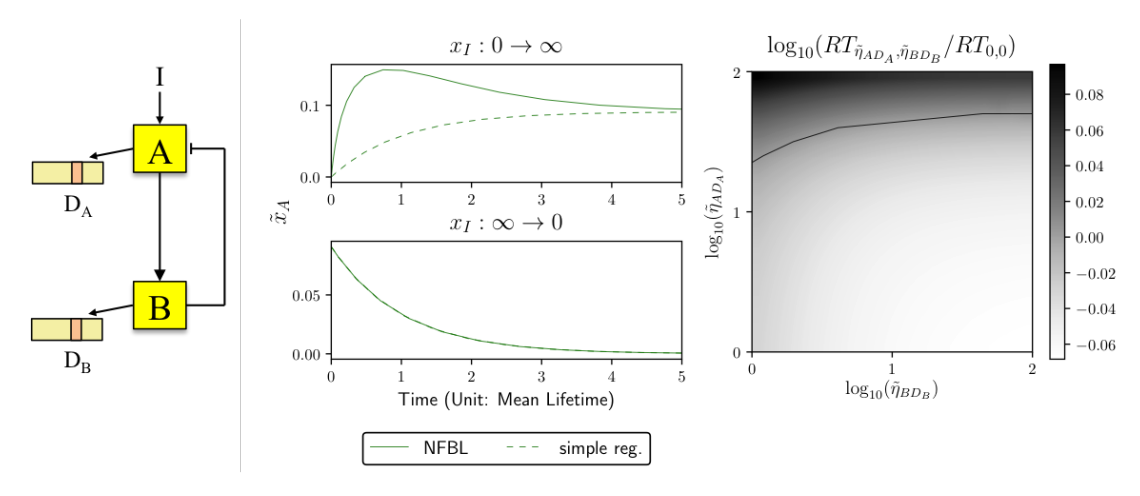


Figure S3: Two-node negative feedback loops (NFBLs). Related to Figure 3. Left: diagram. Middle: sign-sensitive response acceleration of a two-node NFBL in the absence of retroactivity, i.e., $\tilde{\eta}_{AD_A} = \tilde{\eta}_{BD_B} = 0$. The response of \tilde{x}_A is accelerated in response to an ON step, not in response to an OFF step. "Simple reg." represents a simple circuit where A is activated by an external inducer I without additional regulation. The "simple reg." model achieves the same steady state as the NFBL model. Right: response times of the two-node NFBL model at different levels of $\tilde{\eta}_{AD_A}$ and $\tilde{\eta}_{BD_B}$ compared to that of the model with no retroactivity in response to an ON step. The black curve, which we refer to as the "iso-response-time" curve, represents values of $\tilde{\eta}_{XD_X}$ (X = A, B) at which the response time is the same as the response time of the model with no retroactivity. Values of parameters used for making the middle and the right panels are: $\tilde{K}_{AB} = \tilde{K}_{AD_A} = 0.001$, $\tilde{K}_{BA} = \tilde{K}_{BD_B} = 1.0$, $h_{AB} = h_{AD_A} = h_{BD_B} = 1.0$.

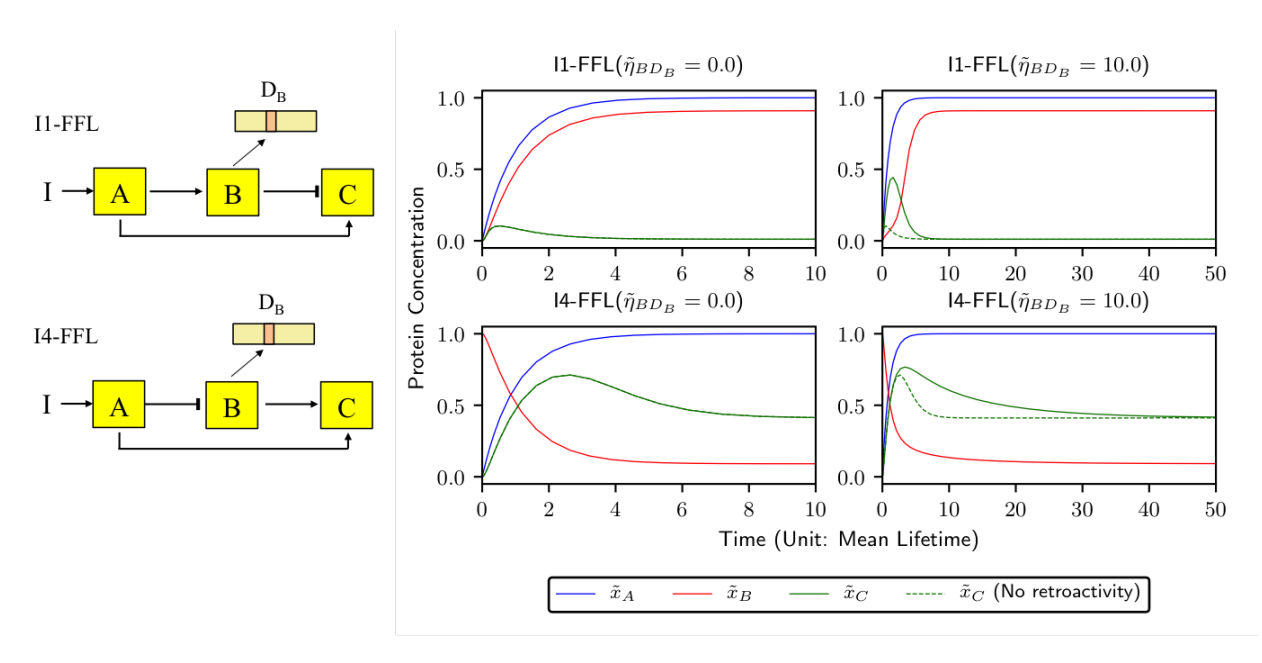


Figure S4: The effect of retroactivity $\tilde{\eta}_{BD_B}$ on pulse amplitude is more pronounced in an I1-FFL (top row) than in an I4-FFL (bottom row). Related to Figure 4C. Values of the parameters are: $\tilde{K}_{AB} = \tilde{K}_{AC} = \tilde{K}_{BC} = \tilde{K}_{BD_B} = 0.1$, $h_{AB} = h_{AC} = 1.0$, $h_{BC} = h_{BD_B} = 2.0$. For comparison, the green dashed curves represent the trajectories of \tilde{x}_C when $\tilde{\eta}_{BD_B}$ equals 0.

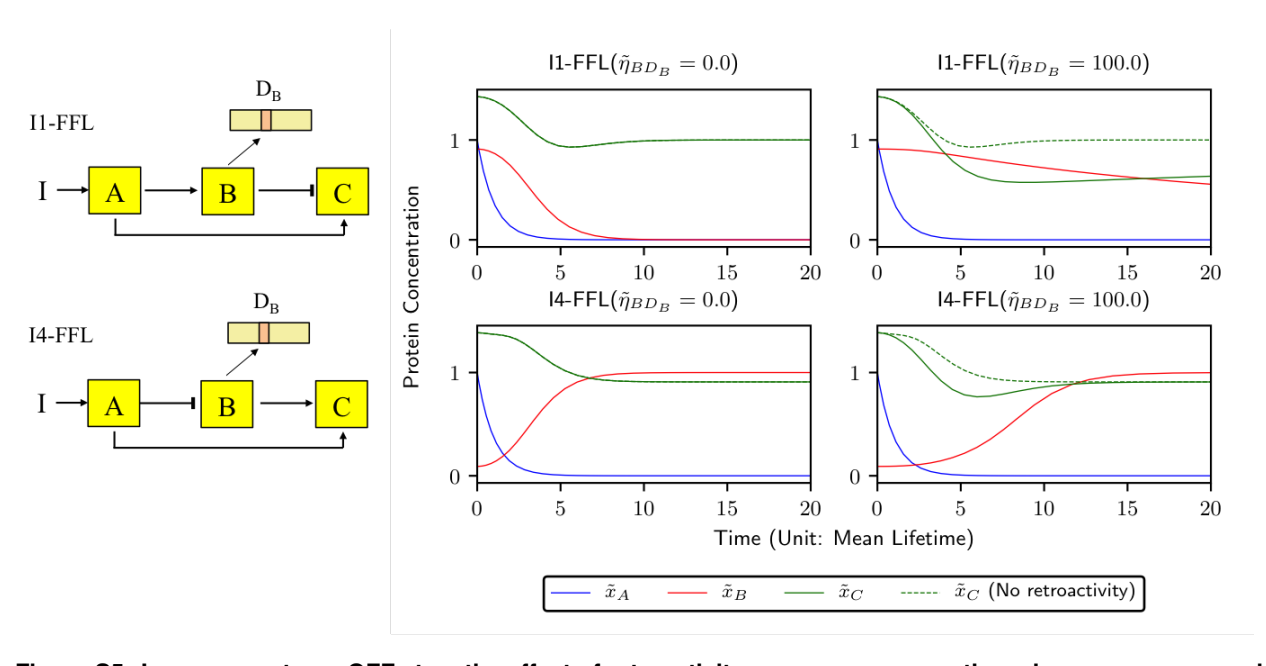


Figure S5: In response to an OFF step, the effect of retroactivity $\tilde{\eta}_{BD_B}$ on response times is more pronounced in an I4-FFL (bottom row) than in an I1-FFL (top row) under the assumption of OR logic. Related to Figure 4C. Values of the parameters are: $\tilde{K}_{AB} = \tilde{K}_{AC} = 0.1$, $\tilde{K}_{BC} = \tilde{K}_{BD_B} = 1.0$, $h_{AB} = h_{AC} = h_{BC} = h_{BD_B} = 1.0$. For comparison, the green dashed curves represent the trajectories of \tilde{x}_C when $\tilde{\eta}_{BD_B}$ equals 0.

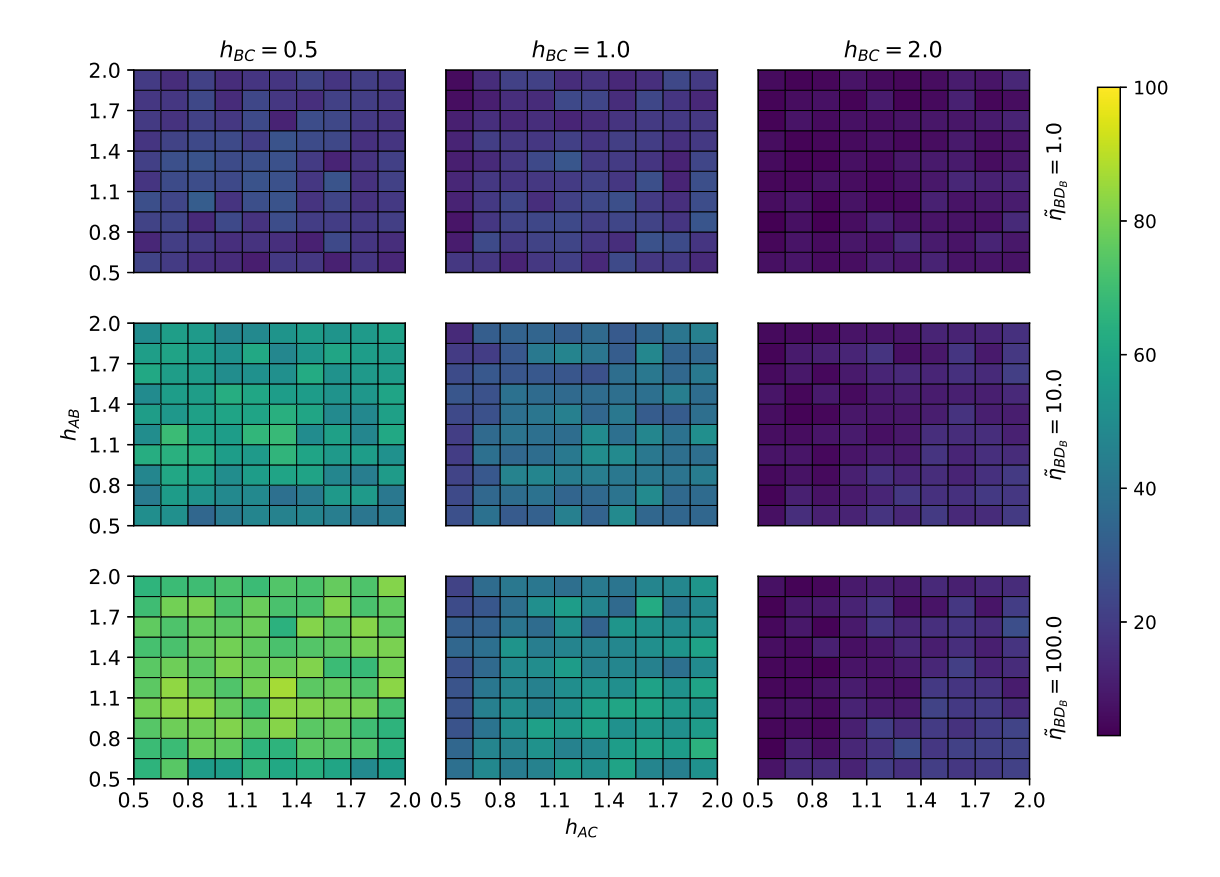


Figure S6: Percent of I1-FFL trajectories whose relative response time is less than 90% of the model in the absence of retroactivity calculated based on systematically exploring parameter space described in Transparent Methods Section 13. Related to Figure 5. The model assumes $0.8h_{BC} \le h_{BD_B} \le 1.2h_{BC}$ and $0.8\tilde{K}_{BC} \le \tilde{K}_{BD_B} \le 1.2\tilde{K}_{BC}$. The trajectories are separated evenly by h_{AB} and h_{AC} into 100 voxels, the color of which represents the percent of trajectories whose relative response time is less than 90% of the model in the absence of retroactivity out of the 100 simulated trajectories falling into that bin. Here, relative response time is defined as the ratio of the response time of the model without retroactivity.

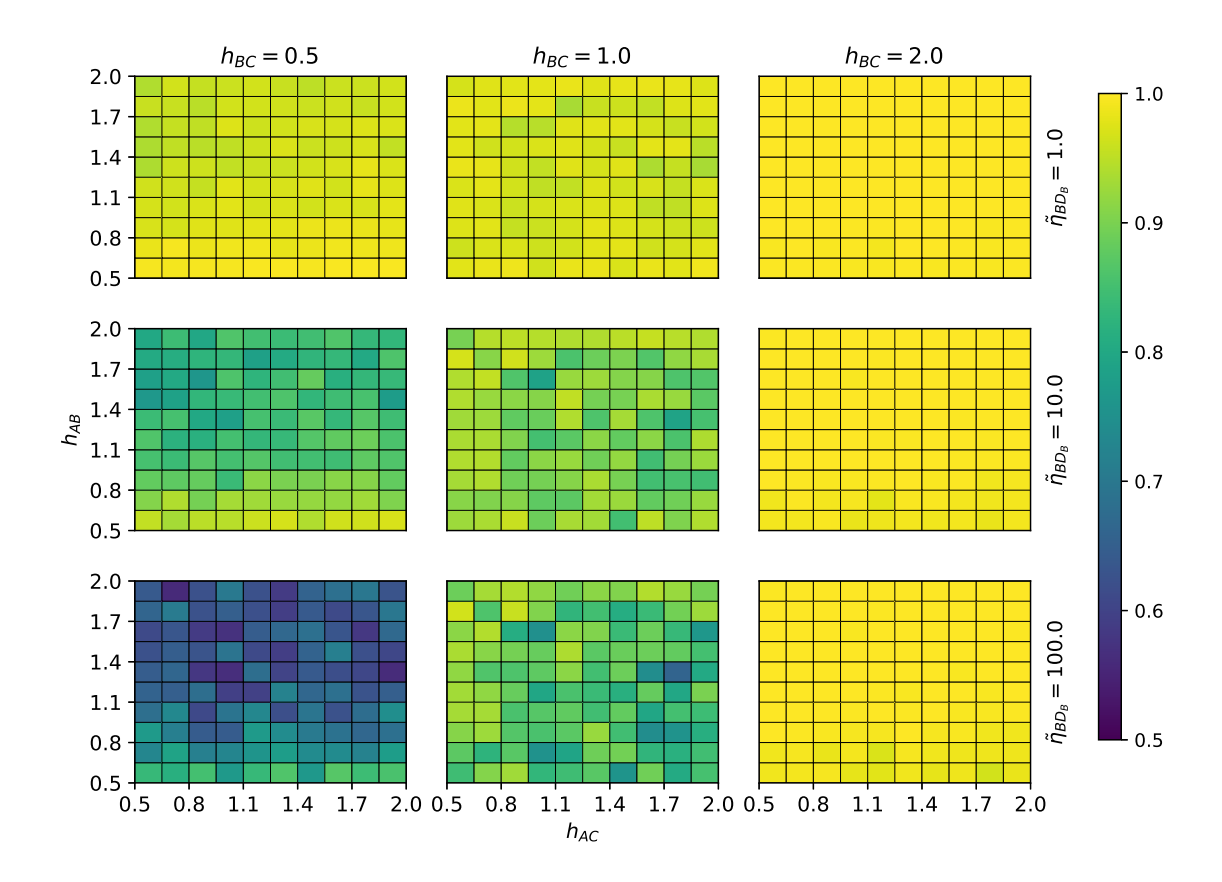


Figure S7: Median relative response time of I1-FFL trajectories calculated based on systematically exploring parameter space as described in Transparent Methods Section 13. Related to Figure 5. The model assumes $h_{BC} = h_{BD_B}$ and $\tilde{K}_{BC} = \tilde{K}_{BD_B}$. The trajectories are separated evenly by h_{AB} and h_{AC} into 100 voxels, the color of which represents the median relative response time of the 100 simulated trajectories falling into that bin. Here, relative response time is defined as the ratio of the response time of the model to the response time of the model without retroactivity.

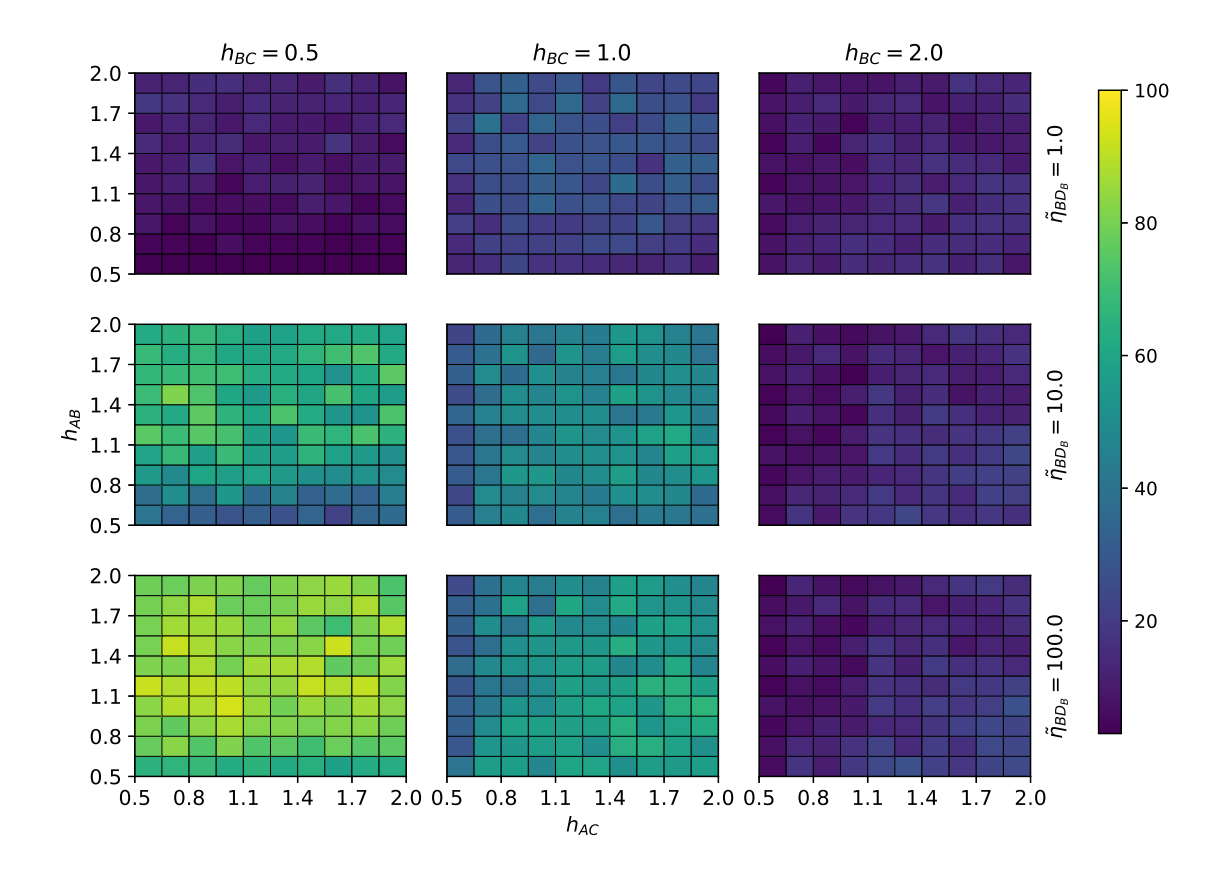


Figure S8: Percent of I1-FFL trajectories whose relative response time is less than 90% of the model in the absence of retroactivity calculated based on systematically exploring parameter space as described in Transparent Methods Section 13. Related to Figure 5. The model assumes $h_{BC} = h_{BD_B}$ and $\tilde{K}_{BC} = \tilde{K}_{BD_B}$. The trajectories are separated evenly by h_{AB} and h_{AC} into 100 voxels, the color of which represents the percent of trajectories whose relative response time is less than 90% of the model in the absence of retroactivity out of the 100 simulated trajectories falling into that bin. Here, relative response time is defined as the ratio of the response time of the model to the response time of the model without retroactivity.

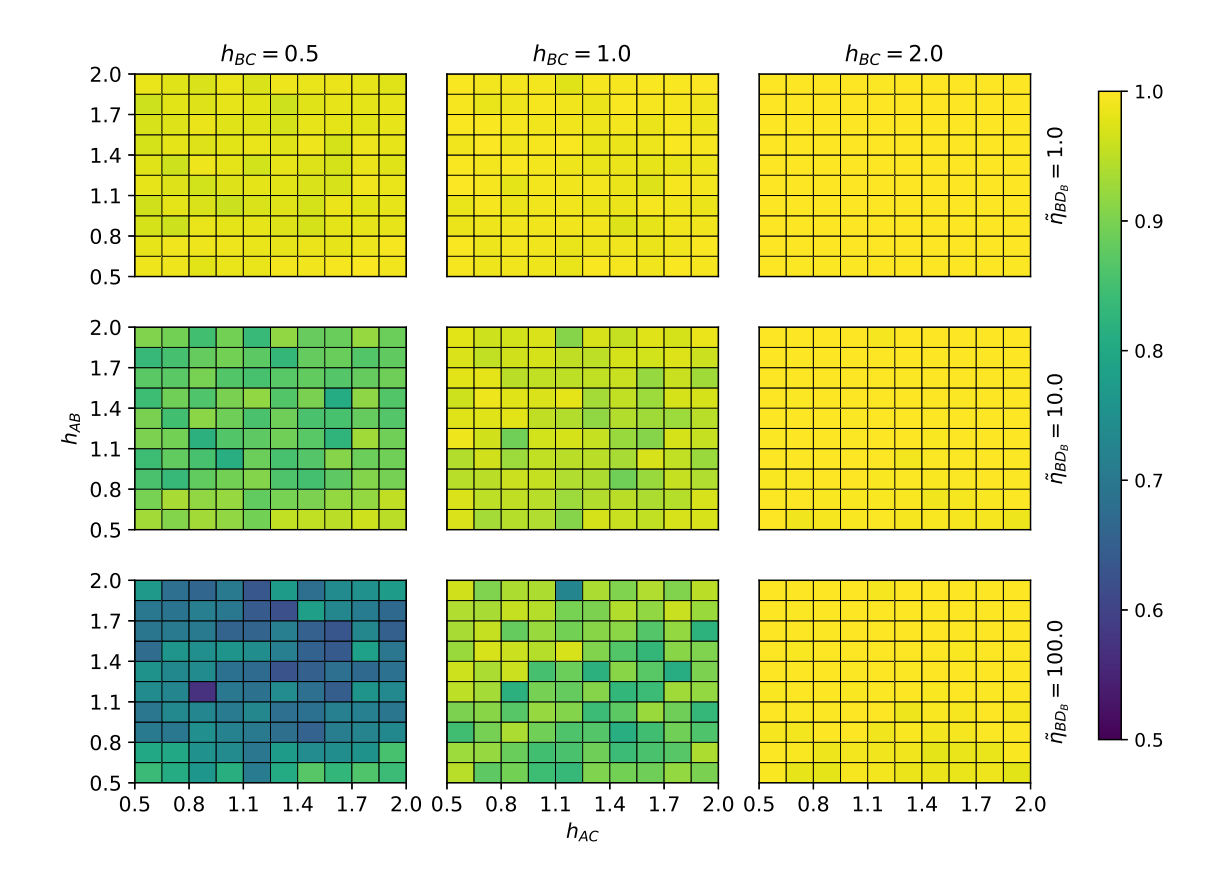


Figure S9: Median relative response time of I1-FFL trajectories calculated based on systematically exploring parameter space as described in Transparent Methods Section 13. Related to Figure 5. The model assumes $0.5h_{BC} \le h_{BD_B} \le 1.5h_{BC}$ and $0.5\tilde{K}_{BC} \le \tilde{K}_{BD_B} \le 1.5\tilde{K}_{BC}$. The trajectories are separated evenly by h_{AB} and h_{AC} into 100 voxels, the color of which represents the median relative response time of the 100 simulated trajectories falling into that bin. Here, relative response time is defined as the ratio of the response time of the model to the response time of the model without retroactivity.

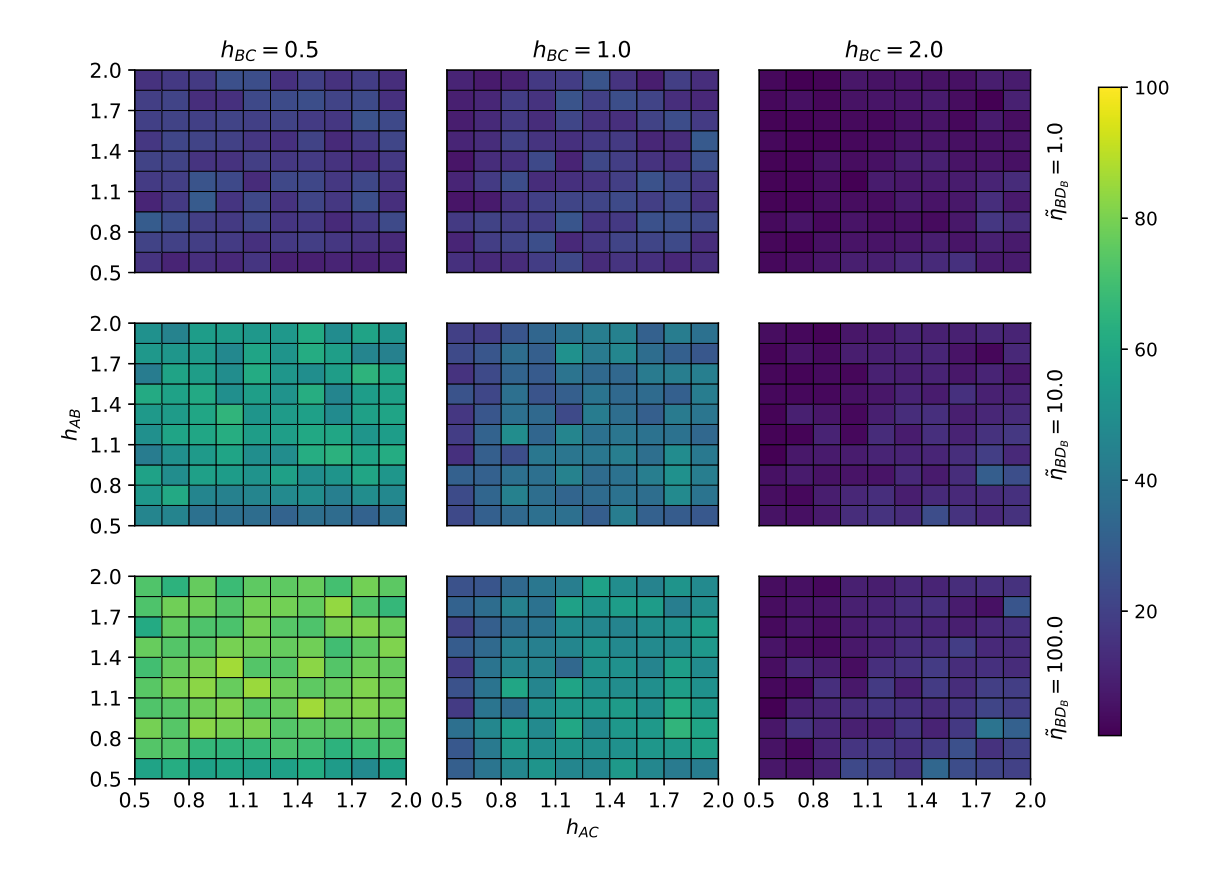


Figure S10: Percent of I1-FFL trajectories whose relative response time is less than 90% of the model in the absence of retroactivity calculated based on systematically exploring parameter space as described in Transparent Methods Section 13. Related to Figure 5. The model assumes $0.5h_{BC} \le h_{BD_B} \le 1.5h_{BC}$ and $0.5\tilde{K}_{BC} \le \tilde{K}_{BD_B} \le 1.5\tilde{K}_{BC}$. The trajectories are separated evenly by h_{AB} and h_{AC} into 100 voxels, the color of which represents the percent of trajectories whose relative response time is less than 90% of the model in the absence of retroactivity out of the 100 simulated trajectories falling into that bin. Here, relative response time is defined as the ratio of the response time of the model to the response time of the model without retroactivity.

Supplemental Tables

		l1	-FFL			14-	FFL	
				h_{CD_C}	= 0.5			
\tilde{R}_{CD_C}	0.0	1.0	10.0	100.0	0.0	1.0	10.0	100.0
0.01	0.16	0.16	0.24	2.14	0.48	0.49	0.53	1.00
0.03	0.16	0.18	0.40	8.06	0.48	0.49	0.63	2.01
0.1	0.16	0.21	1.09	24.73	0.48	0.52	0.90	6.61
0.3	0.16	0.28	3.59	54.33	0.48	0.58	1.48	17.46
1.0	0.16	0.44	9.73	116.91	0.48	0.71	3.13	42.74
				h_{CD_C}	= 1.0			
\tilde{K}_{CDC}	0.0	1.0	10.0	100.0	0.0	1.0	10.0	100.0
0.01	0.16	0.18	0.43	8.90	0.48	0.49	0.61	1.87
0.03	0.16	0.21	1.07	23.40	0.48	0.52	0.86	5.62
0.1	0.16	0.25	2.67	44.21	0.48	0.59	1.54	18.14
0.3	0.16	0.28	3.98	57.73	0.48	0.68	2.66	36.69
1.0	0.16	0.29	4.66	64.44	0.48	0.77	4.04	54.55
				h_{CD_C}	= 2.0			
\tilde{K}_{CD_C}	0.0	1.0	10.0	100.0	0.0	1.0	10.0	100.0
0.01	0.16	0.21	1.12	23.22	0.48	0.51	0.76	3.76
0.03	0.16	0.29	4.36	61.84	0.48	0.57	1.34	13.94
0.1	0.16	0.26	3.42	55.26	0.48	0.74	3.58	48.38
0.3	0.16	0.20	0.77	20.81	0.48	0.83	5.24	69.08
1.0	0.16	0.17	0.29	4.68	0.48	0.64	2.11	30.36

Table S1: Response time of gene C in IFFL models with different values of \tilde{K}_{CDC} , h_{CDC} , and $\tilde{\eta}_{CDC}$ (values rounded to two decimal places). Related to Figure 2A. Values of the other parameters are: $\tilde{K}_{AB} = \tilde{K}_{AC} = \tilde{K}_{BC} = 0.1$, $h_{AB} = h_{AC} = h_{BC} = 1.0$.

		11-	FFL			14-	FFL	
				h_{BD_B}	= 0.5			
\tilde{K}_{BD_B}	0.0	1.0	10.0	100.0	0.0	1.0	10.0	100.0
0.01	0.31	0.30	0.23	0.13	0.75	0.75	0.75	0.75
0.03	0.37	0.36	0.25	0.19	0.68	0.68	0.68	0.68
0.1	0.46	0.43	0.30	0.26	0.59	0.59	0.59	0.58
0.3	0.54	0.50	0.37	0.35	0.51	0.51	0.51	0.50
1.0	0.64	0.58	0.48	0.47	0.44	0.44	0.43	0.43
				h_{BD_B}	= 1.0			
\tilde{K}_{BD_B}	0.0	1.0	10.0	100.0	0.0	1.0	10.0	100.0
0.01	0.04	0.04	0.04	0.04	0.83	0.83	0.83	0.83
0.03	0.08	0.07	0.07	0.07	0.70	0.70	0.70	0.70
0.1	0.16	0.15	0.13	0.13	0.48	0.48	0.48	0.48
0.3	0.30	0.28	0.26	0.26	0.30	0.30	0.30	0.30
1.0	0.54	0.51	0.48	0.47	0.19	0.19	0.19	0.19
				h_{BD_B}	= 2.0			
\tilde{K}_{BD_B}	0.0	1.0	10.0	100.0	0.0	1.0	10.0	100.0
0.01	0.001	0.001	0.001	0.001	0.91	0.91	0.91	0.91
0.03	0.01	0.01	0.01	0.01	0.82	0.82	0.82	0.82
0.1	0.04	0.04	0.04	0.04	0.42	0.42	0.42	0.42
0.3	0.13	0.13	0.13	0.13	0.13	0.13	0.13	0.13
1.0	0.50	0.50	0.50	0.49	0.04	0.04	0.04	0.04

Table S2: Response time of gene C in IFFL models with different values of \tilde{K}_{BD_B} , h_{BD_B} , and $\tilde{\eta}_{BD_B}$ (values rounded to two decimal places). Related to Figure 2A. Values of the other parameters are: $\tilde{K}_{AB} = \tilde{K}_{AC} = 0.1$, $h_{AB} = h_{AC} = 1.0$.

-		I1-	FFL			14-	FFL	
				h:	= 0.5			
\tilde{K}_{CD_C}	0.0	1.0	10.0	100.0	0.0	1.0	10.0	100.0
0.01	0.14	0.14	0.13	0.09	0.60	0.60	0.59	0.55
0.03	0.14	0.14	0.11	0.09	0.60	0.60	0.58	0.47
0.1	0.14	0.13	0.09	NA	0.60	0.60	0.56	0.43
0.3	0.14	0.12	0.09	NA	0.60	0.59	0.49	0.43
1.0	0.14	0.10	0.09	NA	0.60	0.57	0.43	NA
				h:	= 1.0			
\tilde{K}_{CD_C}	0.0	1.0	10.0	100.0	0.0	1.0	10.0	100.0
0.01	0.14	0.14	0.11	0.09	0.60	0.60	0.59	0.49
0.03	0.14	0.13	0.09	NA	0.60	0.60	0.57	0.43
0.1	0.14	0.12	0.09	NA	0.60	0.59	0.49	0.43
0.3	0.14	0.11	0.09	NA	0.60	0.57	0.43	NA
1.0	0.14	0.10	NA	NA	0.60	0.54	0.43	NA
				h:	= 2.0			
\tilde{K}_{CD_C}	0.0	1.0	10.0	100.0	0.0	1.0	10.0	100.0
0.01	0.14	0.13	0.09	0.09	0.60	0.60	0.58	0.44
0.03	0.14	0.12	0.09	NA	0.60	0.59	0.53	0.43
0.1	0.14	0.10	NA	NA	0.60	0.58	0.43	NA
0.3	0.14	0.11	NA	NA	0.60	0.52	NA	NA
1.0	0.14	0.13	NA	NA	0.60	0.51	NA	NA

Table S3: Pulse amplitude of gene C in models with different values of \tilde{K}_{CD_C} , h_{CD_C} , and $\tilde{\eta}_{CD_C}$ (values rounded to two decimal places). Related to Figure 2A. Values of the other parameters are: $\tilde{K}_{AB} = \tilde{K}_{AC} = \tilde{K}_{BC} = 0.1$, $h_{AB} = h_{AC} = h_{BC} = 1.0$. Here, a trajectory is considered to contain a pulse if the trajectory maximum is larger than the pre-induction and post-induction steady states. A trajectory not satisfying this criteria is labeled as "NA".

		l1-	FFL			14-	FFL	
				h:	= 0.5			
\tilde{K}_{BD_B}	0.0	1.0	10.0	100.0	0.0	1.0	10.0	100.0
0.01	0.09	0.09	0.10	0.19	0.71	0.71	0.71	0.71
0.03	0.15	0.15	0.16	0.34	0.62	0.62	0.62	0.64
0.1	0.23	0.23	0.26	0.59	0.51	0.51	0.52	0.57
0.3	0.33	0.34	0.41	0.74	0.40	0.41	0.43	0.50
1.0	0.47	0.47	0.60	0.84	0.29	0.30	0.34	0.41
				h:	= 1.0			
\tilde{K}_{BD_B}	0.0	1.0	10.0	100.0	0.0	1.0	10.0	100.0
0.01	0.03	0.03	0.06	0.28	0.83	0.83	0.83	9.84
0.03	0.06	0.07	0.15	0.49	0.75	0.75	0.75	0.78
0.1	0.14	0.16	0.32	0.70	0.60	0.60	0.63	0.72
0.3	0.27	0.31	0.53	0.81	0.42	0.44	0.51	0.62
1.0	0.49	0.53	0.72	0.87	0.22	0.25	0.33	0.42
				h:	= 2.0			
\tilde{K}_{BD_B}	0.0	1.0	10.0	100.0	0.0	1.0	10.0	100.0
0.01	0.01	0.02	0.09	0.41	0.90	0.90	0.90	0.90
0.03	0.04	0.06	0.22	0.62	0.85	0.85	0.85	0.87
0.1	0.10	0.16	0.44	0.78	0.71	0.72	0.77	0.84
0.3	0.25	0.36	0.65	0.85	0.48	0.52	0.66	0.78
1.0	0.56	0.65	0.81	0.89	0.15	0.22	0.36	0.43

Table S4: Pulse amplitude of gene C in models with different values of \tilde{K}_{BD_B} , h_{BD_B} , and $\tilde{\eta}_{BD_B}$ (values rounded to two decimal places). Related to Figure 2A. Values of the other parameters are: $\tilde{K}_{AB} = \tilde{K}_{AC} = 0.1$, $h_{AB} = h_{AC} = 1.0$.

		I1-FFL				Type-1 Two-Input Circuit			
		$h_{AD_A} = 0.5$							
\tilde{K}_{AD_A} $\tilde{\eta}_{AD_A}$	0.0	1.0	10.0	100.0	0.0	1.0	10.0	100.0	
0.01	0.09	0.09	0.11	0.24	0.09	0.09	0.11	0.33	
0.03	0.11	0.11	0.16	0.44	0.11	0.12	0.18	0.81	
0.1	0.14	0.15	0.26	0.87	0.14	0.16	0.33	2.58	
0.3	0.18	0.21	0.45	1.71	0.18	0.23	0.65	6.20	
1.0	0.25	0.33	0.85	4.06	0.25	0.36	1.61	14.06	
				h_{AI}	$O_A = 1.0$				
\tilde{K}_{AD_A}	0.0	1.0	10.0	100.0	0.0	1.0	10.0	100.0	
0.01	0.08	0.09	0.13	0.37	0.08	0.09	0.15	0.69	
0.03	0.11	0.12	0.21	0.67	0.11	0.12	0.27	1.92	
0.1	0.16	0.19	0.39	1.37	0.16	0.20	0.60	5.72	
0.3	0.24	0.31	0.70	2.92	0.24	0.33	1.43	13.79	
1.0	0.41	0.55	1.40	7.86	0.41	0.61	3.86	31.25	
				h_{AI}	$O_A = 2.0$				
\tilde{K}_{AD_A}	0.0	1.0	10.0	100.0	0.0	1.0	10.0	100.0	
0.01	0.07	0.08	0.17	0.53	0.07	0.09	0.22	1.37	
0.03	0.10	0.13	0.30	1.01	0.10	0.14	0.47	3.89	
0.1	0.17	0.24	0.58	2.24	0.17	0.27	1.36	11.61	
0.3	0.32	0.45	1.13	5.63	0.32	0.53	4.34	34.34	
1.0	0.72	1.00	2.64	18.21	0.72	1.16	10.10	84.06	

Table S5: Response time of gene C in I1-FFLs and type-1 two-input circuits with different values of \tilde{K}_{AD_A} , h_{AD_A} , and $\tilde{\eta}_{AD_A}$ (values rounded to two decimal places). Related to Figure 2B. \tilde{K}_{BC} = 0.1, h_{BC} = 1.0.

		14-	FFL		Тур	pe-4 Two	o-Input Ci	rcuit
				h_{AI}	$D_A = 0.5$			
\tilde{K}_{AD_A}	0.0	1.0	10.0	100.0	0.0	1.0	10.0	100.0
0.01	0.36	0.36	0.38	0.57	0.36	0.36	0.38	0.58
0.03	0.51	0.52	0.57	1.12	0.51	0.52	0.58	1.15
0.1	0.68	0.70	0.87	2.45	0.68	0.70	0.88	2.68
0.3	0.83	0.88	1.33	5.39	0.83	0.88	1.36	5.97
1.0	0.97	1.11	2.29	13.21	0.97	1.11	2.35	14.05
				h_{AI}	$D_A = 1.0$			
\tilde{K}_{AD_A}	0.0	1.0	10.0	100.0	0.0	1.0	10.0	100.0
0.01	0.07	0.08	0.11	0.33	0.07	0.08	0.11	0.33
0.03	0.19	0.21	0.32	1.00	0.19	0.21	0.32	1.05
0.1	0.48	0.52	0.90	3.48	0.48	0.53	0.92	5.34
0.3	0.87	1.00	2.04	10.9	0.87	1.00	2.15	13.79
1.0	1.27	1.60	4.17	29.04	1.27	1.61	4.39	31.25
				h_{AI}	$D_A = 2.0$			
\tilde{K}_{AD_A}	0.0	1.0	10.0	100.0	0.0	1.0	10.0	100.0
0.01	0.01	0.01	0.02	0.05	0.01	0.01	0.02	0.05
0.03	0.03	0.04	0.09	0.26	0.03	0.04	0.09	0.26
0.1	0.15	0.22	0.52	1.87	0.15	0.22	0.53	2.25
0.3	0.68	0.96	2.69	16.90	0.68	0.97	3.33	34.35
1.0	1.72	2.58	9.37	77.33	1.72	2.62	10.11	84.06

Table S6: Response time of gene C in I4-FFLs and type-4 two-input circuits with different values of \tilde{K}_{AD_A} , h_{AD_A} , and $\tilde{\eta}_{AD_A}$ (values rounded to two decimal places). Related to Figure 2B. \tilde{K}_{BC} = 0.1, h_{BC} = 1.0.

		l1-	FFL		Тур	e-1 Two	-Input C	ircuit
				h_{AD}	A = 0.5			
\tilde{K}_{AD_A}	0.0	1.0	10.0	100.0	0.0	1.0	10.0	100.0
0.01	0.12	0.12	0.12	0.12	0.12	0.12	0.11	0.09
0.03	0.12	0.12	0.12	0.11	0.12	0.12	0.11	0.08
0.1	0.12	0.12	0.12	0.10	0.12	0.12	0.10	0.08
0.3	0.12	0.12	0.11	0.09	0.12	0.11	0.08	0.08
1.0	0.11	0.10	0.09	0.08	0.11	0.10	0.08	0.08
				h_{AD}	A = 1.0			
\tilde{K}_{AD_A}	0.0	1.0	10.0	100.0	0.0	1.0	10.0	100.0
0.01	0.15	0.15	0.15	0.14	0.15	0.15	0.13	0.10
0.03	0.15	0.15	0.14	0.12	0.15	0.14	0.12	0.09
0.1	0.14	0.14	0.13	0.10	0.14	0.13	0.10	0.09
0.3	0.13	0.13	0.11	0.09	0.13	0.11	0.09	0.09
1.0	0.11	0.10	0.09	NA	0.11	0.09	0.08	NA
				h_{AD}	A = 2.0			
\tilde{K}_{AD_A}	0.0	1.0	10.0	100.0	0.0	1.0	10.0	100.0
0.01	0.15	0.15	0.15	0.14	0.15	0.15	0.12	0.09
0.03	0.15	0.15	0.15	0.11	0.15	0.14	0.11	0.09
0.1	0.15	0.15	0.13	0.09	0.15	0.13	0.09	0.09
0.3	0.14	0.13	0.10	0.09	0.14	0.10	0.09	NA
1.0	0.10	0.10	0.08	NA	0.10	0.08	NA	NA

Table S7: Pulse amplitude of gene C in I1-FFLs and type-1 two-input circuits with different values of \tilde{K}_{AD_A} , h_{AD_A} , and $\tilde{\eta}_{AD_A}$ (values rounded to two decimal places). Related to Figure 2B. $\tilde{K}_{BC} = 0.1$, $h_{BC} = 1.0$. Here, a trajectory is considered to contain a pulse if the the trajectory maximum is larger than the pre-induction and post-induction steady states. A trajectory not satisfying this criteria is labeled as "NA".

		14-	FFL		Тур	e-4 Two	-Input C	rcuit
		$h_{AD_A} = 0.5$						
\tilde{K}_{AD_A}	0.0	1.0	10.0	100.0	0.0	1.0	10.0	100.0
0.01	0.57	0.57	0.57	0.57	0.57	0.57	0.57	0.55
0.03	0.57	0.57	0.57	0.57	0.57	0.57	0.57	0.52
0.1	0.55	0.55	0.55	0.54	0.55	0.55	0.54	0.53
0.3	0.50	0.50	0.50	0.50	0.50	0.50	0.50	0.50
1.0	0.41	0.41	0.41	0.42	0.41	0.41	0.41	0.42
				h_{AD}	$o_A = 1.0$			
\tilde{K}_{AD_A}	0.0	1.0	10.0	100.0	0.0	1.0	10.0	100.0
0.01	0.62	0.62	0.62	0.62	0.62	0.62	0.61	0.54
0.03	0.62	0.62	0.62	0.60	0.62	0.61	0.60	0.37
0.1	0.60	0.60	0.60	0.57	0.60	0.59	0.54	0.43
0.3	0.56	0.56	0.55	0.54	0.56	0.55	0.54	0.54
1.0	0.42	0.42	0.42	NA	0.42	0.42	0.42	NA
				h_{AD}	$Q_A = 2.0$			
\tilde{K}_{AD_A} $\tilde{\eta}_{AD_A}$	0.0	1.0	10.0	100.0	0.0	1.0	10.0	100.0
0.01	0.62	0.62	0.62	0.62	0.62	0.62	0.61	0.43
0.03	0.62	0.62	0.62	0.60	0.62	0.62	0.57	0.16
0.1	0.62	0.62	0.62	0.56	0.62	0.60	0.42	0.09
0.3	0.60	0.60	0.57	0.54	0.60	0.56	0.42	NA
1.0	0.42	0.42	NA	NA	0.42	0.42	NA	NA

Table S8: Pulse amplitude of gene C in I4-FFLs and type-4 two-input circuits with different values of \tilde{K}_{AD_A} , h_{AD_A} , and $\tilde{\eta}_{AD_A}$ (values rounded to two decimal places). Related to Figure 2B. $\tilde{K}_{BC}=0.1$, $h_{BC}=1.0$. Here, a trajectory is considered to contain a pulse if the the trajectory maximum is larger than the pre-induction and post-induction steady states. A trajectory not satisfying this criteria is labeled as "NA".

	Re	sponse Ti	me	argmax_t	$\operatorname{argmax}_t b(\tilde{x}_B)$		
$ ilde{\eta}_{BD_B}$	1.0	10.0	100.0	1.0	10.0	100.0	
0.01	0.001	0.001	0.001	0.0543	0.1483	0.7416	
0.03	0.0098	0.0098	0.0098	0.1058	0.3187	1.9157	
0.1	0.037	0.037	0.037	0.2394	0.8322	6.0376	
0.3	0.1326	0.1322	0.1321	0.579	2.3339	19.2472	
1.0	0.5004	0.4952	0.4934	2.2718	11.0335	98.8473	

Table S9: Response time and time at which $b(\tilde{x}_B)$ attains its maximum for the I1-FFL model with h_{BC} = 2. Related to Figure 4A.

	I1-FFL			I4-F		
$ ilde{\eta}_{BD_B}$	1.0	10.0	100.0	1.0	10.0	100.0
0.01	Υ	Υ	Υ	N	N	N
0.03	Υ	Υ	Υ	Ν	Ν	Ν
0.1	Υ	Υ	Υ	Υ	Υ	Υ
0.3	Υ	Υ	Υ	Υ	Υ	Υ
1.0	N	Ν	Ν	Ν	Ν	Ν

Table S10: Whether \tilde{x}_B transitions from a value lower (higher) than \tilde{K}_{BC} to a value higher (lower) than \tilde{K}_{BC} for an I1-FFL (I4-FFL) model with h_{BC} = 2. Related to Figure 4B. Y stands for yes; N stands for no.

		l1-	FFL			14-	FFL	
		$h_{BD_B} = 0.5$						
\tilde{K}_{BD_B}	0.0	1.0	10.0	100.0	0.0	1.0	10.0	100.0
0.03	1.22	1.22	1.22	1.23	3.56	3.56	3.55	3.45
0.1	1.55	1.55	1.55	1.54	3.56	3.55	3.5	3.07
0.3	1.93	1.93	1.93	1.9	3.51	3.49	3.3	2.84
1.0	2.37	2.36	2.34	2.29	3.44	3.38	3.05	2.83
3.0	2.71	2.7	2.65	2.61	3.4	3.3	3.02	2.93
				h_{BL}	$O_B = 1.0$			
\tilde{K}_{BD_B}	0.0	1.0	10.0	100.0	0.0	1.0	10.0	100.0
0.03	NA	NA	NA	NA	3.71	3.7	3.68	3.43
0.1	0.34	0.34	0.34	0.34	3.96	3.93	3.51	2.5
0.3	1.44	1.44	1.42	1.39	3.7	3.45	2.37	2.14
1.0	2.48	2.44	2.34	2.29	3.16	2.91	2.53	2.45
3.0	3.1	3.04	2.93	2.89	3.23	3.12	2.96	2.92
				h_{BL}	$O_B = 2.0$			
\tilde{K}_{BD_B}	0.0	1.0	10.0	100.0	0.0	1.0	10.0	100.0
0.03	NA	NA	NA	NA	3.61	3.6	3.6	3.5
0.1	NA	NA	NA	NA	4.71	4.65	2.71	2.15
0.3	0.3	0.3	0.3	0.3	5.68	1.14	0.99	0.97
1.0	2.88	2.59	2.39	2.35	2.45	2.36	2.27	2.24
3.0	3.42	3.36	3.26	3.24	3.26	3.24	3.22	3.2

Table S11: Response time of gene C in IFFL models under the assumption of OR logic with different values of \tilde{K}_{BD_B} , h_{BD_B} , and $\tilde{\eta}_{BD_B}$ (values rounded to two decimal places). Related to Figure 4C. Values of the other parameters are: $\tilde{K}_{AB} = \tilde{K}_{AC} = 0.1$, $h_{AB} = h_{AC} = 1.0$. In response to an OFF step, \tilde{x}_C transitions from a high pre-stimulus state to a low post-stimulus state in I1-FFLs, I4-FLLs, and their simple regulation counterparts. NA represents cases where the post-induction steady state and the mid-point are larger than the pre-induction steady state.

	E. coli	mouse	human
\overline{N}	2870	1858	2072
E	8149	4197	5071
k_+	0.71	0.68	0.62
k_{-}	0.29	0.32	0.38
$\hat{N_G}$	1258	470	1171
$< N_G >$	10.60	5.49	7.23
$\frac{\hat{N_G}}{\langle N_G \rangle}$	118.68	85.61	161.96

Table S12: Number of IFFLs in real and randomized *E. coli*, mouse, and human TRNs. Related to Figure 3 and Transparent Methods Section 15.

	E. coli	mouse	human
\overline{N}	2870	1858	2072
E	8149	4197	5071
k_{-}	0.29	0.32	0.38
$\hat{N_G}$	86	5	4
$< N_G >$	0.82	0.72	0.93
$\frac{\hat{N_G}}{\langle N_G \rangle}$	104.88	6.94	4.30

Table S13: Number of negative autoregulatory loops in real and randomized *E. coli*, mouse, and human TRNs. Related to Figure 3 and Transparent Methods Section 15.

	E. coli	mouse	human
\overline{N}	2870	1858	2072
E	8149	4197	5071
k_+	0.71	0.68	0.62
k_{-}	0.29	0.32	0.38
$\hat{N_G}$	8	20	26
$< N_G >$	1.66	1.11	1.41
$\frac{\hat{N_G}}{\langle N_G \rangle}$	4.82	18.02	18.44

Table S14: Number of two-node NFBLs in real and randomized *E. coli*, mouse, and human TRNs. Related to Figure 3 and Transparent Methods Section 15.

Transparent Methods

1 Hill Function

Hill functions are commonly used to model transcriptional regulation in ODE models. Here, we consider the case where species x_i is regulated by multiple TFs. Let m_i be the number of parents of node i and M_i be the collection of all nonempty subsets of \vec{p}_i , i.e., $\{1,2,...,m_i\}$. Then under the assumption of independent binding, $H_i(\vec{p}_i)$ can be expressed as:

$$H_i(\vec{p}_i) = \frac{\sum_{X \in M_i} \pi_{i,X} \prod_{j \in X} \left(\frac{p_{ij}}{K_{ij}}\right)^{h_{ij}}}{1 + \sum_{X \in M_i} \prod_{j \in X} \left(\frac{p_{ij}}{K_{ij}}\right)^{h_{ij}}},\tag{1}$$

where p_{ij} , h_{ij} , and K_{ij} are counterparts of p_i , h_i , K_i for the j-th parent of node i. Similar to a previous study (Gyorgy and Del Vecchio, 2014), here we assume that no parents of the same node are identical. X corresponds to each complex formed by a different combination of TFs, and $\pi_{i,X}$ denotes the normalized production rate of species x_i due to the corresponding complex.

Under the assumption of AND logic, the regulated gene is turned on only when all the corresponding activators aggregate and bind to the promoter. Let $M_{i,A} = \{j | j \in \{1,2,...,m_i\}$ and p_{ij} is an activator} denote the complex formed by all the activators. Then

$$\pi_{i,X} = \begin{cases} 1, & \text{if } X = M_{i,A}, \\ 0, & \text{otherwise.} \end{cases}$$
 (2)

2 Retroactivity Matrix

Under the assumption of AND logic, $R_i(\vec{p}_i)$ is a diagonal matrix, and the k-th entry on the diagonal r_{ik} is (Gyorgy and Del Vecchio, 2014):

$$r_{ik} = \eta_i \frac{h_{ik}^2 p_{ik}^{h_{ik}-1}}{K_{ik}^{h_{ik}}} \left(1 + \left(\frac{p_{ik}}{K_{ik}} \right)^{h_{ik}} \right)^{-2}, \tag{3}$$

where η_i stands for the number of downstream binding sites (DNA copy number) of node i. p_{ik} , h_{ik} , and K_{ik} are the protein concentration, the Hill coefficient, and the dissociation coefficient of the k-th parent of node i.

3 Proof of Diagonality

Here, we prove that $V_i^T R_i(\vec{p}_i) V_i$ is a diagonal matrix. Let V_i^T be an $n \times m$ matrix and a_{kj} denote the (k,j)-th entry of V_i^T . Recall that each row of V_i has only one non-zero entry by definition. Similarly, let $R_i(\vec{p}_i)$ be an $m \times m$ diagonal matrix and $x_{k'j'}$ denote the (k',j')-th entry of $R_i(\vec{p}_i)$. This implies that the product $V_i^T R_i(\vec{p}_i)$ is an $n \times m$ matrix. The (k^*,j^*) -th entry of the product $V_i^T R_i(\vec{p}_i)$ can be expressed as:

$$\sum_{u=1}^{m} a_{k^*u} x_{uj^*} = a_{k^*j^*} x_{j^*j^*},$$

as $R_i(\vec{p_i})$ is diagonal. The (\hat{k}, \hat{j}) -th entry of the product $V_i^T R_i(\vec{p_i}) V_i$ can be expressed as:

$$\sum_{\nu=1}^{n} \left(a_{\hat{k}\nu} x_{\nu\nu} \right) a_{\hat{j}\nu} = \sum_{\nu=1}^{n} \left(a_{\hat{k}\nu} a_{\hat{j}\nu} \right) x_{\nu\nu}.$$

Here $a_{\hat{k}v}a_{\hat{j}v}=0$ for $\hat{k}\neq\hat{j}$ as otherwise there would be two non-zero entries in the same row of V_i , which contradicts the definition of V_i . Hence, the (\hat{k},\hat{j}) -th entry of the product $V_i^TR_i(\vec{p}_i)V_i$ is always zero if $\hat{k}\neq\hat{j}$. In other words, $V_i^TR_i(\vec{p}_i)V_i$ is a diagonal matrix.

4 ODE Models for IFFL

Without retroactivity, the ODE model for the I1-FFL is given as:

$$\frac{dx_A}{dt} = f_A = \beta_A \left[\left(1 - \gamma_A \right) \frac{\left(\frac{x_I}{K_{IA}} \right)^{h_{IA}}}{1 + \left(\frac{x_I}{K_{IA}} \right)^{h_{IA}}} + \gamma_A \right] - \delta_A x_A$$

$$\frac{dx_B}{dt} = f_B = \beta_B \left[\left(1 - \gamma_B \right) \frac{\left(\frac{x_A}{K_{AB}} \right)^{h_{AB}}}{1 + \left(\frac{x_A}{K_{AB}} \right)^{h_{AB}}} + \gamma_B \right] - \delta_B x_B$$

$$\frac{dx_C}{dt} = f_C = \beta_C \left[\left(1 - \gamma_C \right) \frac{\left(\frac{x_A}{K_{AC}} \right)^{h_{AC}}}{\left(1 + \left(\frac{x_A}{K_{AC}} \right)^{h_{AC}} \right) \left(1 + \left(\frac{x_B}{K_{BC}} \right)^{h_{BC}}} + \gamma_C \right] - \delta_C x_C.$$

I2-FFL:

$$\begin{aligned}
\frac{dx_A}{dt} &= f_A = \beta_A \left[\left(1 - \gamma_A \right) \frac{\left(\frac{x_I}{K_{IA}} \right)^{h_{IA}}}{1 + \left(\frac{x_I}{K_{IA}} \right)^{h_{IA}}} + \gamma_A \right] - \delta_A x_A \\
\frac{dx_B}{dt} &= f_B = \beta_B \left[\frac{1 - \gamma_B}{1 + \left(\frac{x_A}{K_{AB}} \right)^{h_{AB}}} + \gamma_B \right] - \delta_B x_B \\
\frac{dx_C}{dt} &= f_C = \beta_C \left[\frac{1 - \gamma_C}{\left(1 + \left(\frac{x_A}{K_{AC}} \right)^{h_{AC}} \right) \left(1 + \left(\frac{x_B}{K_{BC}} \right)^{h_{BC}} \right)} + \gamma_C \right] - \delta_C x_C.
\end{aligned}$$

I3-FFL:

$$\frac{dx_A}{dt} = f_A = \beta_A \left[\left(1 - \gamma_A \right) \frac{\left(\frac{x_I}{K_{IA}} \right)^{h_{IA}}}{1 + \left(\frac{x_I}{K_{IA}} \right)^{h_{IA}}} + \gamma_A \right] - \delta_A x_A$$

$$\frac{dx_B}{dt} = f_B = \beta_B \left[\left(1 - \gamma_B \right) \frac{\left(\frac{x_A}{K_{AB}} \right)^{h_{AB}}}{1 + \left(\frac{x_A}{K_{AB}} \right)^{h_{AB}}} + \gamma_B \right] - \delta_B x_B$$

$$\frac{dx_C}{dt} = f_C = \beta_C \left[\left(1 - \gamma_C \right) \frac{\left(\frac{x_B}{K_{AC}} \right)^{h_{BC}}}{\left(1 + \left(\frac{x_A}{K_{AC}} \right)^{h_{AC}} \right) \left(1 + \left(\frac{x_B}{K_{BC}} \right)^{h_{BC}}} + \gamma_C \right] - \delta_C x_C.$$

I4-FFL:

$$\frac{dx_A}{dt} = f_A = \beta_A \left[\left(1 - \gamma_A \right) \frac{\left(\frac{x_I}{K_{IA}} \right)^{h_{IA}}}{1 + \left(\frac{x_I}{K_{IA}} \right)^{h_{IA}}} + \gamma_A \right] - \delta_A x_A$$

$$\frac{dx_B}{dt} = f_B = \beta_B \left[\frac{1 - \gamma_B}{1 + \left(\frac{x_A}{K_{AB}} \right)^{h_{AB}}} + \gamma_B \right] - \delta_B x_B$$

$$\frac{dx_C}{dt} = f_C = \beta_C \left[\left(1 - \gamma_C \right) \frac{\left(\frac{x_A}{K_{AC}} \right)^{h_{AC}} \left(\frac{x_B}{K_{BC}} \right)^{h_{BC}}}{\left(1 + \left(\frac{x_A}{K_{AC}} \right)^{h_{AC}} \right) \left(1 + \left(\frac{x_B}{K_{BC}} \right)^{h_{BC}}} + \gamma_C \right] - \delta_C x_C.$$

When only retroactivity on A is considered, the retroactivity matrix $R(\vec{x})$, which is the same for all four IFFLs, is calculated as (Gyorgy and Del Vecchio, 2014):

$$R(\vec{x}) = \begin{bmatrix} \eta_{D_A} \frac{h_{AD_A}^2 x_A^{h_{AD_A} - 1}}{K_{AD_A}^{h_{AD_A}}} \left(1 + \left(\frac{x_A}{K_{AD_A}} \right)^{h_{AD_A}} \right)^{-2} & 0 & 0 \\ & 0 & 0 & 0 \\ & 0 & 0 & 0 \end{bmatrix}.$$

When only retroactivity on B is considered, the retroactivity matrix $R(\vec{x})$, which is the same for all four IFFLs, is calculated as (Gyorgy and Del Vecchio, 2014):

$$R(\vec{x}) = \begin{bmatrix} 0 & 0 & 0 \\ 0 & \eta_{D_B} \frac{h_{BD_B}^2 x_B^{h_{BD_B} - 1}}{K_{BD_B}^{h_{BD_B}}} \left(1 + \left(\frac{x_B}{K_{BD_B}} \right)^{h_{BD_B}} \right)^{-2} & 0 \\ 0 & 0 & 0 \end{bmatrix}.$$

When only retroactivity on C is considered, the retroactivity matrix $R(\vec{x})$, which is the same for all four IFFLs, is calculated as (Gyorgy and Del Vecchio, 2014):

5 Non-dimensionalization and Parameter Sampling

In order to reduce the dimensions of parameter space, we non-dimensionalized our models via methods shown in a previous study (Cao et al., 2016). We rescaled the model parameters via the following equations:

$$\tilde{x}_{A} = \frac{x_{A}\delta_{A}}{\beta_{A}} \qquad \tilde{x}_{B} = \frac{x_{B}\delta_{B}}{\beta_{B}} \qquad \tilde{x}_{C} = \frac{x_{C}\delta_{C}}{\beta_{C}}$$

$$\tilde{K}_{AB} = \frac{K_{AB}\delta_{A}}{\beta_{A}} \qquad \tilde{K}_{AC} = \frac{K_{AC}\delta_{A}}{\beta_{A}} \qquad \tilde{K}_{BC} = \frac{K_{BC}\delta_{B}}{\beta_{B}}$$

$$\tilde{K}_{AD_{A}} = \frac{K_{AD_{A}}\delta_{A}}{\beta_{A}} \qquad \tilde{K}_{BD_{B}} = \frac{K_{BD_{B}}\delta_{B}}{\beta_{B}} \qquad \tilde{K}_{CD_{C}} = \frac{K_{CD_{C}}\delta_{C}}{\beta_{C}}$$

$$\tilde{\eta}_{AD_{A}} = \frac{\eta_{A}}{K_{AD_{A}}} \qquad \tilde{\eta}_{BD_{B}} = \frac{\eta_{B}}{K_{BD_{B}}} \qquad \tilde{\eta}_{CD_{C}} = \frac{\eta_{C}}{K_{CD_{C}}}$$

$$(4)$$

For simplicity, we assumed proteins A, B, and C have equal decay rates, i.e., $\delta_A = \delta_B = \delta_C$. To non-dimensionalize time, we rescaled t against the mean lifetime (equal to the reciprocal of the decay rate):

$$\tau = \frac{t}{\frac{1}{\delta}} = t \cdot \delta. \tag{5}$$

Non-dimensionlized models of IFFLs with and without retroactivity, are provided in Transparent Methods Section 6. To simplify our analysis, we assume the following for all simulations carried out in this work except for extensive simulations as described in Transparent Methods Section 13: each protein binds to its downstream binding sites, including both the functional target site and accessible ND sites, with equal affinity and equal cooperativity, i.e., $\tilde{K}_{AB} = \tilde{K}_{AC} = \tilde{K}_{AD_A}$, $\tilde{K}_{BC} = \tilde{K}_{BD_B}$, $h_{AB} = h_{AC} = h_{AD_A}$, and $h_{BC} = h_{BD_B}$. To ensure sufficient coverage of parameter space, we sampled the kinetic parameters \tilde{K}_{XD_X} (X = A, B, C) spanning two orders of magnitude: $\tilde{K}_{XD_X} \in \{0.01, 0.03, 0.1, 0.3, 1.0\}$ and included both positive and negative cooperative binding, sampling Hill coefficients h_{XD_X} (X = A, B, C) at 0.5, 1,0, and 2.0 (Mangan and Alon, 2003). The retroactivity coefficient $\tilde{\eta}$ is the total concentration of the accessible ND sites for a given TF divided by the corresponding dissociation constant (Wang and Belta, 2019). Without loss of generality, the basal fraction of the promoter that is active, γ_X (X = A, B, C) is assumed to be 10^{-5} .

6 Non-Dimensionalized ODE Models for IFFL

Without retroactivity, the non-dimensionalized ODE model for the I1-FFL is given as:

$$\begin{split} \frac{d\tilde{x}_{A}}{d\tau} &= f_{\tilde{A}} = \left(1 - \gamma_{A}\right) \frac{\left(\frac{x_{I}}{K_{IA}}\right)^{h_{IA}}}{1 + \left(\frac{x_{I}}{K_{IA}}\right)^{h_{IA}}} + \gamma_{A} - \tilde{x}_{A} \\ \frac{d\tilde{x}_{B}}{d\tau} &= f_{\tilde{B}} = \left(1 - \gamma_{B}\right) \frac{\left(\frac{\tilde{x}_{A}}{K_{AB}}\right)^{h_{AB}}}{1 + \left(\frac{\tilde{x}_{A}}{K_{AB}}\right)^{h_{AB}}} + \gamma_{B} - \tilde{x}_{B} \\ \frac{d\tilde{x}_{C}}{d\tau} &= f_{\tilde{C}} = \left(1 - \gamma_{C}\right) \frac{\left(\frac{\tilde{x}_{A}}{K_{AC}}\right)^{h_{AC}}}{\left(1 + \left(\frac{\tilde{x}_{A}}{K_{AC}}\right)^{h_{AC}}\right) \left(1 + \left(\frac{\tilde{x}_{B}}{K_{BC}}\right)^{h_{BC}}\right)} + \gamma_{C} - \tilde{x}_{C}. \end{split}$$

I2-FFL:

$$\begin{split} \frac{d\tilde{x}_A}{d\tau} &= f_{\tilde{A}} = \left(1 - \gamma_A\right) \frac{\left(\frac{x_I}{K_{IA}}\right)^{h_{IA}}}{1 + \left(\frac{x_I}{K_{IA}}\right)^{h_{IA}}} + \gamma_A - \tilde{x}_A \\ \frac{d\tilde{x}_B}{d\tau} &= f_{\tilde{B}} = \frac{1 - \gamma_B}{1 + \left(\frac{\tilde{x}_A}{\tilde{K}_{AB}}\right)^{h_{AB}}} + \gamma_B - \tilde{x}_B \\ \frac{d\tilde{x}_C}{d\tau} &= f_{\tilde{C}} = \frac{1 - \gamma_C}{\left(1 + \left(\frac{\tilde{x}_A}{\tilde{K}_{AC}}\right)^{h_{AC}}\right) \left(1 + \left(\frac{\tilde{x}_B}{\tilde{K}_{BC}}\right)^{h_{BC}}\right)} + \gamma_C - \tilde{x}_C. \end{split}$$

I3-FFL:

$$\begin{split} \frac{d\tilde{x}_A}{d\tau} &= f_{\tilde{A}} = \left(1 - \gamma_A\right) \frac{\left(\frac{x_I}{K_{IA}}\right)^{h_{IA}}}{1 + \left(\frac{x_I}{K_{IA}}\right)^{h_{IA}}} + \gamma_A - \tilde{x}_A \\ \frac{d\tilde{x}_B}{d\tau} &= f_{\tilde{B}} = \left(1 - \gamma_B\right) \frac{\left(\frac{\tilde{x}_A}{\tilde{K}_{AB}}\right)^{h_{AB}}}{1 + \left(\frac{\tilde{x}_A}{\tilde{K}_{AB}}\right)^{h_{AB}}} + \gamma_B - \tilde{x}_B \\ \frac{d\tilde{x}_C}{d\tau} &= f_{\tilde{C}} = \left(1 - \gamma_C\right) \frac{\left(\frac{\tilde{x}_B}{\tilde{K}_{AC}}\right)^{h_{BC}}}{\left(1 + \left(\frac{\tilde{x}_A}{\tilde{K}_{AC}}\right)^{h_{AC}}\right) \left(1 + \left(\frac{\tilde{x}_B}{\tilde{K}_{BC}}\right)^{h_{BC}}\right)} + \gamma_C - \tilde{x}_C. \end{split}$$

I4-FFL:

$$\begin{split} \frac{d\tilde{x}_{A}}{d\tau} &= f_{\tilde{A}} = \left(1 - \gamma_{A}\right) \frac{\left(\frac{x_{I}}{K_{IA}}\right)^{h_{IA}}}{1 + \left(\frac{x_{I}}{K_{IA}}\right)^{h_{IA}}} + \gamma_{A} - \tilde{x}_{A} \\ \frac{d\tilde{x}_{B}}{d\tau} &= f_{\tilde{B}} = \frac{1 - \gamma_{B}}{1 + \left(\frac{\tilde{x}_{A}}{K_{AB}}\right)^{h_{AB}}} + \gamma_{B} - \tilde{x}_{B} \\ \frac{d\tilde{x}_{C}}{d\tau} &= f_{\tilde{C}} = \left(1 - \gamma_{C}\right) \frac{\left(\frac{\tilde{x}_{A}}{K_{AC}}\right)^{h_{AC}} \left(\frac{\tilde{x}_{B}}{K_{BC}}\right)^{h_{BC}}}{\left(1 + \left(\frac{\tilde{x}_{A}}{K_{AC}}\right)^{h_{AC}}\right) \left(1 + \left(\frac{\tilde{x}_{B}}{K_{C}}\right)^{h_{BC}}\right)} + \gamma_{C} - \tilde{x}_{C}. \end{split}$$

 $R(\vec{\tilde{x}})$ with only retroactivity on A can be written as (Gyorgy and Del Vecchio, 2014):

 $R(\vec{x})$ with only retroactivity on B can be written as (Gyorgy and Del Vecchio, 2014):

$$R(\vec{\tilde{x}}) = \begin{bmatrix} 0 & 0 & 0 \\ 0 & \tilde{\eta}_{BD_B} h_{BD_B}^2 \left(\frac{\tilde{x}_B}{\tilde{K}_{BD_B}} \right)^{h_{BD_B} - 1} \left(1 + \left(\frac{\tilde{x}_B}{\tilde{K}_{BD_B}} \right)^{h_{BD_B}} \right)^{-2} & 0 \\ 0 & 0 & 0 \end{bmatrix}.$$

 $R(\vec{x})$ with only retroactivity on C can be written as (Gyorgy and Del Vecchio, 2014):

7 Proof of the Effects of $ilde{\eta}_{BD_R}$ on Response Time and Pulse Amplitude in IFFLs

Here we show that for any parameters, increases in retroactivity on node B, $\tilde{\eta}_{BD_B}$, in an I1-FFL lead to a decrease in response time and an increase in pulse amplitude.

According to Transparent Methods Section 6, $\frac{d\tilde{x}_A}{d\tau}$, $\frac{d\tilde{x}_B}{d\tau}$, and $\frac{d\tilde{x}_C}{d\tau}$ in an I1-FFL where only $\tilde{\eta}_{BD_B}$ is allowed to vary can be expressed as:

$$\begin{bmatrix} \frac{d\tilde{x}_{A}}{d\tau} \\ \frac{d\tilde{x}_{B}}{d\tau} \\ \frac{d\tilde{x}_{C}}{d\tau} \end{bmatrix} = \begin{bmatrix} \frac{1}{1+r_{AD_{A}}(\tilde{x}_{A})} & 0 & 0 \\ 0 & \frac{1}{1+r_{BD_{B}}(\tilde{x}_{B})} & 0 \\ 0 & 0 & \frac{1}{1+r_{CD_{C}}(\tilde{x}_{C})} \end{bmatrix} \begin{bmatrix} f_{\tilde{A}} \\ f_{\tilde{B}} \\ f_{\tilde{C}} \end{bmatrix}, \tag{6}$$

$$f_{\tilde{A}} = \frac{\left(\frac{x_I}{K_{IA}}\right)^{h_{IA}}}{1 + \left(\frac{x_I}{K_{IA}}\right)^{h_{IA}}} (1 - \gamma_A) + \gamma_A - \tilde{x}_A$$

$$f_{\tilde{B}} = \frac{\left(\frac{\tilde{x}_A}{K_{AB}}\right)^{h_{AB}}}{1 + \left(\frac{\tilde{x}_A}{K_{AB}}\right)^{h_{AB}}} (1 - \gamma_B) + \gamma_B - \tilde{x}_B$$

$$f_{\tilde{C}} = \frac{\left(\frac{\tilde{x}_A}{K_{AC}}\right)^{h_{AC}}}{\left(1 + \left(\frac{\tilde{x}_A}{K_{AC}}\right)^{h_{AC}}\right) \left(1 + \left(\frac{\tilde{x}_B}{K_{BC}}\right)^{h_{BC}}\right)} (1 - \gamma_C) + \gamma_C - \tilde{x}_C,$$

$$(7)$$

$$r_{AD_A}(\tilde{x}_A) = \tilde{\eta}_{AD_A} h_{AD_A}^2 \left(\frac{\tilde{x}_A}{\tilde{K}_{AD_A}}\right)^{h_{AD_A} - 1} \left(1 + \left(\frac{\tilde{x}_A}{\tilde{K}_{AD_A}}\right)^{h_{AD_A}}\right)^{-2}$$

$$r_{BD_B}(\tilde{x}_B) = \tilde{\eta}_{BD_B} h_{BD_B}^2 \left(\frac{\tilde{x}_B}{\tilde{K}_{BD_B}}\right)^{h_{BD_B} - 1} \left(1 + \left(\frac{\tilde{x}_B}{\tilde{K}_{BD_B}}\right)^{h_{BD_B}}\right)^{-2}$$

$$r_{CD_C}(\tilde{x}_C) = \tilde{\eta}_{CD_C} h_{CD_C}^2 \left(\frac{\tilde{x}_C}{\tilde{K}_{CD_C}}\right)^{h_{CD_C} - 1} \left(1 + \left(\frac{\tilde{x}_C}{\tilde{K}_{CD_C}}\right)^{h_{CD_C}}\right)^{-2},$$

$$(8)$$

where $\gamma_A, \gamma_B, \gamma_C \in (0, 1)$ such that $\tilde{x}_A, \tilde{x}_B, \tilde{x}_C \in (0, 1)$.

Let $\vec{x_1}$ and $\vec{x_2}$ denote the concentrations of A, B, and C in two I1-FFL models (i.e., $\vec{x_1} = [\tilde{x}_{A_1}, \tilde{x}_{B_1}, \tilde{x}_{C_1}]$, $\vec{x_2} = [\tilde{x}_{A_2}, \tilde{x}_{B_2}, \tilde{x}_{C_2}]$), in which all parameters are held identical except that node B is connected to different numbers of downstream targets such that retroactivity coefficient $\tilde{\eta}_{BD_B}$ equals $\tilde{\eta}_{BD_{B_1}}$ and $\tilde{\eta}_{BD_{B_2}}$, respectively. At $\tau = 0$, x_I undergoes a stepwise increase and is kept constant afterwards. The initial values of \tilde{x}_A , \tilde{x}_{B_i} (i = 1, 2), and \tilde{x}_C are the corresponding steady values before the increase in x_I . Without loss of generality, we assume $\tilde{\eta}_{BD_{B_1}} < \tilde{\eta}_{BD_{B_2}}$. We now show that $\forall \tau > 0$, $\tilde{x}_{C_1}(\tau) < \tilde{x}_{C_2}(\tau)$, i.e., the concentration of C in I1-FFL model #1 is less than the concentration of C in I1-FFL model #2 at all positive times.

First, we prove the following two lemmas:

Lemma 1. Let $\frac{d\tilde{x}}{d\tau} = g(\tilde{x})(c - \tilde{x})$. If $0 < \tilde{x}(0) < c$, and $g(\tilde{x})$ is positive and smooth for all $\tilde{x} \in (0, \infty)$, then $\frac{d\tilde{x}}{d\tau} > 0$ for all $\tau \ge 0^+$.

Proof. It is clear that \tilde{x} has a unique steady state equal to c for $\tilde{x} \in (0,\infty)$. Because $\frac{d\tilde{x}}{d\tau} > 0$ for $\tilde{x} < c$ and $0 < \tilde{x}(0) < c$, we have $\frac{d\tilde{x}}{d\tau} > 0$ for all $\tau \ge 0^+$.

Lemma 2. Suppose that a smooth function $h(\tau)$ defined on $[0,\infty)$ satisfies the following properties: (i) there exists a positive integer k such that $\frac{d^k h}{d\tau^k}(0^+) > 0$ and $\frac{d^i h}{d\tau^i}(0^+) = 0$ for all i = 0, 1, 2, ..., k-1; (ii) for any τ^* in $(0,\infty)$ where $h(\tau^*) = 0$ we always have $\frac{dh}{d\tau}(\tau^*) > 0$. Then $h(\tau) > 0$ for all $\tau > 0$.

Proof. Property (i) of $h(\tau)$ implies that $h(\tau) > 0$ on some interval $(0, \delta)$. Let (0, T) be the largest interval where $h(\tau) > 0$. We claim that $T = \infty$. If $T < \infty$, then by continuity, h(T) = 0. We immediately arrive at a contradiction as property (ii) implies that $h(\tau)$ for τ near but less than T cannot be decreasing.

Theorem 1. $\forall \tau > 0$, $\tilde{x}_{C_1}(\tau) < \tilde{x}_{C_2}(\tau)$.

Proof. We begin by showing that \tilde{x}_A and \tilde{x}_B are monotonically increasing in time. Based on (7), we know $0 < \tilde{x}_A(0) < \tilde{x}_{A_{ss}}$ for nonzero x_I . From Lemma 1 it follows that $\frac{d\tilde{x}_A}{d\tau} > 0$ for all $\tau \ge 0^+$.

Let $H_{\tilde{A}}(\tilde{x}_A) = \frac{\left(\frac{\tilde{x}_A}{\tilde{K}_{AB}}\right)^{h_{AB}}}{1 + \left(\frac{\tilde{x}_A}{\tilde{K}_{AB}}\right)^{h_{AB}}}$. Assume that there exists $\tau^* \ge 0^+$ at which $f_{\tilde{B}}(\tau^*) = 0$. Using that $f_{\tilde{B}}(\tau^*) = 0$, $\frac{dH_A(\tilde{x}_A)}{d\tilde{x}_A} > 0$ for $\tilde{x}_A > 0$, and $\frac{d\tilde{x}_A}{d\tau} > 0$ for $\tau \ge 0^+$, we get

$$\begin{split} \frac{d^2\tilde{x}_B}{d\tau^2}\bigg|_{\tau=\tau^*} &= \frac{d}{d\tau} \left[\frac{1}{1+r_{BD_B}(\tilde{x}_B)} f_{\tilde{B}}\right]\bigg|_{\tau=\tau^*} \\ &= \frac{d}{d\tau} \left[\frac{1}{1+r_{BD_B}(\tilde{x}_B)}\right] \cdot f_{\tilde{B}}\bigg|_{\tau=\tau^*} + \frac{1}{1+r_{BD_B}(\tilde{x}_B)} \cdot \frac{df_{\tilde{B}}}{d\tau}\bigg|_{\tau=\tau^*} \\ &= \frac{1}{1+r_{BD_B}(\tilde{x}_B)} \cdot \frac{df_{\tilde{B}}}{d\tau}\bigg|_{\tau=\tau^*} \\ &= \frac{1}{1+r_{BD_B}(\tilde{x}_B)} \cdot \left[\frac{dH_A(\tilde{x}_A)}{d\tau} (1-\gamma_B) - \frac{d\tilde{x}_B}{d\tau}\right]\bigg|_{\tau=\tau^*} \\ &= \frac{1}{1+r_{BD_B}(\tilde{x}_B)} \frac{dH_A(\tilde{x}_A)}{d\tilde{x}_A} \frac{d\tilde{x}_A}{d\tau} (1-\gamma_B)\bigg|_{\tau=\tau^*} > 0. \end{split}$$

Because (i) $\frac{d\tilde{x}_B}{d\tau}\Big|_{\tau=0^+}=0$, $\frac{d^2\tilde{x}_B}{d\tau^2}\Big|_{\tau=0^+}>0$ (ii) $\frac{d^2\tilde{x}_B}{d\tau^2}\Big|_{\tau=\tau^*}>0$ wherever $\frac{d\tilde{x}_B}{d\tau}\Big|_{\tau=\tau^*}=0$ and $\tau^*>0$, based on Lemma 2 we know that $\frac{d\tilde{x}_B}{d\tau}>0$ for all $\tau>0$.

Next, we will show that $\forall \tau > 0$, $\tilde{x}_{B_1}(\tau) > \tilde{x}_{B_2}(\tau)$. Let $w_B(\tau) = \tilde{x}_{B_1}(\tau) - \tilde{x}_{B_2}(\tau)$. Based on (7), we know that $\tilde{x}_{B_1}(0^+) = \tilde{x}_{B_2}(0^+)$, i.e., $w_B(0^+) = 0$. Consider any $\tau^* \geq 0^+$ at which $w_B(\tau^*) = 0$, i.e., $\tilde{x}_{B_1}(\tau^*) = \tilde{x}_{B_2}(\tau^*)$. Because $\tilde{\eta}_{BD_{B_1}} < \tilde{\eta}_{BD_{B_2}}$, based on (8) we know $\frac{1}{1+r_{BD_{B_1}}(\tilde{x}_{B_1})}\Big|_{\tau=\tau^*} > \frac{1}{1+r_{BD_{B_2}}(\tilde{x}_{B_2})}\Big|_{\tau=\tau^*}$. Hence,

$$\begin{split} \frac{dw_B}{d\tau}\bigg|_{\tau=\tau^*} &= \frac{d}{d\tau} \left[\tilde{x}_{B_1} - \tilde{x}_{B_2} \right] \bigg|_{\tau=\tau^*} \\ &= \left[\frac{1}{1 + r_{BD_{B_1}}(\tilde{x}_{B_1})} f_{\tilde{B}_1} - \frac{1}{1 + r_{BD_{B_2}}(\tilde{x}_{B_2})} f_{\tilde{B}_2} \right] \bigg|_{\tau=\tau^*} \\ &= \left(\frac{1}{1 + r_{BD_{B_1}}(\tilde{x}_B)} - \frac{1}{1 + r_{BD_{B_2}}(\tilde{x}_B)} \right) f_{\tilde{B}} \bigg|_{\tau=\tau^*} \\ &= 0, \quad \text{if } \tau^* = 0^+ \quad \text{as } f_{\tilde{B}} \bigg|_{\tau=0^+} = 0 \\ &> 0, \quad \text{if } \tau^* > 0 \quad \text{as } \frac{d\tilde{x}_B}{d\tau} > 0 \text{ for } \tau > 0 \Longrightarrow f_{\tilde{B}} \bigg|_{\tau=\tau^*} > 0. \end{split}$$

If $\tau^* = 0^+$, we can further show that

$$\begin{split} \frac{d^2 w_B}{d\tau^2} \bigg|_{\tau=0^+} &= \left. \frac{d^2}{d\tau^2} \left[\tilde{x}_{B_1} - \tilde{x}_{B_2} \right] \right|_{\tau=0^+} \\ &= \left(\frac{1}{1 + r_{BD_{B_1}}(\tilde{x}_B)} - \frac{1}{1 + r_{BD_{B_2}}(\tilde{x}_B)} \right) \frac{dH_A(\tilde{x}_A)}{d\tilde{x}_A} \frac{d\tilde{x}_A}{d\tau} (1 - \gamma_B) \bigg|_{\tau=0^+} > 0. \end{split}$$

Now because (i) $w_B(0^+) = 0$, $\frac{dw_B}{d\tau}\Big|_{\tau=0^+} = 0$, $\frac{d^2w_B}{d\tau^2}\Big|_{\tau=0^+} > 0$ (ii) $\frac{dw_B}{d\tau}\Big|_{\tau=\tau^*} > 0$ wherever $w_B(\tau^*) = 0$ and $\tau^* > 0$, based on Lemma 2 we know that $w_B(\tau) > 0$, i.e., $\tilde{x}_{B_1}(\tau) > \tilde{x}_{B_2}(\tau)$ for all $\tau > 0$.

Finally, we will show that $\forall \tau > 0$, $\tilde{x}_{C_1}(\tau) < \tilde{x}_{C_2}(\tau)$. Let $w_C(\tau) = \tilde{x}_{C_2}(\tau) - \tilde{x}_{C_1}(\tau)$. Based on (7), we know $\tilde{x}_{C_1}(0^+) = \tilde{x}_{C_2}(0^+)$, i.e., $w_C(0^+) = 0$. Consider any $\tau^* \geq 0^+$ at which $w_C(\tau^*) = 0$, i.e., $\tilde{x}_{C_1}(\tau^*) = \tilde{x}_{C_2}(\tau^*)$. Let $\tilde{x}_C = \tilde{x}_{C_1}(\tau^*) = \tilde{x}_{C_2}(\tau^*)$.

$$\left. \frac{dw_C}{d\tau} \right|_{\tau=\tau^*} = \left. \frac{1}{1 + r_{CD_C}(\tilde{x}_C)} \left(f_{\tilde{C}_2} - f_{\tilde{C}_1} \right) \right|_{\tau=\tau^*}.$$

If $\tau^* > 0^+$, then $\tilde{x}_{B_1}(\tau^*) > \tilde{x}_{B_2}(\tau^*)$, which based on (7) indicates that $f_{\tilde{C}_2}(\tau^*) > f_{\tilde{C}_1}(\tau^*)$. In this case, $\frac{dw_C}{d\tau}\Big|_{\tau=\tau^*} > 0$.

Now consider the case where $\tau^* = 0^+$. Because $\tilde{x}_{B_1}(0^+) = \tilde{x}_{B_2}(0^+)$ and $\tilde{x}_{C_1}(0^+) = \tilde{x}_{C_2}(0^+)$, we know that $\forall n \in \mathbb{N}, \ \frac{\partial^n}{\partial \tilde{x}_i^n} \left(\frac{d\tilde{x}_{C_1}}{d\tau}\right)\Big|_{\tau=0^+} = \frac{\partial^n}{\partial \tilde{x}_i^n} \left(\frac{d\tilde{x}_{C_2}}{d\tau}\right)\Big|_{\tau=0^+}$ ($i = A, B_1, B_2, C_1, C_2$). Using the chain rule we can further show that

$$\begin{split} \frac{d^2 w_C}{d\tau^2} \bigg|_{\tau=0^+} &= \frac{d}{d\tau} \left(\frac{d\tilde{x}_{C_2}}{d\tau} \right) - \frac{d}{d\tau} \left(\frac{d\tilde{x}_{C_1}}{d\tau} \right) \bigg|_{\tau=0^+} \\ &= \frac{\partial}{\partial \tilde{x}_A} \left(\frac{d\tilde{x}_{C_2}}{d\tau} \right) \frac{d\tilde{x}_A}{d\tau} + \frac{\partial}{\partial \tilde{x}_{B_2}} \left(\frac{d\tilde{x}_{C_2}}{d\tau} \right) \frac{d\tilde{x}_{B_2}}{d\tau} + \frac{\partial}{\partial \tilde{x}_{C_2}} \left(\frac{d\tilde{x}_{C_2}}{d\tau} \right) \frac{d\tilde{x}_{C_2}}{d\tau} \\ &- \frac{\partial}{\partial \tilde{x}_A} \left(\frac{d\tilde{x}_{C_1}}{d\tau} \right) \frac{d\tilde{x}_A}{d\tau} - \frac{\partial}{\partial \tilde{x}_{B_1}} \left(\frac{d\tilde{x}_{C_1}}{d\tau} \right) \frac{d\tilde{x}_{B_1}}{d\tau} - \frac{\partial}{\partial \tilde{x}_{C_1}} \left(\frac{d\tilde{x}_{C_1}}{d\tau} \right) \frac{d\tilde{x}_{C_1}}{d\tau} \bigg|_{\tau=0^+} \\ &= \frac{\partial}{\partial \tilde{x}_A} \left(\frac{d\tilde{x}_{C_2}}{d\tau} \right) \frac{d\tilde{x}_A}{d\tau} - \frac{\partial}{\partial \tilde{x}_A} \left(\frac{d\tilde{x}_{C_1}}{d\tau} \right) \frac{d\tilde{x}_A}{d\tau} \bigg|_{\tau=0^+} = 0, \end{split}$$

$$\begin{split} \frac{d^3w_C}{d\tau^3}\Big|_{\tau=0^+} &= \frac{d^2}{d\tau^2} \left(\frac{d\tilde{x}_{C_2}}{d\tau}\right) - \frac{d^2}{d\tau^2} \left(\frac{d\tilde{x}_{C_1}}{d\tau}\right)\Big|_{\tau=0^+} \\ &= \frac{d}{d\tau} \left[\frac{\partial}{\partial \tilde{x}_A} \left(\frac{d\tilde{x}_{C_2}}{d\tau}\right) \frac{d\tilde{x}_A}{d\tau}\right] + \frac{d}{d\tau} \left[\frac{\partial}{\partial \tilde{x}_{B_2}} \left(\frac{d\tilde{x}_{C_2}}{d\tau}\right) \frac{d\tilde{x}_{B_2}}{d\tau}\right] + \frac{d}{d\tau} \left[\frac{\partial}{\partial \tilde{x}_{C_2}} \left(\frac{d\tilde{x}_{C_2}}{d\tau}\right) \frac{d\tilde{x}_{C_2}}{d\tau}\right] \\ &- \frac{d}{d\tau} \left[\frac{\partial}{\partial \tilde{x}_A} \left(\frac{d\tilde{x}_{C_1}}{d\tau}\right) \frac{d\tilde{x}_A}{d\tau}\right] - \frac{d}{d\tau} \left[\frac{\partial}{\partial \tilde{x}_{B_1}} \left(\frac{d\tilde{x}_{C_1}}{d\tau}\right) \frac{d\tilde{x}_{B_1}}{d\tau}\right] - \frac{d}{d\tau} \left[\frac{\partial}{\partial \tilde{x}_{C_1}} \left(\frac{d\tilde{x}_{C_1}}{d\tau}\right) \frac{d\tilde{x}_{C_1}}{d\tau}\right]\right] \\ &= \frac{\partial}{\partial \tilde{x}_A} \left(\frac{d\tilde{x}_{C_2}}{d\tau}\right) \frac{d}{d\tau} \left(\frac{d\tilde{x}_A}{d\tau}\right) + \frac{d}{d\tau} \left[\frac{\partial}{\partial \tilde{x}_A} \left(\frac{d\tilde{x}_{C_2}}{d\tau}\right)\right] \frac{d\tilde{x}_A}{d\tau} + \frac{\partial}{\partial \tilde{x}_{B_2}} \left(\frac{d\tilde{x}_{C_2}}{d\tau}\right) \frac{d}{d\tau} \left(\frac{d\tilde{x}_{B_2}}{d\tau}\right) \\ &+ \frac{d}{d\tau} \left[\frac{\partial}{\partial \tilde{x}_{B_2}} \left(\frac{d\tilde{x}_{C_2}}{d\tau}\right)\right] \frac{d\tilde{x}_{B_2}}{d\tau} + \frac{\partial}{\partial \tilde{x}_{C_2}} \left(\frac{d\tilde{x}_{C_2}}{d\tau}\right) \frac{d}{d\tau} \left(\frac{d\tilde{x}_{C_2}}{d\tau}\right) + \frac{d}{d\tau} \left[\frac{\partial}{\partial \tilde{x}_{C_2}} \left(\frac{d\tilde{x}_{C_2}}{d\tau}\right)\right] \frac{d\tilde{x}_{B_2}}{d\tau} \\ &- \frac{\partial}{\partial \tilde{x}_A} \left(\frac{d\tilde{x}_{C_1}}{d\tau}\right) \frac{d}{d\tau} \left(\frac{d\tilde{x}_{A}}{d\tau}\right) - \frac{d}{d\tau} \left[\frac{\partial}{\partial \tilde{x}_{A}} \left(\frac{d\tilde{x}_{C_2}}{d\tau}\right) \frac{d\tilde{x}_{A}}{d\tau} - \frac{\partial}{\partial \tilde{x}_{B_1}} \left(\frac{d\tilde{x}_{C_2}}{d\tau}\right) \frac{d}{d\tau} \left(\frac{d\tilde{x}_{C_1}}{d\tau}\right) \right] \frac{d\tilde{x}_{B_1}}{d\tau} \\ &- \frac{d}{d\tau} \left[\frac{\partial}{\partial \tilde{x}_{B_1}} \left(\frac{d\tilde{x}_{C_1}}{d\tau}\right)\right] \frac{d\tilde{x}_{B_1}}{d\tau} - \frac{\partial}{\partial \tilde{x}_{C_1}} \left(\frac{d\tilde{x}_{C_1}}{d\tau}\right) \frac{d\tilde{x}_{C_1}}{d\tau} \left(\frac{d\tilde{x}_{C_1}}{d\tau}\right) - \frac{d}{d\tau} \left[\frac{\partial}{\partial \tilde{x}_{C_1}} \left(\frac{d\tilde{x}_{C_1}}{d\tau}\right)\right] \frac{d\tilde{x}_{B_1}}{d\tau} - \frac{\partial}{\partial \tilde{x}_{C_1}} \left(\frac{d\tilde{x}_{C_1}}{d\tau}\right) \frac{d}{d\tau} \left(\frac{d\tilde{x}_{C_1}}{d\tau}\right) \frac{d\tilde{x}_{C_2}}{d\tau} \left(\frac{d\tilde{x}_{C_1}}{d\tau}\right) \frac{d\tilde{x}_{C_1}}{d\tau} \right] \\ &- \frac{\partial}{\partial \tilde{x}_A} \left(\frac{d\tilde{x}_{C_1}}{d\tau}\right) \frac{d\tilde{x}_{B_1}}{d\tau^2} - \frac{\partial}{\partial \tilde{x}_A} \left(\frac{d\tilde{x}_{C_1}}{d\tau}\right) \left(\frac{d\tilde{x}_{A_1}}{d\tau}\right)^2 + \frac{\partial}{\partial \tilde{x}_{B_1}} \left(\frac{d\tilde{x}_{C_1}}{d\tau}\right) \frac{d\tilde{x}_{C_1}}{d\tau^2} + \frac{\partial}{\partial \tilde{x}_{C_1}} \left(\frac{d\tilde{x}_{C_1}}{d\tau}\right) \left(\frac{d\tilde{x}_{A_1}}{d\tau}\right)^2 - \frac{\partial}{\partial \tilde{x}_{B_1}} \left(\frac{d\tilde{x}_{C_1}}{d\tau}\right) \frac{d\tilde{x}_{A_1}}{d\tau^2} - \frac{\partial}{\partial \tilde{x}_{C_1}} \left(\frac{d\tilde{x}_{C_1}}{d\tau}\right) \left(\frac{d\tilde{x}_{A_1}}{d\tau}\right)^2 - \frac{\partial}{\partial \tilde{x}_{B$$

 $\begin{array}{l} \text{Then because } \left. \frac{\partial}{\partial \tilde{x}_{B_1}} \left(\frac{d \tilde{x}_{C_1}}{d \tau} \right) \right|_{\tau = 0^+} = \left. \frac{\partial}{\partial \tilde{x}_{B_2}} \left(\frac{d \tilde{x}_{C_2}}{d \tau} \right) \right|_{\tau = 0^+} < 0 \text{ and } \left. \frac{d^2 w_B}{d \tau^2} \right|_{\tau = 0^+} > 0, \text{ we know } \left. \frac{d^3 w_C}{d \tau^3} \right|_{\tau = 0^+} > 0. \\ \text{Now as (i) } \left. w_C(0^+) = 0, \left. \frac{d w_C}{d \tau} \right|_{\tau = 0^+} = 0, \left. \frac{d^2 w_C}{d \tau^2} \right|_{\tau = 0^+} = 0, \left. \frac{d^3 w_C}{d \tau^3} \right|_{\tau = 0^+} > 0 \text{ (ii) } \left. \frac{d w_C}{d \tau} \right|_{\tau = \tau^*} > 0 \text{ wherever } w_C(\tau^*) = 0 \\ \text{and } \tau^* > 0, \text{ based on Lemma 2 we know that } w_C(\tau) > 0, \text{ i.e., } \tilde{x}_{C_1}(\tau) < \tilde{x}_{C_2}(\tau) \text{ for all } \tau > 0. \\ \end{array}$

Theorem 2. $RT_{\tilde{x}_{C_1}} > RT_{\tilde{x}_{C_2}}$ (RT: response time).

Proof. Based on the previous lemmas and previous theorem, we know that \tilde{x}_C has a unique steady state \tilde{x}_{Css} . Note also that neither \tilde{x}_{Css} nor $\tilde{x}_C(0)$ depends on the choice of $\tilde{\eta}_{XD_X}$ (X = A, B, C).

Based on Theorem 1, we know that \tilde{x}_{C_2} is larger than \tilde{x}_{C_1} . This means when \tilde{x}_{C_1} reaches the midpoint between $\tilde{x}_C(0)$ and $\tilde{x}_{C_{ss}}$ (for biological implications, we only consider $\tilde{x}_C(0) < \tilde{x}_{C_{ss}}$), \tilde{x}_{C_2} has reached a value larger than the midpoint. By continuity of \tilde{x}_C , we know that \tilde{x}_{C_2} must have reached the midpoint earlier than \tilde{x}_{C_1} . This in turn implies that the response time of \tilde{x}_{C_1} is larger than the response time of \tilde{x}_{C_2} .

Proof of the Effects of Intermodular Retroactivity on Response Time and Pulse **Amplitude in IFFLs**

We now consider the model of an IFFL where node B is connected to, and hence, serves as the input to other circuits (Figure S2). Using the method shown in a previous study (Gyorgy and Del Vecchio, 2014), we can derive a model for an IFFL in which intermodular retroactivity is accounted for. $\frac{d\tilde{x}_A}{d\tau}$, $\frac{d\tilde{x}_B}{d\tau}$, and $\frac{d\tilde{x}_C}{d\tau}$ in an I1-FFL where only node B is connected to n additional modules (nodes) can be expressed as:

$$\begin{bmatrix} \frac{d\tilde{x}_{A}}{d\tau} \\ \frac{d\tilde{x}_{B}}{d\tau} \\ \frac{d\tilde{x}_{C}}{d\tau} \end{bmatrix} = \begin{bmatrix} 1 & 0 & 0 \\ 0 & \frac{1+r_{BD_{B}}(\tilde{x}_{B})}{1+r_{BD_{B}}(\tilde{x}_{B})+\Sigma_{i=1}^{n}S_{B^{i}}(\tilde{x}_{B})} & 0 \\ 0 & 0 & 1 \end{bmatrix} \begin{bmatrix} g_{\tilde{A}} \\ g_{\tilde{B}} \\ g_{\tilde{C}} \end{bmatrix}$$
(9)

where

$$S_{B^{i}}(\tilde{x}_{B}) = \tilde{\eta}_{B^{i}} h_{B^{i}}^{2} \left(\frac{\tilde{x}_{B}}{\tilde{K}_{B^{i}}} \right)^{h_{B^{i}} - 1} \left(1 + \left(\frac{\tilde{x}_{B}}{\tilde{K}_{B^{i}}} \right)^{h_{B^{i}}} \right)^{-2}$$
(10)

and

$$g_{\tilde{A}} = \frac{1}{1 + r_{AD_A}(\tilde{x}_A)} f_{\tilde{A}}$$

$$g_{\tilde{B}} = \frac{1}{1 + r_{BD_B}(\tilde{x}_B)} f_{\tilde{B}}$$

$$g_{\tilde{C}} = \frac{1}{1 + r_{BD_B}(\tilde{x}_B)} f_{\tilde{C}},$$

$$(11)$$

where r_{AD_A} , r_{BD_B} , r_{CD_C} , $f_{\tilde{A}}$, $f_{\tilde{B}}$, and $f_{\tilde{C}}$ are defined the same as in (6). Let $\vec{\tilde{x_1}}$ and $\vec{\tilde{x_2}}$ denote the concentrations of A, B, and C in two I1-FFL models (i.e., $\vec{\tilde{x_1}} = [\tilde{x}_{A_1}, \tilde{x}_{B_1}, \tilde{x}_{C_1}]$, $\vec{\tilde{x}}_2 = [\tilde{x}_{A_2}, \tilde{x}_{B_2}, \tilde{x}_{C_2}]$), in which all parameters are held identical except that node B is connected to different numbers of binding sites in the k-th module of its context $(1 \le k \le n)$. $\tilde{\eta}_{B^k}$ equals $\tilde{\eta}_{B^k_1}$ and $\tilde{\eta}_{B^k_2}$, respectively. At $\tau = 0$, x_I undergoes a stepwise increase and is kept constant afterwards. The initial values of \tilde{x}_A , \tilde{x}_{B_i} (i = 1, 2), and \tilde{x}_C are the corresponding steady values before the increase in x_I . Without loss of generality, we assume that for one given k, $\tilde{\eta}_{B_1^k} < \tilde{\eta}_{B_2^k}$. We now show that $\forall \tau > 0$, $\tilde{x}_{C_1}(\tau) < \tilde{x}_{C_2}(\tau)$, i.e., the concentration of C in I1-FFL model #1 is less than the concentration of C in I1-FFL model #2 at all positive times.

We begin by showing that \tilde{x}_A and \tilde{x}_B are monotonically increasing in time. From the proof of Theorem 1, we already know that $\frac{d\tilde{x}_A}{d\tau} > 0$ for all $\tau \geq 0^+$. Assume that there exists $\tau^* \geq 0^+$ at which $\frac{d\tilde{x}_B}{d\tau} = 0$, i.e., $g_{\tilde{B}} = 0$. Using that $\frac{dg_{\bar{B}}}{d\tau}\Big|_{\tau=\tau^*} > 0$ wherever $g_{\bar{B}}\Big|_{\tau=\tau^*} = 0$ and $\tau^* \ge 0^+$ from the proof of Theorem 1, we get

$$\left. \frac{d^2 \tilde{x}_B}{d \tau^2} \right|_{\tau = \tau^*} = \left. \frac{1 + r_{BD_B}(\tilde{x}_B)}{1 + r_{BD_B}(\tilde{x}_B) + \sum_{i=1}^n S_{B^i}(\tilde{x}_B)} \frac{d g_{\tilde{B}}}{d \tau} \right|_{\tau = \tau^*} > 0.$$

Then because(i) $\frac{d\tilde{x}_B}{d\tau}\Big|_{\tau=0^+}=0$, $\frac{d^2\tilde{x}_B}{d\tau^2}\Big|_{\tau=0^+}>0$ (ii) $\frac{d^2\tilde{x}_B}{d\tau^2}\Big|_{\tau=\tau^*}>0$ wherever $\frac{d\tilde{x}_B}{d\tau}\Big|_{\tau=\tau^*}=0$ and $\tau^*>0$, based on

Lemma 2 we know that $\frac{d\tilde{x}_B}{d\tau} > 0$ for all $\tau > 0$. Next, we will show that $\forall \tau > 0$, $\tilde{x}_{B_1}(\tau) > \tilde{x}_{B_2}(\tau)$. Let $w_B(\tau) = \tilde{x}_{B_1}(\tau) - \tilde{x}_{B_2}(\tau)$. Based on (7) and (9), we know that $\tilde{x}_{B_1}(0^+) = \tilde{x}_{B_2}(0^+)$, i.e., $w_B(0^+) = 0$. Consider any $\tau^* \ge 0^+$ at which $w_B(\tau^*) = 0$, i.e., $\tilde{x}_{B_1}(\tau^*) = \tilde{x}_{B_2}(\tau^*) = 0$ $\tilde{x}_B(\tau^*)$. Because $\tilde{\eta}_{B_1^k} < \tilde{\eta}_{B_2^k}$, based on (10) we know $S_{B_1^k}(\tilde{x}_B)\Big|_{\tau=\tau^*} < S_{B_2^k}(\tilde{x}_B)\Big|_{\tau=\tau^*}$. Hence,

$$\begin{split} \frac{d\,w_B}{d\tau} \bigg|_{\tau=\tau^*} &= \left(\frac{1 + r_{BD_B}(\tilde{x}_B)}{1 + r_{BD_B}(\tilde{x}_B) + \sum_{i=1, i \neq k}^n S_{B^i}(\tilde{x}_B) + S_{B_1^k}(\tilde{x}_B)} - \frac{1 + r_{BD_B}(\tilde{x}_B)}{1 + r_{BD_B}(\tilde{x}_B) + \sum_{i=1, i \neq k}^n S_{B^i}(\tilde{x}_B) + S_{B_2^k}(\tilde{x}_B)} \right) g_{\tilde{B}} \bigg|_{\tau=\tau^*} \\ &= 0, \quad \text{if } \tau^* = 0^+ \quad \text{as } g_{\tilde{B}} \bigg|_{\tau=0^+} = 0 \\ &> 0, \quad \text{if } \tau^* > 0 \quad \quad \text{as } \frac{d\tilde{x}_B}{d\tau} > 0 \text{ for } \tau > 0 \implies g_{\tilde{B}} \bigg|_{\tau=\tau^*} > 0. \end{split}$$

If $\tau^* = 0^+$, we can further show that

$$\begin{split} \left. \frac{d^2 w_B}{d\tau^2} \right|_{\tau=0^+} &= \left(\frac{1 + r_{BD_B}(\tilde{x}_B)}{1 + r_{BD_B}(\tilde{x}_B) + \sum_{i=1, i \neq k}^n S_{B^i}(\tilde{x}_B) + S_{B^k_1}(\tilde{x}_B)} - \frac{1 + r_{BD_B}(\tilde{x}_B)}{1 + r_{BD_B}(\tilde{x}_B) + \sum_{i=1, i \neq k}^n S_{B^i}(\tilde{x}_B) + S_{B^k_2}(\tilde{x}_B)} \right) \\ & \cdot \left. \frac{dg_{\tilde{B}}}{d\tau} \right|_{\tau=0^+} &> 0. \end{split}$$

Now because (i) $w_B(0^+)=0$, $\frac{dw_B}{d\tau}\Big|_{\tau=0^+}=0$, $\frac{d^2w_B}{d\tau^2}\Big|_{\tau=0^+}>0$ (ii) $\frac{dw_B}{d\tau}\Big|_{\tau=\tau^*}>0$ wherever $w_B(\tau^*)=0$ and $\tau^*>0$, based on Lemma 2 we know that $w_B(\tau)>0$, i.e., $\tilde{x}_{B_1}(\tau)>\tilde{x}_{B_2}(\tau)$ for all $\tau>0$.

Finally, following the rest of the proof for Theorem 1, we know that $\tilde{x}_{C_1}(\tau) < \tilde{x}_{C_2}(\tau)$ for all $\tau > 0$. Then, similar to the proof of Theorem 2, we conclude that the response time of \tilde{x}_{C_1} is larger than the response time of \tilde{x}_{C_2} .

9 Non-Dimensionalized ODE Models for Other Sign-Sensitive Response-Acceleration Motifs

Without retroactivity, the non-dimensionalized ODE model for a type-1 two-input circuit is given as:

$$\begin{split} \frac{d\tilde{x}_A}{d\tau} &= f_{\tilde{A}} = \left(1 - \gamma_A\right) \frac{\left(\frac{x_I}{K_{IA}}\right)^{h_{IA}}}{1 + \left(\frac{x_I}{K_{IA}}\right)^{h_{IA}}} + \gamma_A - \tilde{x}_A \\ \frac{d\tilde{x}_{A_2}}{d\tau} &= f_{\tilde{A}_2} = \left(1 - \gamma_{A_2}\right) \frac{\left(\frac{x_{I_2}}{K_{IA_2}}\right)^{h_{IA_2}}}{1 + \left(\frac{x_{I_2}}{K_{IA_2}}\right)^{h_{IA_2}}} + \gamma_{A_2} - \tilde{x}_{A_2} \\ \frac{d\tilde{x}_B}{d\tau} &= f_{\tilde{B}} = \left(1 - \gamma_B\right) \frac{\left(\frac{\tilde{x}_{A_2}}{\tilde{K}_{A_2B}}\right)^{h_{A_2B}}}{1 + \left(\frac{\tilde{x}_{A_2}}{\tilde{K}_{A_2B}}\right)^{h_{A_2B}}} + \gamma_B - \tilde{x}_B \\ \frac{d\tilde{x}_C}{d\tau} &= f_{\tilde{C}} = \left(1 - \gamma_C\right) \frac{\left(\frac{\tilde{x}_A}{\tilde{K}_{AC}}\right)^{h_{AC}}}{\left(1 + \left(\frac{\tilde{x}_A}{\tilde{K}_{AC}}\right)^{h_{AC}}\right) \left(1 + \left(\frac{\tilde{x}_B}{\tilde{K}_{BC}}\right)^{h_{BC}}\right)} + \gamma_C - \tilde{x}_C. \end{split}$$

The non-dimensionalized ODE model for a type-4 two-input circuit is given as:

$$\begin{split} \frac{d\tilde{x}_A}{d\tau} &= f_{\tilde{A}} = \left(1 - \gamma_A\right) \frac{\left(\frac{x_I}{K_{IA}}\right)^{h_{IA}}}{1 + \left(\frac{x_I}{K_{IA}}\right)^{h_{IA}}} + \gamma_A - \tilde{x}_A \\ \frac{d\tilde{x}_{A_2}}{d\tau} &= f_{\tilde{A}_2} = \left(1 - \gamma_{A_2}\right) \frac{\left(\frac{x_{I_2}}{K_{IA_2}}\right)^{h_{IA_2}}}{1 + \left(\frac{x_{I_2}}{K_{IA_2}}\right)^{h_{IA_2}}} + \gamma_{A_2} - \tilde{x}_{A_2} \\ \frac{d\tilde{x}_B}{d\tau} &= f_{\tilde{B}} = \left(1 - \gamma_B\right) \frac{1}{1 + \left(\frac{\tilde{x}_{A_2}}{K_{A_2B}}\right)^{h_{A_2B}}} + \gamma_B - \tilde{x}_B \\ \frac{d\tilde{x}_C}{d\tau} &= f_{\tilde{C}} = \left(1 - \gamma_C\right) \frac{\left(\frac{\tilde{x}_A}{K_{AC}}\right)^{h_{AC}} \left(\frac{\tilde{x}_B}{K_{BC}}\right)^{h_{BC}}}{\left(1 + \left(\frac{\tilde{x}_A}{K_{AC}}\right)^{h_{AC}}\right) \left(1 + \left(\frac{\tilde{x}_B}{K_{BC}}\right)^{h_{BC}}} + \gamma_C - \tilde{x}_C. \end{split}$$

The non-dimensionalized ODE model for a negative autoregulated circuit is given as:

$$\begin{split} \frac{d\tilde{x}_{A}}{d\tau} &= f_{\tilde{A}} = \left(1 - \gamma_{A}\right) \frac{\left(\frac{x_{I}}{K_{IA}}\right)^{h_{IA}}}{1 + \left(\frac{x_{I}}{K_{IA}}\right)^{h_{IA}}} + \gamma_{A} - \tilde{x}_{A} \\ \frac{d\tilde{x}_{C}}{d\tau} &= f_{\tilde{C}} = \left(1 - \gamma_{C}\right) \frac{\left(\frac{\tilde{x}_{A}}{K_{IA}}\right)^{h_{AC}}}{\left(1 + \left(\frac{\tilde{x}_{A}}{K_{AC}}\right)^{h_{AC}}\right) \left(1 + \left(\frac{\tilde{x}_{C}}{K_{CC}}\right)^{h_{CC}}\right)} + \gamma_{C} - \tilde{x}_{C}. \end{split}$$

When only retroactivity on A is considered, the retroactivity matrix $R(\vec{x})$, which is the same for both type-1

and type-4 two-input circuits, is given as:

When only retroactivity on A is considered, the retroactivity matrix $R(\vec{\tilde{x}})$ for a negative autoregulated circuit is given as:

When only retroactivity on C is considered, the retroactivity matrix $R(\vec{\tilde{x}})$ for a negative autoregulated circuit is given as:

10 Proof of the Effects of $\tilde{\eta}_{AD_A}$ and $\tilde{\eta}_{CD_C}$ on Response Time in a Negative Autoregulated Circuit

In this section, we show that for any parameters, response time always increases in a negative autoregulated circuit if retroactivity on node A or C, $\tilde{\eta}_{AD_A}$ or $\tilde{\eta}_{CD_C}$, increases.

 $\frac{d\tilde{x}_A}{d\tau}$ and $\frac{d\tilde{x}_C}{d\tau}$ in a negative autoregulated circuit where only $\tilde{\eta}_{AD_A}$ may be allowed to vary can be expressed as:

$$\begin{bmatrix} \frac{d\tilde{x}_A}{d\tau} \\ \frac{d\tilde{x}_C}{d\tau} \end{bmatrix} = \begin{bmatrix} \frac{1}{1+r_{AD_A}(\tilde{x}_A)} & 0 \\ 0 & \frac{1}{1+r_{CD_C}(\tilde{x}_C)} \end{bmatrix} \begin{bmatrix} f_{\tilde{A}} \\ f_{\tilde{C}} \end{bmatrix}, \tag{12}$$

$$f_{\tilde{A}} = \frac{\left(\frac{x_I}{K_{IA}}\right)^{h_{IA}}}{1 + \left(\frac{x_I}{K_{IA}}\right)^{h_{IA}}} (1 - \gamma_A) + \gamma_A - \tilde{x}_A$$

$$f_{\tilde{C}} = \frac{\left(\frac{\tilde{x}_A}{\tilde{K}_{AC}}\right)^{h_{AC}}}{\left(1 + \left(\frac{\tilde{x}_A}{\tilde{K}_{AC}}\right)^{h_{AC}}\right) \left(1 + \left(\frac{\tilde{x}_C}{\tilde{K}_{CC}}\right)^{h_{CC}}\right)} (1 - \gamma_C) + \gamma_C - \tilde{x}_C,$$
(13)

$$r_{AD_A}(\tilde{x}_A) = \tilde{\eta}_{AD_A} h_{AD_A}^2 \left(\frac{\tilde{x}_A}{\tilde{K}_{AD_A}}\right)^{h_{AD_A} - 1} \left(1 + \left(\frac{\tilde{x}_A}{\tilde{K}_{AD_A}}\right)^{h_{AD_A}}\right)^{-2}$$

$$r_{CD_C}(\tilde{x}_C) = \tilde{\eta}_{CD_C} h_{CD_C}^2 \left(\frac{\tilde{x}_C}{\tilde{K}_{CD_C}}\right)^{h_{CD_C} - 1} \left(1 + \left(\frac{\tilde{x}_C}{\tilde{K}_{CD_C}}\right)^{h_{CD_C}}\right)^{-2},$$

$$(14)$$

where $\gamma_A, \gamma_C \in (0, 1)$ such that $\tilde{x}_A, \tilde{x}_C \in (0, 1)$.

Let $\vec{x_1}$ and $\vec{x_2}$ denote the concentrations of A and C in two negative autoregulated circuit models (i.e., $\vec{x_1} = [\tilde{x}_{A_1}, \tilde{x}_{C_1}], \ \vec{x_2} = [\tilde{x}_{A_2}, \tilde{x}_{C_2}])$, in which all parameters are held identical except that node A is connected to different numbers of downstream targets such that retroactivity coefficient $\tilde{\eta}_{AD_A}$ equals $\tilde{\eta}_{AD_{A_1}}$ and $\tilde{\eta}_{AD_{A_2}}$, respectively. At $\tau = 0$, x_I undergoes a stepwise increase and is kept constant afterwards. The initial values of \tilde{x}_{A_i} and \tilde{x}_{C_i} (i = 1,2) are the corresponding steady values before the increase in x_I . Without loss of generality, we assume $\tilde{\eta}_{AD_{A_1}} < \tilde{\eta}_{AD_{A_2}}$. Now we will show that $\forall \tau > 0$, $\tilde{x}_{C_1}(\tau) > \tilde{x}_{C_2}(\tau)$, i.e., the concentration of C in I1-FFL model #1 is larger than the concentration of C in I1-FFL model #2 at all positive times.

Theorem 3. $\forall \tau > 0$, $\tilde{x}_{C_1} > \tilde{x}_{C_2}$ and $RT_{\tilde{x}_{C_1}} < RT_{\tilde{x}_{C_2}}$ (RT: response time).

Proof. We begin by showing that \tilde{x}_A and \tilde{x}_C are monotonically increasing in time. Based on (12), we know $\tilde{x}_A(0) < \tilde{x}_{A_{ss}}$ for nonzero x_I . From Lemma 1 it follows that $\frac{d\tilde{x}_A}{d\tau} > 0$ for all $\tau \ge 0^+$.

Let $H_{\tilde{A}}(\tilde{x}_A) = \frac{\left(\frac{\tilde{x}_A}{\tilde{k}_{AC}}\right)^{h_{AC}}}{1 + \left(\frac{\tilde{x}_A}{\tilde{k}_{AC}}\right)^{h_{AC}}}$ and $H_{\tilde{C}}(\tilde{x}_C) = \frac{1}{1 + \left(\frac{\tilde{x}_C}{\tilde{k}_{CC}}\right)^{h_{CC}}}$. Assume that there exists $\tau^* \ge 0^+$ at which $f_{\tilde{C}}(\tau^*) = 0$.

Because $f_{\tilde{C}}(\tau^*) = 0$, $\frac{d\tilde{H}_A(\tilde{x}_A)}{d\tilde{x}_A} > 0$ for $\tilde{x}_A > 0$, and $\frac{d\tilde{x}_A}{d\tau} > 0$ for $\tau \ge 0^+$, we get

$$\begin{split} \frac{d^2\tilde{x}_C}{d\tau^2}\bigg|_{\tau=\tau^*} &= \frac{1}{1+r_{CD_C}(\tilde{x}_C)} \frac{df_{\tilde{C}}}{d\tau}\bigg|_{\tau=\tau^*} + \frac{d}{d\tau} \left[\frac{1}{1+r_{CD_C}(\tilde{x}_C)}\right] f_{\tilde{C}}\bigg|_{\tau=\tau^*} \\ &= \frac{1}{1+r_{CD_C}(\tilde{x}_C)} \left[\frac{d\left[H_A(\tilde{x}_A)H_C(\tilde{x}_C)\right]}{d\tau}(1-\gamma_C) - \frac{d\tilde{x}_C}{d\tau}\right]\bigg|_{\tau=\tau^*} \\ &= \frac{1}{1+r_{CD_C}(\tilde{x}_C)} \left[\frac{dH_A(\tilde{x}_A)}{d\tilde{x}_A} \frac{d\tilde{x}_A}{d\tau} H_C(\tilde{x}_C) + \frac{dH_C(\tilde{x}_C)}{d\tilde{x}_C} \frac{d\tilde{x}_C}{d\tau} H_A(\tilde{x}_A)\right] (1-\gamma_C)\bigg|_{\tau=\tau^*} \\ &= \frac{1}{1+r_{CD_C}(\tilde{x}_C)} \frac{dH_A(\tilde{x}_A)}{d\tilde{x}_A} \frac{d\tilde{x}_A}{d\tau} H_C(\tilde{x}_C) (1-\gamma_C)\bigg|_{\tau=\tau^*} > 0. \end{split}$$

Because (i) $\frac{d\tilde{x}_C}{d\tau}\Big|_{\tau=0^+}=0$, $\frac{d^2\tilde{x}_C}{d\tau^2}\Big|_{\tau=0^+}>0$ (ii) $\frac{d^2\tilde{x}_C}{d\tau^2}\Big|_{\tau=\tau^*}>0$ wherever $\frac{d\tilde{x}_C}{d\tau}\Big|_{\tau=\tau^*}=0$ and $\tau^*>0$, based on Lemma 2 we know that $\frac{d\tilde{x}_C}{d\tau}>0$ for all $\tau>0$.

Next, we will show that $\forall \tau > 0$, $\tilde{x}_{A_1} > \tilde{x}_{A_2}$. Let $w_A(\tau) = \tilde{x}_{A_1}(\tau) - \tilde{x}_{A_2}(\tau)$. Based on (13), we know $\tilde{x}_{A_1}(0^+) = \tilde{x}_{A_2}(0^+)$, i.e., $w_A(0^+) = 0$. Consider any $\tau^* \ge 0^+$ at which $w_A(\tau^*) = 0$, i.e., $\tilde{x}_{A_1}(\tau^*) = \tilde{x}_{A_2}(\tau^*)$. Since $\tilde{\eta}_{AD_{A_1}} < \tilde{\eta}_{AD_{A_2}}$, based on (14) we know $\frac{1}{1+r_{AD_{A_1}}(\tilde{x}_{A_1})}\Big|_{\tau=\tau^*} > \frac{1}{1+r_{AD_{A_2}}(\tilde{x}_{A_2})}\Big|_{\tau=\tau^*}$. Hence,

$$\begin{aligned} \frac{dw_{A}}{d\tau} \bigg|_{\tau=\tau^{*}} &= \frac{1}{1 + r_{AD_{A_{1}}}(\tilde{x}_{A_{1}})} f_{\tilde{A}_{1}} - \frac{1}{1 + r_{AD_{A_{2}}}(\tilde{x}_{A_{2}})} f_{\tilde{A}_{2}} \bigg|_{\tau=\tau^{*}} \\ &= \left[\frac{1}{1 + r_{AD_{A_{1}}}(\tilde{x}_{A})} - \frac{1}{1 + r_{AD_{A_{2}}}(\tilde{x}_{A})} \right] f_{\tilde{A}} \bigg|_{\tau=\tau^{*}} > 0. \end{aligned}$$

Now because (i) $w_A(0^+)=0$, $\left.\frac{dw_A}{d\tau}\right|_{\tau=0^+}>0$ (ii) $\left.\frac{dw_A}{d\tau}\right|_{\tau=\tau^*}>0$ wherever $w_A(\tau^*)=0$ and $\tau^*>0$, based on Lemma 2 we know that $w_A(\tau)>0$, i.e., $\tilde{x}_{A_1}(\tau)>\tilde{x}_{A_2}(\tau)$ for all $\tau>0$.

Finally, we will show that $\forall \tau > 0$, $\tilde{x}_{C_1} > \tilde{x}_{C_2}$. Let $w_C(\tau) = \tilde{x}_{C_1}(\tau) - \tilde{x}_{C_2}(\tau)$. Based on (13), we know that $\tilde{x}_{C_1}(0^+) = \tilde{x}_{C_2}(0^+)$, i.e., $w_C(0^+) = 0$. Consider any $\tau^* \geq 0^+$ at which $w_C(\tau^*) = 0$, i.e., $\tilde{x}_{C_1}(\tau^*) = \tilde{x}_{C_2}(\tau^*)$. Because $\tilde{x}_{A_1}(\tau) > \tilde{x}_{A_2}(\tau)$ for all $\tau > 0$, we know $H_A(\tilde{x}_{A_1}) > H_A(\tilde{x}_{A_2})$ for all $\tau > 0$. Thus,

$$\begin{split} \frac{d \, w_C}{d \tau} \bigg|_{\tau = \tau^*} &= \frac{d}{d \tau} \left[\tilde{x}_{C_1} - \tilde{x}_{C_2} \right] \bigg|_{\tau = \tau^*} \\ &= \frac{1}{1 + r_{CD_{C_1}}(\tilde{x}_{C_1})} f_{\tilde{C}_1} - \frac{1}{1 + r_{CD_{C_2}}(\tilde{x}_{\tilde{C}_2})} f_{\tilde{C}_2} \bigg|_{\tau = \tau^*} \\ &= \frac{1}{1 + r_{CD_C}(\tilde{x}_C)} \left(f_{\tilde{C}_1} - f_{\tilde{C}_2} \right) \bigg|_{\tau = \tau^*} \\ &= 0, \quad \text{if } \tau^* = 0^+ \\ &> 0, \quad \text{if } \tau^* > 0. \end{split}$$

If $\tau^* = 0^+$, then using $\frac{dH_A(\tilde{x}_A)}{d\tilde{x}_A} > 0$ for $\tilde{x}_A > 0$, $\frac{dw_A}{d\tau}\Big|_{\tau=0^+} > 0$, and $\frac{dw_C}{d\tau}\Big|_{\tau=0^+} = 0$, we can further show that

$$\begin{split} \frac{d^2 w_C}{d\tau^2} \bigg|_{\tau=0^+} &= \frac{d^2}{d\tau^2} \left[\tilde{x}_{C_1} - \tilde{x}_{C_2} \right] \bigg|_{\tau=0^+} \\ &= \frac{1}{1 + r_{CD_C}(\tilde{x}_{C_1})} \frac{dH_A(\tilde{x}_{A_1})}{d\tilde{x}_{A_1}} \frac{d\tilde{x}_{A_1}}{d\tau} H_C(\tilde{x}_{C_1}) (1 - \gamma_C) \\ &- \frac{1}{1 + r_{CD_C}(\tilde{x}_{C_2})} \frac{dH_A(\tilde{x}_{A_2})}{d\tilde{x}_{A_2}} \frac{d\tilde{x}_{A_2}}{d\tau} H_C(\tilde{x}_{C_2}) (1 - \gamma_C) \bigg|_{\tau=0^+} \\ &= \frac{1}{1 + r_{CD_C}(\tilde{x}_C)} \frac{dH_A(\tilde{x}_A)}{d\tilde{x}_A} \left(\frac{d\tilde{x}_{A_1}}{d\tau} - \frac{d\tilde{x}_{A_2}}{d\tau} \right) H_C(\tilde{x}_C) (1 - \gamma_C) \bigg|_{\tau=0^+} > 0. \end{split}$$

As (i) $w_C(0^+) = 0$, $\frac{dw_C}{d\tau}\Big|_{\tau=0^+} = 0$, $\frac{d^2w_C}{d\tau^2}\Big|_{\tau=0^+} > 0$ (ii) $\frac{dw_C}{d\tau}\Big|_{\tau=\tau^*} > 0$ wherever $w_C(\tau^*) = 0$ and $\tau^* > 0$, based on Lemma 2 we know that $w_C(\tau) > 0$, i.e., $\tilde{x}_{C_1}(\tau) > \tilde{x}_{C_2}(\tau)$ for all $\tau > 0$.

Then, similar to the proof of Theorem 2, we conclude that the response time of \tilde{x}_{C_1} is shorter than the response time of \tilde{x}_{C_2} .

Now we consider $\frac{d\tilde{x}_A}{d\tau}$ and $\frac{d\tilde{x}_C}{d\tau}$ in a negative autoregulated circuit where only $\tilde{\eta}_{CDC}$ may be allowed to vary. Let \vec{x}_1 and \vec{x}_2 denote the concentrations of A and C in two negative autoregulated circuit models (i.e., $\vec{x}_1 = [\tilde{x}_{A_1}, \tilde{x}_{C_1}], \ \vec{x}_2 = [\tilde{x}_{A_2}, \tilde{x}_{C_2}]$), in which all parameters are held identical except that node C is connected to different numbers of downstream targets such that retroactivity coefficient $\tilde{\eta}_{CDC}$ equals $\tilde{\eta}_{CDC_1}$ and $\tilde{\eta}_{CDC_2}$, respectively. At $\tau = 0$, x_I undergoes a stepwise increase and is kept constant afterwards. The initial values of \tilde{x}_{A_i} and \tilde{x}_{C_i} (i = 1, 2) are the corresponding steady values before the increase in x_I . Without loss of generality, we assume $\tilde{\eta}_{CDC_1} < \tilde{\eta}_{CDC_2}$. Now we will show that $\forall \tau > 0$, $\tilde{x}_{C_1}(\tau) > \tilde{x}_{C_2}(\tau)$, i.e., the concentration of C in I1-FFL model #1 is larger than the concentration of C in I1-FFL model #2 at all positive times.

Theorem 4. $\forall \tau > 0$, $\tilde{x}_{C_1} > \tilde{x}_{C_2}$ and $RT_{\tilde{x}_{C_1}} < RT_{\tilde{x}_{C_2}}$ (RT: response time).

Proof. Similar to before, we have that \tilde{x}_A and \tilde{x}_C are monotonically increasing in time, i.e., (i) $\forall \tau \geq 0^+$, $\frac{d\tilde{x}_A}{d\tau} > 0$ (ii) $\forall \tau > 0$, $\frac{d\tilde{x}_C}{d\tau} > 0$ (see proof of Theorem 3). Next, we will show that $\forall \tau > 0$, $\tilde{x}_{C_1}(\tau) > \tilde{x}_{C_2}(\tau)$. We define $w_C(\tau)$ and τ^* similarly as in the proof of

Next, we will show that $\forall \tau > 0$, $\tilde{x}_{C_1}(\tau) > \tilde{x}_{C_2}(\tau)$. We define $w_C(\tau)$ and τ^* similarly as in the proof of Theorem 3 such that $w_C(\tau^*) = 0$. Because $\tilde{\eta}_{CD_{C_1}} < \tilde{\eta}_{CD_{C_2}}$, we have $\frac{1}{1+r_{CD_{C_1}}(\tilde{x}_{C_1})}\Big|_{\tau=\tau^*} > \frac{1}{1+r_{CD_{C_2}}(\tilde{x}_{C_2})}\Big|_{\tau=\tau^*}$. Thus,

$$\begin{split} \frac{dw_{C}}{d\tau}\bigg|_{\tau=\tau^{*}} &= \left(\frac{1}{1+r_{CD_{C_{1}}}(\tilde{x}_{C})} - \frac{1}{1+r_{CD_{C_{2}}}(\tilde{x}_{C})}\right)f_{C}\bigg|_{\tau=\tau^{*}} \\ &= 0, \quad \text{if } \tau^{*} = 0^{+} \\ &> 0, \quad \text{if } \tau^{*} > 0. \end{split}$$

If $\tau^* = 0^+$, then using $\frac{dH_A(\tilde{x}_A)}{d\tilde{x}_A} > 0$ for $\tilde{x}_A > 0$ and $\frac{d\tilde{x}_A}{d\tau} > 0$ for $\tau \ge 0^+$, we can further show that

$$\left. \frac{d^2 w_C}{d\tau^2} \right|_{\tau=0^+} = \left[\frac{1}{1 + r_{CD_{C_1}}(\tilde{x}_{C_1})} - \frac{1}{1 + r_{CD_{C_2}}(\tilde{x}_{C_2})} \right] \frac{dH_A(\tilde{x}_A)}{d\tilde{x}_A} \frac{d\tilde{x}_A}{d\tau} H_C(\tilde{x}_C) (1 - \gamma_C) \right|_{\tau=0^+} > 0.$$

Now because (i) $w_C(0^+) = 0$, $\frac{dw_C}{d\tau}\Big|_{\tau=0^+} = 0$, $\frac{d^2w_C}{d\tau^2}\Big|_{\tau=0^+} > 0$ (ii) $\frac{dw_C}{d\tau}\Big|_{\tau=\tau^*} > 0$ wherever $w_C(\tau^*) = 0$ and $\tau^* > 0$, based on Lemma 2 we know that $w_C(\tau) > 0$, i.e., $\tilde{x}_{C_1}(\tau) > \tilde{x}_{C_2}(\tau)$ for all $\tau > 0$. Then similar to the proof of Theorem 2, we conclude that the response time of \tilde{x}_{C_1} is shorter than the response time of \tilde{x}_{C_2} .

11 Two-node Negative Feedback Loops

Model for the two-node NFBL is:

$$\begin{bmatrix} \frac{d\tilde{x}_A}{d\tau} \\ \frac{d\tilde{x}_B}{d\tau} \end{bmatrix} = \begin{bmatrix} \frac{1}{1+r_{AD_A}(\tilde{x}_A)} & 0 \\ 0 & \frac{1}{1+r_{BD_B}(\tilde{x}_B)} \end{bmatrix} \begin{bmatrix} f_{\tilde{A}} \\ f_{\tilde{B}} \end{bmatrix},$$

$$f_{\tilde{A}} = (1-\gamma_A) \frac{\left(\frac{x_I}{K_{IA}}\right)^{h_{IA}}}{1+\left(\frac{x_I}{K_{IA}}\right)^{h_{IA}}} \frac{1}{1+\left(\frac{\tilde{x}_B}{K_{BA}}\right)^{h_{BA}}} + \gamma_A - \tilde{x}_A$$

$$f_{\tilde{B}} = (1-\gamma_B) \frac{\left(\frac{\tilde{x}_A}{K_{AB}}\right)^{h_{AB}}}{1+\left(\frac{\tilde{x}_A}{K_{AB}}\right)^{h_{AB}}} + \gamma_B - \tilde{x}_B,$$

$$\begin{split} r_{AD_A}(\tilde{x}_A) &= \tilde{\eta}_{AD_A} h_{AD_A}^2 \left(\frac{\tilde{x}_A}{\tilde{K}_{AD_A}}\right)^{h_{AD_A} - 1} \left(1 + \left(\frac{\tilde{x}_A}{\tilde{K}_{AD_A}}\right)^{h_{AD_A}}\right)^{-2} \\ r_{BD_B}(\tilde{x}_B) &= \tilde{\eta}_{BD_B} h_{BD_B}^2 \left(\frac{\tilde{x}_B}{\tilde{K}_{BD_B}}\right)^{h_{BD_B} - 1} \left(1 + \left(\frac{\tilde{x}_B}{\tilde{K}_{BD_B}}\right)^{h_{BD_B}}\right)^{-2}. \end{split}$$

12 Response Time of IFFLs with OR Logic at Different Levels of $\tilde{\eta}_{BD_B}$

Under the assumption of OR logic, the non-dimensionalized ODE model for an I1-FFL without retroactivity is given as:

$$\begin{split} \frac{d\tilde{x}_{A}}{d\tau} &= f_{\tilde{A}} = \left(1 - \gamma_{A}\right) \frac{\left(\frac{x_{I}}{K_{IA}}\right)^{h_{IA}}}{1 + \left(\frac{x_{I}}{K_{IA}}\right)^{h_{IA}}} + \gamma_{A} - \tilde{x}_{A} \\ \frac{d\tilde{x}_{B}}{d\tau} &= f_{\tilde{B}} = \left(1 - \gamma_{B}\right) \frac{\left(\frac{\tilde{x}_{A}}{\tilde{K}_{AB}}\right)^{h_{AB}}}{1 + \left(\frac{\tilde{x}_{A}}{\tilde{K}_{AB}}\right)^{h_{AB}}} + \gamma_{B} - \tilde{x}_{B} \\ \frac{d\tilde{x}_{C}}{d\tau} &= f_{\tilde{C}} = \left(1 - \gamma_{C}\right) \left[\frac{\left(\frac{\tilde{x}_{A}}{\tilde{K}_{AC}}\right)^{h_{AC}}}{1 + \left(\frac{\tilde{x}_{A}}{\tilde{K}_{AC}}\right)^{h_{AC}}} + \frac{1}{1 + \left(\frac{\tilde{x}_{B}}{\tilde{K}_{BC}}\right)^{h_{BC}}}\right] + \gamma_{C} - \tilde{x}_{C}. \end{split}$$

Under the assumption of OR logic, the non-dimensionalized ODE model for an I4-FFL without retroactivity is given as:

$$\begin{split} \frac{d\tilde{x}_A}{d\tau} &= f_{\tilde{A}} = \left(1 - \gamma_A\right) \frac{\left(\frac{x_I}{K_{IA}}\right)^{h_{IA}}}{1 + \left(\frac{x_I}{K_{IA}}\right)^{h_{IA}}} + \gamma_A - \tilde{x}_A \\ \frac{d\tilde{x}_B}{d\tau} &= f_{\tilde{B}} = \left(1 - \gamma_B\right) \frac{1}{1 + \left(\frac{\tilde{x}_A}{\tilde{K}_{AB}}\right)^{h_{AB}}} + \gamma_B - \tilde{x}_B \\ \frac{d\tilde{x}_C}{d\tau} &= f_{\tilde{C}} = \left(1 - \gamma_C\right) \left[\frac{\left(\frac{\tilde{x}_A}{\tilde{K}_{AC}}\right)^{h_{AC}}}{1 + \left(\frac{\tilde{x}_A}{\tilde{K}_{AC}}\right)^{h_{AC}}} + \frac{\left(\frac{\tilde{x}_B}{\tilde{K}_{BC}}\right)^{h_{BC}}}{1 + \left(\frac{\tilde{x}_B}{\tilde{K}_{BC}}\right)^{h_{BC}}}\right] + \gamma_C - \tilde{x}_C. \end{split}$$

13 IFFL Acceleration Persists in the Absence of Parameter Isometry

We generated random kinetic parameters via Latin hypercube sampling. To ensure an even distribution over the large space, \tilde{K}_X (X=AB,AC,BC) and δ_X (X=A,B,C) were sampled uniformly on a log scale from the same ranges of values used in the literature (Cao et al., 2016; Shi et al., 2017): $\tilde{K}_X \sim 0.001-1$ and $\delta_X \sim 0.01-1$. Hill coefficients h_X (X=AB,AC,BC) were sampled uniformly from a linear interval starting at 0.5 and ending at 2, including both positive and negative cooperativity.

14 Simulated Synthetic IFFL

The I2-FFL model shown in Figure 6 is given as:

$$\begin{split} \frac{dx_{L}}{dt} &= f_{L} = \beta_{L} \left[\left(1 - \gamma_{L} \right) \frac{\left(\frac{x_{L}}{K_{IL}} \right)^{h_{IL}}}{1 + \left(\frac{x_{L}}{K_{IL}} \right)^{h_{IL}}} + \gamma_{L} \right] - \delta_{L} x_{L} \\ \frac{dx_{T}}{dt} &= f_{T} = \frac{1}{1 + \eta_{D_{T}} \frac{h_{TE}^{2} x_{T}^{h_{TE}-1}}{K_{TE}^{h_{TE}}} \left(1 + \left(\frac{x_{T}}{K_{TE}} \right)^{h_{TE}} \right)^{-2}} \left\{ \beta_{T} \left[\frac{1 - \gamma_{T}}{1 + \left(\frac{x_{L}}{K_{LT}} \right)^{h_{LT}}} + \gamma_{T} \right] - \delta_{T} x_{T} \right\} \\ \frac{dx_{E}}{dt} &= f_{E} = \beta_{E} \left[\frac{1 - \gamma_{E}}{\left(1 + \left(\frac{x_{L}}{K_{LE}} \right)^{h_{LE}} \right) \left(1 + \left(\frac{x_{T}}{K_{TE}} \right)^{h_{TE}}} \right) + \gamma_{E} \right] - \delta_{E} x_{E}, \end{split}$$

where L, T, and E represent LmrA, TAL21, and EYFP, respectively. TAL21 is assumed to bind to pUAS-Rep2 (promoter) and D_T (decoy sites) with the same affinity and cooperativity, as they share the same operator binding sites. η_{DT} is the concentration of the decoy sites of TAL21. The kinetic parameters used in the model are taken from Supplementary Figure 3 (Wang et al., 2019): $\beta_L = 5 \times 10^4$ MEFL/hr, $\gamma_L = 1 \times 10^{-4}$, $\delta_L = 9.5$ /hr, $\beta_T = 1.66 \times 10^5$ MEFL/hr, $\gamma_T = 2.36 \times 10^{-5}$, $K_{LT} = 3.73 \times 10^5$ MEFL, $h_{LT} = 0.59$, $\delta_T = 1.5$ /hr, $\beta_E = 4.68 \times 10^5$ MEFL/hr, $\gamma_E = 1.1 \times 10^{-3}$, $K_{LE} = 3.73 \times 10^5$ MEFL, $h_{LE} = 0.59$, $K_{TE} = 2.9 \times 10^5$ MEFL, $h_{TE} = 0.72$, $\delta_E = 0.3$ /hr. Production rates β_X (X = L, T, E) are ten times the values given in the earlier study (Wang et al., 2019) as the rates given in the earlier study (Wang et al., 2019) represent the cell subpopulation with the lowest production rates. δ_X (X = L, T, E) are increased for the sake of a faster response time. Biologically, this can be achieved by adding degradation tags to the proteins.

15 Significance of Motifs

Following the method outlined in a previous study (Alon, 2007), we compared the number of the times an IFFL is observed in real networks to the number of times an IFFL is expected in a randomized network. We began by computing the number of times an IFFL is expected to appear in a randomized ER network. Let G denote a network (graph) consisting of E edges and E nodes. The probability of an edge in a given direction with the correct interaction type between a pair of nodes is (Alon, 2007):

$$p = E/N^2 * k, (15)$$

where k is the probability that a given edge is positive (activation) or negative (inhibition).

According to the same study (Alon, 2007), the average number of occurrences of an IFFL in the randomized ER network is approximately equal to the number of ways of choosing n nodes out of N times the probability to get g edges with correct interaction types in the correct places:

$$\langle N_G \rangle = N^n p^g, \tag{16}$$

where both n and g equal 3, since an IFFL contains three nodes and three edges. For convenience of notations, we denote the number of occurrences of an IFFL in real networks by \hat{N}_G .

We searched the Regulon database v10.0 (Santos-Zavaleta et al., 2018) and the TRRUST database v2 (Han et al., 2018) for TF-gene interactions in the *E. coli* (Regulon), mouse (TRRUST), and human (TTRUST) TRNs. The number of genes (nodes), number of edges (interactions), percentage of activation, percentage of inhibition, and the number of IFFLs are listed in Table S12. Plugging these values into (16), we obtained $< N_G >$.

The comparison between real and randomized networks is shown in Table S12. The number of occurrences of an IFFL in a real *E. coli*, mouse, and human TRN is approximately 118.68, 85.61, and 161.96 times the number of occurrences of an IFFL in a randomized *E. coli*, mouse, and human TRN.

In addition, we found 86 out of 154 inhibitors in *E. coli* (Regulon) are negatively auto-regulated, whereas only 5 out of 448 inhibitors in mouse (TTRUST) and 4 out of 470 inhibitors in human (TTRUST) are auto-repressors. The number of occurrences of a negative autoregulatory loop in a real *E. coli*, mouse, and human TRN is approximately 104.88, 6.94, and 4.30 times the number of occurrences of a negative autoregulatory loop in a randomized *E. coli*, mouse, and human TRN (Table S13).

Following the same method as above, we compared the number of real and randomized two-node negative feedback loops (NFBLs) in different organisms. The number of occurrences of a two-node NFBL in a real *E. coli*, mouse, and human TRN is approximately 4.82, 18.02, and 18.44 times the number of occurrences of a two-node NBFL in a randomized *E. coli*, mouse, and human TRN (Table S14).

Supplemental References

- Alon, U. (2007), *An Introduction to Systems Biology Design Principles of Biological Circuits*, Chapman and Hall.
- Cao, L.-H., Jing, B.-Y., Yang, D., Zeng, X., Shen, Y., Tu, Y. and Luo, D.-G. (2016), 'Distinct signaling of *Drosophila* chemoreceptors in olfactory sensory neurons', *Proc. Natl. Acad. Sci. U.S.A* **113**(7), 902–911.
- Gyorgy, A. and Del Vecchio, D. (2014), 'Modular composition of gene transcription networks', *PLOS Comput. Biol.*.
- Han, H., Cho, J.-W., Lee, S., Yun, A., Kim, H., Bae, D., Yang, S., Kim, C. Y., Lee, M., Kim, E., Lee, S., Kang, B., Jeong, D., Kim, Y., Jeon, H.-N., Jung, H., Nam, S., Chung, M., Kim, J.-H. and Lee, I. (2018), 'Trrust v2: an expanded reference database of human and mouse transcriptional regulatory interactions', *Nucleic Acids Res.* **46**(D1), D380–D386.
- Mangan, S. and Alon, U. (2003), 'Structure and function of the feed-forward loop network motif', *Proc. Natl. Acad. Sci. U.S.A* **100**(21), 11980–11985.
- Santos-Zavaleta, A., Sánchez-Pérez, M., Salgado, H., Velázquez-Ramírez, D. A., Gama-Castro, S., Tierrafría, V. H., Busby, S. J. W., Aquino, P., Fang, X., Palsson, B. O., Galagan, J. E. and Collado-Vides, J. (2018), 'A unified resource for transcriptional regulation in escherichia coli k-12 incorporating high-throughput-generated binding data into regulondb version 10.0', *BMC Biol.* **16**(1), 91.
- Shi, W., Ma, W., Xiong, L., Zhang, M. and Tang, C. (2017), 'Adaptation with transcriptional regulation', *Sci. Rep.* **7**, 42648.
- Wang, J. and Belta, C. (2019), Retroactivity affects the adaptive robustness of transcriptional regulatory networks, *in* '2019 American Control Conference (ACC)', Philadelphia, PA, USA, pp. 5396–5401.
- Wang, J., Isaacson, S. A. and Belta, C. (2019), 'Modeling genetic circuit behavior in transiently transfected mammalian cells.', *ACS Synth. Biol.* **8**(4), 697–707.